

Unravelling the sources of uncertainty in glacier runoff projections in the Patagonian Andes Assessing the glacier projection uncertainties in the Patagonian Andes (40–56° S) from a catchment perspective

Rodrigo Aguayo<sup>1,2</sup>, Fabien Maussion<sup>23,43</sup>, Lilian Schuster<sup>32</sup>, Marius Schaefer<sup>45</sup>, Alexis Caro<sup>56</sup>, Patrick Schmitt<sup>23</sup>, Jonathan Mackay<sup>76,87</sup>, Lizz Ultee<sup>89</sup>, Jorge Leon-Muñoz<sup>9,10,11,12</sup>, and Mauricio Aguayo<sup>1</sup>

<sup>1</sup>Centro EULA, Facultad de Ciencias Ambientales, Universidad de Concepción, Concepción, Chile.  
<sup>2</sup>Department of Water and Climate, Vrije Universiteit Brussel, Brussels, Belgium  
<sup>43</sup>Department of Atmospheric and Cryospheric Sciences (ACINN), Universität Innsbruck, Innsbruck, Austria  
<sup>44</sup>School of Geographical Sciences, University of Bristol, Bristol, UK  
<sup>45</sup>Instituto de Ciencias Físicas y Matemáticas, Universidad Austral de Chile, Valdivia, Chile  
<sup>56</sup>Univ. Grenoble Alpes, CNRS, IRD, INRAE, Grenoble-INP, Institut des Géosciences de l'Environnement, Grenoble, France  
<sup>76</sup>British Geological Survey, Keyworth, Nottingham, United Kingdom  
<sup>89</sup>School of Geography, Earth and Environmental Sciences, University of Birmingham, Edgbaston, Birmingham, UK  
<sup>89</sup>Department of Earth & Climate Sciences, Middlebury College, Middlebury, US  
<sup>109</sup>Departamento de Química Ambiental, Universidad Católica de la Santísima Concepción, Concepción, Chile  
<sup>116</sup>Centro Interdisciplinario para la Investigación Acuícola (INCAR), Concepción, Chile  
<sup>12</sup>Centro de Energía, Universidad Católica de la Santísima Concepción, Concepción, Chile

Correspondence to: Rodrigo Aguayo (rodaguayo@udec.cl)

**Abstract.** Glaciers are retreating globally and are projected to continue to lose mass in the coming decades, directly affecting downstream ecosystems through changes in glacier runoff. Estimating the future evolution of glacier runoff involves several sources of data uncertainty in the modelling chain, which to date have not been comprehensively assessed on a regional scale. In this study, we used the Open Global Glacier Model (OGGM) to estimate the glacier evolution of each glacier (area > 1 km<sup>2</sup>) in the Patagonian Andes (40–56° S), which are distributed in 847 catchments covering 9 different hydrological zones together represent 82% of the glacier area of the Andes. We used different glacier inventories (n = 2), ice thickness datasets (n = 2), historical climate datasets (n = 4), general circulation models (GCMs; n = 10), emission scenarios (SSPs; n = 4), and bias correction methods (BCMs; n = 3) to generate 1,920 possible scenarios over the period 1980–2099. For In each scenario and catchment, glacier runoff and melt on glacier time series were characterized by ten glacio-hydrological signatures (i.e., metrics). We used the permutation feature importance of random forest regression models to assess the relative importance of each source on the signatures of each catchment. Considering all scenarios, 61% ± 14% of the catchment area (34% ± 13% (mean ± one standard deviation) 30% ± 13% of the glacier area) has already peaked in terms of glacier melt (year 2020), and 43% ± 8% of the catchment area (68% ± 21% 48% ± 7% of the glacier area) will lose more than 8050% of its volume this century. Considering the glacier melt on glacier signatures, the future sources of uncertainty (GCMs, SSPs and

Formatted: English (United States), Superscript  
Formatted: English (United States)

Formatted  
Formatted: Normal

BCMs) were the main source in only  $17\% \pm 21\%$   ~~$18\% \pm 21\%$~~  of the total ~~catchment-glacier~~ area. In contrast, the reference climate was the ~~most important~~main source in  $69\% \pm 22\%$   ~~$78\% \pm 21\%$~~  of the ~~glacier catchment~~ area, highlighting the importance of the choices we make in the calibration procedure. The results provide a basis for prioritizing future efforts (e.g., improve reference climate ~~eharacterization~~characterisation) to reduce glacio-hydrological modelling gaps in poorly instrumented regions, such as the Patagonian Andes.



## 1 Introduction

Glaciers are retreating worldwide (Hugonnet et al., 2021) and are projected to continue to lose mass (Marzeion et al., 2020). Recent projections by Rounce et al. (2023) indicate that glaciers will lose  $26 \pm 6\%$  ( $\pm 1.5^\circ\text{C}$ -scenario) to  $41 \pm 11\%$  ( $\pm 4^\circ\text{C}$ -scenario) of their present mass by 2100 (median  $\pm 95\%$  confidence interval), contributing between  $90 \pm 26$  and  $154 \pm 44$  mm to sea-level rise, respectively. The rapid glacier shrinkage has led to cascading effects on downstream systems (Huss et al., 2017; Milner et al., 2017), affecting the availability and quality of water resources (IPCC, 2022), and causing changes in the ecological (Cauvy-Fraunié and Dangles, 2019) and socio-economic (Rasul and Molden, 2019) aspects of downstream environments. As glaciers retreat increases due to climate change, hazards such as glacial lake outburst floods (GLOFs) are undergoing shift in their occurrence rate (Veh et al., 2022), posing an increasing risk to nearby communities (Taylor et al., 2023).

One of the most important impacts of glaciers on downstream systems is the contribution of meltwater to streamflow (Huss and Hock, 2018), which is essential for irrigation, industry, domestic use, hydropower and ecosystems (Immerzeel et al., 2020; Viviroli et al., 2020). However, as glaciers continue to shrink, the reliability and quantity of this water reserve becomes increasingly uncertain, potentially increasing drought stress (Kaser et al., 2010; Pritchard, 2019; Van Tiel et al., 2021, 2023). Ultee et al. (2022) showed globally that accounting for glacier runoff reduces simulated drought frequency and severity, even in basins with low glacier cover ( $< 2\%$ ). The buffering effect is higher in moderately glaciated arid regions, such as the Central Andes, and is projected to increase through the 21st century. In this region, glaciers have provided an important drought mitigation capacity during the current Mega Drought (Ayala et al., 2020; McCarthy et al., 2022), which is unprecedented in recent centuries according to dendrochronological studies (Garreaud et al., 2017; Morales et al., 2020).

Recent global estimates suggest that Andean glaciers are likely to be one of the largest per unit area contributors to sea level rise, with a contribution of  $0.057 \pm 0.006$  mm SLE  $\text{yr}^{-1}$  ( $-20.7 \pm 2.1$  Gt  $\text{yr}^{-1}$ ) representing 7.7% of the global mass loss between 2000 and 2019 (mean  $\pm 95\%$  confidence interval) (Hugonnet et al., 2021). Glaciers in the Patagonian Andes account for 96% of the total ice loss in the Southern Andes (Braun et al., 2019), which has accelerated in recent decades (Davies and Glasser, 2012; Dussaillant et al., 2019). Due to the high precipitation levels in the Patagonian Andes (Aguayo et al., 2024), the contribution of glaciers to regional water supply is generally low, with glacier runoff serving as a flow buffer during dry periods rather than a major source of streamflow (Ruiz et al., 2022). Nevertheless, recent studies have reported increased flows in rivers with important glacier cover the accelerated mass loss over recent decades has significantly increased streamflow in many Patagonian rivers (Masiokas et al., 2019; Vries et al., 2023), some of which have only begun to show significant trends ( $p < 0.01$ ) in the last decade (e.g., Santa Cruz; Pasquini et al., 2021).

70 Despite efforts to improve the understanding of glacier processes in the Patagonian Andes, there are still important limitations  
due to the lack of ground-based validation data. ~~Lowland meteorological stations far from glaciers have had to be used, but~~  
~~their scarcity and lack of continuity remain significant issues in this region (Table 1).~~ To address these limitations, many  
modelling studies have used dynamic and/or statistical downscaling methods based on climate reanalyses (). However, the  
different approaches and data sources have ~~diverged towards systematic overestimations~~ overestimated the precipitation  
75 according to numerical simulations of regional moisture fluxes (Sauter, 2020). Despite the severe lack of data on melt patterns  
and snow accumulation in the upper plateaus of the Patagonian Icefields (Bravo et al., 2019a, b), most regional modelling  
efforts have focused on this region (). In this area, glacier modelling has generally relied on energy balance approaches based  
on downscaled reanalysis data. Only two studies have modelled the regional hydrological contribution of the Patagonian  
glaciers (Mernild et al., 2017; Caro et al., 2023). Using the SnowModel (1979-2014), Mernild et al. (2017) estimated a mean  
80 specific runoff of 6,240 and 6,700 mm yr<sup>-1</sup> for the SPI and NPI, respectively. More Recently, (Caro et al., (2024) used the  
Open Global Glacier Model (OGGM) to compare the hydrological response of Andean catchments between 2000-2009 and  
2010-2019. In the Patagonian Andes, an -positive-increase in glacier melt was found, ranging from 6% to 14% depending on  
the zone. Although recent modelling efforts have benefited from the increased availability of geodetic mass balances to  
calibrate and validate surface mass balance models (), important sources of uncertainty in the future evolution of Patagonian  
85 glaciers remain.

There are several sources of uncertainty in the modelling chain of glacier projections. At the global scale, results from the  
Glacier Model Intercomparison Project Phase 2 (GlacierMIP2) showed that the emission scenario is the largest source of  
uncertainty by the end of the century, but the uncertainty from the glacier models, which use different data sources and  
calibration setups, is the largest source until 2050 (Marzeion et al., 2020). Locally, several studies have shown that individual  
90 choices during model initialization and calibration, such as the historical climate (Compagno et al., 2021; Watanabe et al.,  
2019), the glacier inventory (Li et al., 2022), the ice thickness (Gabbi et al., 2012), and the downscaling strategy (Schuster et  
al., 2023), have an impact on glacier evolution. However, few studies have examined the influence of multiple components of  
the modelling chain on projected glacio-hydrological changes. ~~Huss et al. (2014)~~ ~~Huss et al. (2014)~~ found that winter snow  
accumulation and the glacier retreat model have the greatest influence on the glacier runoff projections in the Findelengletscher  
95 basin (Switzerland), while the downscaling strategy, calibration data quality and the surface mass balance model are of  
secondary importance. Mackay et al. (2019) used hydrological signatures, which are quantitative metrics that describe the  
dynamic properties of hydrological time series (McMillan, 2021), to measure changes in the hydrology of the Virkisá basin  
(southern Iceland). They found that the main source of uncertainty were the climate model chain components (global  
circulation models and emission scenarios), but for certain hydrological signatures; the most important source was the  
100 representation of glacio-hydrological processes. Overall, adding additional data (e.g., snow cover area, glacier mass change)

Field Code Changed

to the calibration of glacio-hydrological processes has shown to be more important than increasing the complexity of the model (Van Tiel et al., 2020).

In this study, we investigated the importance of six sources of data uncertainty in the glacier modelling chain for ten glacio-hydrological signatures (i.e., metrics) that characterize the evolution of hydrological regime glacier runoff of each catchment. The sources of uncertainty were glacier inventories (n = 2), ice thickness datasets (n = 2), historical climates (n = 4), global circulation models (n = 10), emission scenarios (n = 4) and bias correction methods (n = 3). The scenarios were tested with using the Open Global Glacier Model (OGGM) to project the evolution of each glacier (area > 1 km<sup>2</sup>) in the Patagonian Andes (40–56° S) over the period 1980–2099. Finally, the importance of each source of data uncertainty was measured using we used the permutation feature importance of random forest regression models to assess the importance of each source of uncertainty on the different glacio-hydrological signatures of each catchment.

**Table 1. Regional surface mass balance models applied in the Patagonian Andes (40–56° S). In parenthesis the initial spatial resolution of the gridded climate. AWS: Automatic weather station. PP: Precipitation. T2M: Air temperature at 2m. GMB: Geodetic mass balance. The area acronyms are defined in Section 2.**

Area	Period	Reference climate	Downscaling	Target resolution	Timestep	SMB-model	Calibration/validation of mass balance	Reference
NPI	1975–2099	Output from WRF run (5 km)-based on NCEP-NCAR (2.5°)	T2M: Constant lapse rate of 6.5 °C km <sup>-1</sup> ; PP: Gradient of 0.05% m <sup>-1</sup> . AWSs were used for validation.	450 m	Daily	Simplified energy balance	GMB: Willis et al. (2012) and Rignot et al. (2003)	Schaefer et al. (2013)
GCN	2000–2005	PP: NCEP-NCAR (2.5°); T2M: AWSs	T2M: Constant lapse rate of 5.8 °C km <sup>-1</sup> ; PP: Gradient of 0.15% m <sup>-1</sup> . Orographic precipitation model as an alternative.	90 m	Daily	Degree-day model	Ablation stakes for validation	Weidemann et al. (2013)
NPI+SPI	1979–2012	Output from RACMO run based on ERA-Interim (~80 km)	No downscaling. AWSs were used for model evaluation	5.5 km	6 hours	Energy balance (RACMO2.3)	Ice cores for validation	Lenaerts et al. (2014)
SPi	1975–2011	Follows Schaefer et al. (2013)	Follows Schaefer et al. (2013)	180 m	Daily	Simplified energy balance	Parameters from Schaefer et al. (2013). Ablation stakes and ice cores for validation	Schaefer et al. (2015)
Andes	1979–2014	NASA MERRA (~0.5°)	Downscaling based on MicroMet (Liston and Elder, 2006)	1 km	3 hours	Energy balance (SnowModel)	SMB observations of seven glaciers (only one in the Patagonian Andes)	Mernild et al. (2017)
NPI+SPI	1976–2050	RegCM4.6 output (~10 km)-based on MPI-ESM-MR model	No downscaling. AWSs were used for model evaluation	10 km	Daily	Energy balance	Validation based on multiple GMBs (NPI and SPI)	Bravo et al. (2021)

NPI+ SPI	1980– 2015	RegCM4.6 output (10 km) based on ERA-Interim model	Follows Schaefer et al. (2013). CR2MET was used for validation	450 m	3 hours	Simplified energy balance	Calibration based on SMB estimates from Minowa et al. (2021)	Carrasco- Escaff et al. (2023)
CDI	2000– 2022	ERA5 (0.25°) and AWSs	Several methods depending on the variable	200 m	3 hours	Four different models	Multiple strategies using ablation stakes, geodetic mass balance and mass budgeting	Temme et al. (2023)
Andes	2000– 2019	Bias-corrected version of TerraClimate (4 km)	Lapse rates depend on the glaciological zones	f (glacier area)	Monthly	Degree-day model (OGGM)	GMB from Hugonnet et al. (2021) and volume from Farinotti et al. (2019)	Caro et al. (2023)

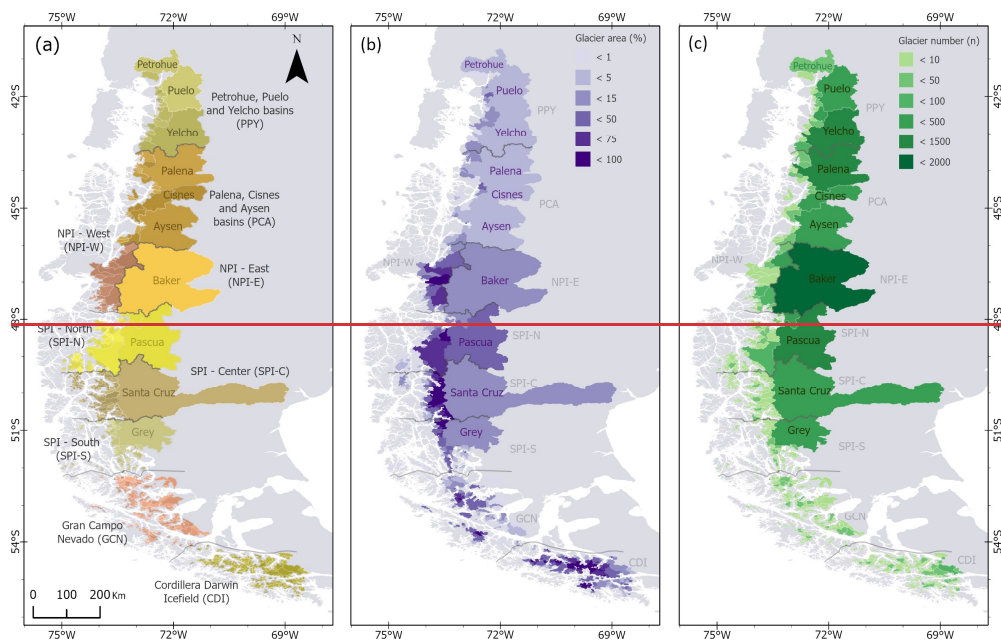
## 2 Study area

Our study area comprises the Patagonian Andes (40–56° S; Fig. 1), which is characterized by an almost-pristine environment, where freshwater ecosystems interact with the adjacent coastal system. In this region, where the glaciers are a crucial natural feature of the terrestrial geography and their seasonal melting of glaciers is essential for the long-term sustainability of the local ecosystems and coastal human populations (Iriarte et al., 2014). Glaciers in the Patagonian Andes cover an extensive area of 25,886 km<sup>2</sup>, which represents 82% of the total glacierized area of the Andes at the time of the inventory (year ~2000; RGI Consortium, 2017). This region includes the Northern and Southern Patagonian Icefields (NPI and SPI), which form the largest freshwater reservoir in the Southern Hemisphere outside of Antarctica, with a total area of 17,195 km<sup>2</sup> in 2011 (Davies and Glasser, 2012), and an estimated ice volume of 4,756 ± 923 km<sup>3</sup> (Millan et al., 2019).

We selected 847 glacierized catchments, each with at least one glacier and a glacier area greater than 0.1%. The 0.1% glacier area threshold was selected as a conservative threshold for drought buffering effect (see Fig. 3 in Ultee et al. 2022). The catchments were and aggregated into nine hydrological zones (Fig. 1), which. Each catchment has at least one glacier and presents a glacier area greater than 0.1% of the catchment area. The hydrological zones were selected based on the spatial patterns of precipitation and temperature that have showed a high-explanatory powerstrong capacity to reproduce -of recent glacier changes (Caro et al., 2021). Along the latitudinal gradient covered by the nine zones, the mean annual 0 °C isotherm decreases with elevation from about 3,000 m a.s.l. in the northern area to less than 1,000 m a.s.l. in the southern area (Condom et al., 2007; Carrasco et al., 2008). The northern area (~ 41–46° S; Fig. 1) is characterized by two zones (PPY and PCA) that aggregate large catchments with a low glacier area: Petrohue, Puelo and Yelcho (PPY) basins, and Palena, Cisnes and Aysen (PCA) basins. The Northern Patagonian Icefield (NPI; ~ 46–48° S) was divided into two zones according to its main aspect (NPI-E and NPI-W). The eastern side (NPI-E) coincides with the location of the Baker River Basin, one of the catchments with the largest glacier area in the study area and the focus of regional (Dussailant et al., 2019) and global (Huss and Hock, 2018) glacio-hydrological studies. The Southern Patagonian Icefield (SPI; ~ 48–52° S) was divided latitudinally according to

Field Code Changed

the main catchments on the eastern side (Pascua in SPI-N, Santa Cruz in SPI-C and Grey in SPI-S). Finally, the southern area was divided into the Gran Campo Nevado (GCN; ~ 52–54° S) and the Cordillera Darwin Icefield (CDI; < ~ 54° S), which hosts many small catchments~~are characterized by many small catchments~~. In contrast to the rest of the area, both southern zones receive uniform precipitation throughout the year, with no clear seasonality.



**Formatted:** Normal (Web), Left, Space After: 0 pt, Line spacing: single, Don't keep with next

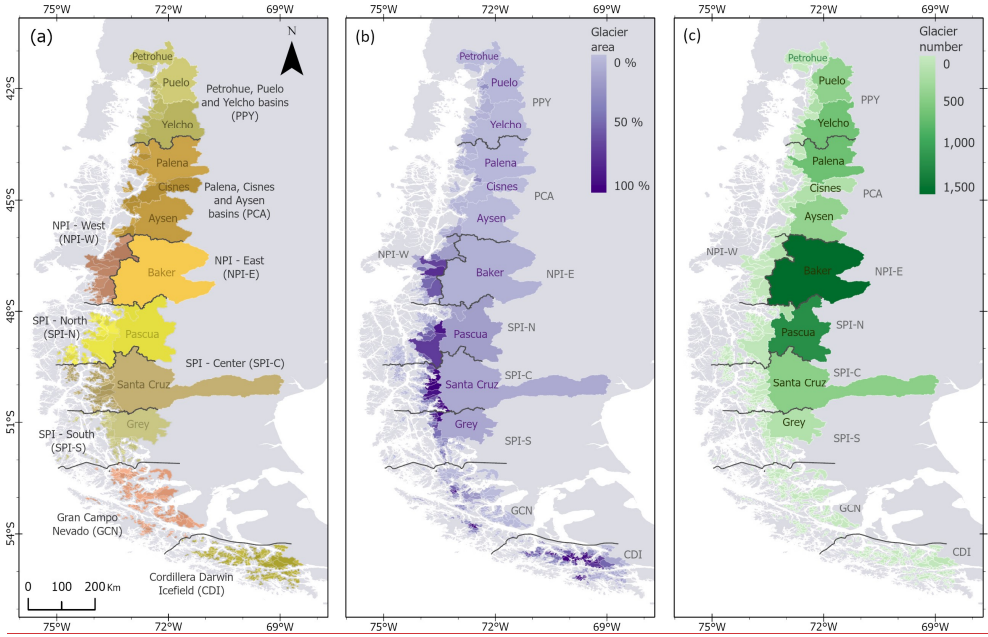


**Figure 1. Study area. a) Hydrological zones (n = 9) for the 847 catchments. The names in grey correspond to the names of the main catchments (area > 5,000 km<sup>2</sup>) in the study area, which account for the 68% of the total catchment area. b) Glacier area for each catchment. c) Number of glaciers in RGI6 per catchment.**

### 3 Methods

#### 3.1 The Open Global Glacier Model (OGGM)

We used the Open Global Glacier Model v1.5.4 (OGGM, Maussion et al., 2019) to model the evolution of all the glaciers in the study area. The OGGM is an open-source model that couples a surface mass balance model with a model of glacier dynamics. The model has been used in global studies (Marzeion et al., 2020; Rounce et al., 2023; Zekollari et al., 2024) and regional-hydrological studies (e.g., Caro et al., 2024; Hanus et al., 2024; Pesci et al., 2023; Zhao et al., 2023). The surface climatic mass balance model is based on an extended version of the temperature-index model used by Marzeion et al. (2012). In this approach, the monthly mass balance ( $B_i$ ) at elevation  $z$  is calculated as:

$$B_i(z) = P_i \cdot P_i^s(z) - \mu^* \cdot \max(T_i(z) - T_{\text{melt}}, 0), \quad (1)$$

Formatted: Dutch (Belgium)

Formatted: Dutch (Belgium)

Field Code Changed

Formatted: French (France)

Formatted: French (France)

Formatted: French (France)

Field Code Changed

where  $P_r$  is a precipitation factor used to account for measurement biases in mountainous topography, to further downscale precipitation to the glacier resolution, and to account for missing processes (e.g., debris cover, firn densification, avalanches) not explicitly included in the mass balance.  $P_i^*$  and  $T_i$  are the monthly solid precipitation and air temperature,  $\mu^*$  is the temperature sensitivity of the glacier, and  $T_{melt}$  is the monthly mean air temperature above which ice melt is assumed to occur. The air temperature climate variables are obtained from the nearest grid-grid point. In the case of temperature, this itself and at each reference grid elevation is adjusted to the glacier surface elevation using a constant lapse rates of  $-6.5\text{ }^{\circ}\text{C km}^{-1}$ , a value commonly used in the study area (Table S11). The solid precipitation fraction is calculated using an upper and a lower temperature thresholds  $[0, 2\text{ }^{\circ}\text{C}]$ . Positive degree-months and solid precipitation are calculated using Given the low availability of regional ground-based data, we used the default thresholds for melting ( $T_{melt} = -1\text{ }^{\circ}\text{C}$  since melting can still occur on some days when the monthly mean temperature is below  $0\text{ }^{\circ}\text{C}$ ) and accumulation ( $T_{solid} = 0\text{ }^{\circ}\text{C}$  and  $T_{liquid} = 2\text{ }^{\circ}\text{C}$ ). When the temperature is within between  $T_{solid}$  and  $T_{liquid}$  range defined by the thresholds, the solid precipitation varies linearly between 100% and 0% at the lower and upper limits, respectively. The contributions of positive degree-months and solid precipitation are combined to calculate the monthly mass balance, which is used to update the glacier geometry annually.

Glacier geometry (i.e., outlines) is derived from global or local inventories that are projected onto a local grid for each glacier, with a spatial resolution that depends on the area of each glacier (between 10 and 200 m). In this study, the elevation data is obtained from NASADEM (NASA JPL, 2020). Based on this dataset, each glacier was divided into binned elevation bands following the algorithm proposed by Werder et al. (2020). ModelGridded glacier geometry is obtained by overlaying global or local glacier inventory outlines and NASADEM elevation data (NASA JPL, 2020) onto a regular grid. The resolution of the grid 's resolution varies with the glacier size, ranging from 10 to 200 meters. Based on this dataset, gGlaciers are then segmented into elevation bands, each of which covers an elevation difference of 30 m, following the algorithm proposed by described in Werder et al. (2020), each of which covers an elevation difference of 30 m. The spacing of the resulting elevation band flowline cross-sections mirrors the initial dataset's resolution, also between 10 and 200 meters. The ice dynamics flowline model of OGGM uses a relies on a depth-integrated ice velocity  $u$  ( $\text{m s}^{-1}$ ), utilizing the shallow ice approximation (SIA):

$$u = \frac{2A}{n+1} \cdot h \cdot (\rho \cdot g \cdot h \cdot \alpha)^n, \quad (2)$$

$$U = (2A)/(n+2) \cdot h \cdot (\rho \cdot g \cdot h \cdot \alpha)^n, \quad (2)$$

- Formatted: Superscript
- Formatted: Not Superscript/ Subscript
- Formatted: Font: +Headings (Times New Roman)
- Formatted: Font: +Headings (Times New Roman)
- Formatted: Font: +Headings (Times New Roman)
- Formatted: Font: +Headings (Times New Roman)
- Formatted: Font: +Headings (Times New Roman)
- Formatted: Font: +Headings (Times New Roman)
- Formatted: Font: +Headings (Times New Roman)
- Formatted: Font: +Headings (Times New Roman)
- Formatted: Font: +Headings (Times New Roman)
- Formatted: Font: +Headings (Times New Roman)
- Formatted: Font: +Headings (Times New Roman)



shallow ice approximation (SIA) with a depth-integrated flowline model where  $A$  is the ice creep parameter ( $\text{s}^{-1} \text{PA}^3$ ),  $n$  is the exponent of Glen's flow law ( $n=3$ ),  $h$  is the local ice thickness (m),  $\rho_{\text{ice}}$  is the ice density ( $900 \text{ kg m}^{-3}$ ),  $g$  is the gravitational acceleration ( $9.81 \text{ m s}^{-2}$ ), and  $\alpha$  is the surface slope computed numerically along the flowline (following Eq. 3 and 4 of Maussion et al. 2019). With this velocity, the flux of ice along the glacier is to explicitly computed, the flux of ice along the glacier.

In this study, we set the precipitation factor ( $P_f$ ) to 1.0 to assess the influence of different reference climates on the evolution of each glacier (Fig. 2), assuming that the estimated precipitation from the different products corresponds to the "true" values. Given the low availability of regional ground-based data, we used the default thresholds for melting ( $T_{\text{melt}} = -1^\circ\text{C}$  since melting can still occur on some days when the monthly mean temperature is below  $0^\circ\text{C}$ ) and accumulation ( $T_{\text{solid}} = 0^\circ\text{C}$  and  $T_{\text{liquid}} = 2^\circ\text{C}$ ). The frontal ablation of marine-terminating and lake-terminating glaciers was not explicitly simulated explicitly. However, Malles et al. (2023) recently showed that the mass-balance model (through different temperature sensitivities) implicitly accounts for the effect of frontal ablation when calibrated against the Hugonnet et al. (2021) observations, resulting in relatively small changes in the projections. This is an acknowledged shortcoming of our study and should be further investigated in future studies.

The calibration of each glacier consisted of a newly developed iterative process that involves three parameters: the temperature sensitivity ( $\mu^*$ ; Eq. 1), the composite ice creep parameter deformation-sliding-parameter ( $A$ ; encapsulating basal sliding and ice deformation, Eq. 2) following Glen's flow law; Eq. 3 in Maussion et al. 2019), and finally, the spin-up temperature ( $T_{\text{spinup}}$ ; used to find a historical glacier state). The calibration procedure, shown in Fig. 2, unfolds through the following steps:

i. Define a new the initial value of  $\mu^*$  (Eq. 1). The first value is obtained by matching the modelled specific mass balance with the geodetic mass balance of Hugonnet et al. (2021). This is calculated using the period 2000 to 2020, the reference climate and the static surface geometry, which refers to the outline obtained from the Randolph Glacier Inventory (RGI; see next section).

ii. Compute an apparent mass balance using the static surface geometry and the reference climate in the geodetic mass balance period (2000–2020). In particular, this step searches for a mass balance residual to add to the mass balance profile so that the average specific mass balance is zero. This is needed for the underlying equilibrium assumption during the inversion, as described in Maussion et al. (2019). The apparent mass balance is defined as the specific mass balance plus a residual term, which shifts the complete mass balance profile. This adjustment ensures that the resulting specific mass balance is equals to zero, adhering following to the equilibrium assumption in the inversion process described by Maussion et al. (2019) Maussion et al. (2019).

2.

Formatted: Superscript

Formatted: Superscript

Formatted: Superscript

Formatted: Superscript

Formatted: Numbered + Level: 1 + Numbering Style: i, ii, iii, ... + Start at: 1 + Alignment: Right + Aligned at: 0" + Indent at: 0.25"

Formatted: Indent: Left: 0.25", No bullets or numbering

iii. Use the derived apparent mass balance for an inversion for the underlying glacier bed. Throughout this inversion, parameter A (Eq. 2) is defined such that the resulting inversion glacier volume matches the estimates for each hydrological zone defined in Fig. 1. The inversion method follows Maussion et al. (2019) when the sliding parameter is set to 0.

3.

215 iv. The next step is to find a glacier state in the past (first ~~try attempt~~ 1980) from which a dynamic glacier run to the RGI date (approx. year 2000) results in the given RGI area. To define different glacier states in the past, the temperature spin-up  $T_{\text{spinup}}$  (first guess is  $-1^{\circ}\text{C}$ ) ~~is was~~ added to the reference climate ~~and we define a mean mass balance using the reference climate between 1980 and the RGI date. With this mean mass balance during a 20-year dynamic model run is conducted and the resulting glacier state defines the 1980 extend~~ constant mass balance run (first guess of  $T_{\text{spinup}}$  is  $-1^{\circ}\text{C}$ ). The

220 ~~constant mass balance is defined as the mean mass balance given by the reference climate between 1980 and the RGI date.~~ How consecutive guesses of  $T_{\text{spinup}}$  are found is described in Appendix A. If the resulting glacier is too large even when we start from an ice-free initial glacier state in the past, or the resulting glacier is too small and the algorithm grows the glacier outside the domain, a shorter spin-up period is tried two times (starting ~~at year in~~ 1985 or 1990). If the spin-up period is shortened, a fixed geometry volume is calculated by going backwards to 1980, using the calculated mass change on the constant surface geometry ~~(assuming a bulk density of  $900\text{ kg m}^{-3}$ ). This is done ~~to~~ have a continuous volume~~ time-series for all glaciers. We only move on if this step has successfully found a proper past glacier state to match the RGI area within  $1\text{ km}^2$  or 1% of the total area, whatever is smaller.

225

4.

5-v. Initiate a dynamic simulation from 1980 to 2020, using the reference climate inputs and starting from the glacier state

230 inferred in the previous step.

6-vi. Finally, the geodetic mass balance resulting from the dynamic simulation is calculated and compared ~~it~~ with the observed values from Hugonnet et al. (2021). If the difference between these values is within the defined uncertainty ( $\pm 250\text{ kg m}^{-2}\text{ yr}^{-1}$ ), the calibration/initialization workflow is terminated and the resulting glacier in 2020 and the parameters  $\mu^*$  and A are used as inputs for the projection runs. If not, a new  $\mu^*$  is defined (Appendix A) and the ~~whole~~ process starts again

235 from ~~the beginning step N°1~~.

**Formatted:** Numbered + Level: 1 + Numbering Style: i, ii, iii, ... + Start at: 1 + Alignment: Right + Aligned at: 0" + Indent at: 0.25"

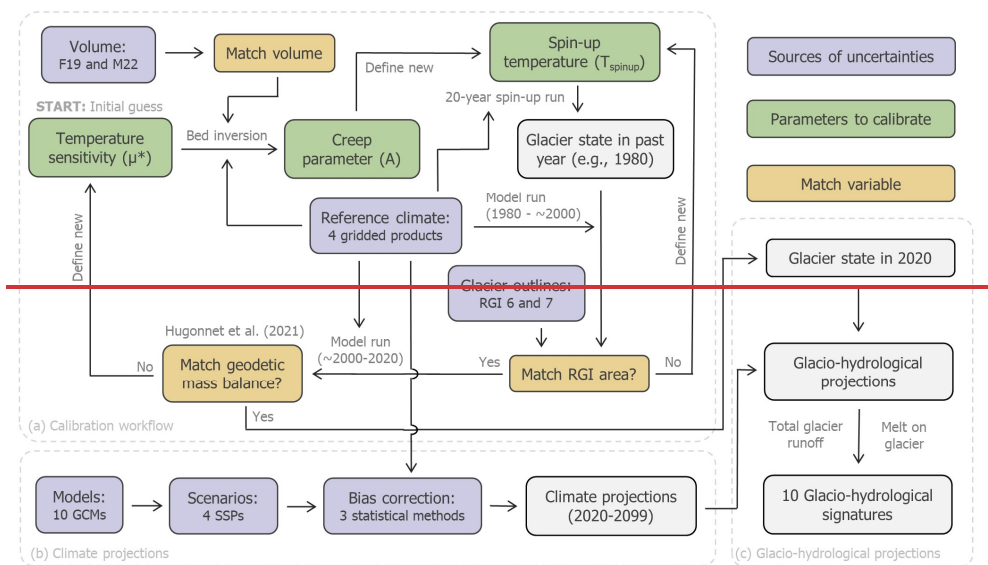
**Formatted:** Indent: Left: 0.25", No bullets or numbering

**Formatted:** Numbered + Level: 1 + Numbering Style: i, ii, iii, ... + Start at: 1 + Alignment: Right + Aligned at: 0" + Indent at: 0.25"

**Formatted:** Superscript

**Formatted:** Indent: Left: 0.25", No bullets or numbering

**Formatted:** Numbered + Level: 1 + Numbering Style: i, ii, iii, ... + Start at: 1 + Alignment: Right + Aligned at: 0" + Indent at: 0.25"



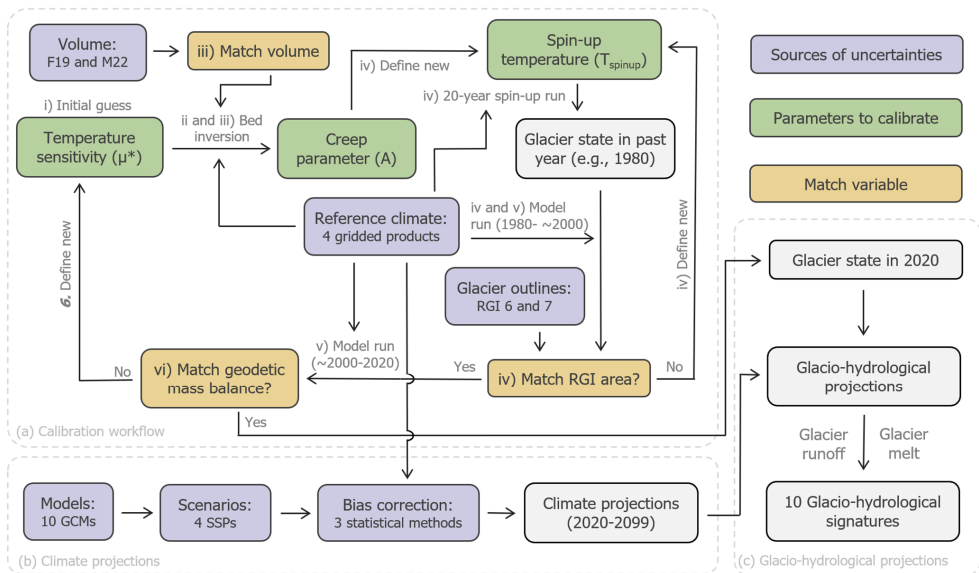


**Figure 2. Methodological framework.** a) Open Global Glacier Model (OGGM) dynamic calibration workflow. **Roman numerals refer to the calibration steps in Section 3.1.** b) Climate projections. c) Glacio-hydrological projections. GCM: General Circulation Models. SSP: Shared Socioeconomic Pathways. F19 and M22: Thickness estimated from Farinotti et al. (2019) and Millan et al. (2022). RGI: Randolph Glacier Inventory.

### 3.2 Sources of uncertainty

#### 3.2.1 Geometry and volume

The geometry, represented by the glacier outlines, was obtained from RGI6 (Randolph Glacier Inventory - Version 6) (RGI Consortium, 2017) and RGI7 (RGI Consortium, 2023). In the latest version, RGI7 integrates the national inventories of Chile (Barcaza et al., 2017) and Argentina (Zalazar et al., 2020). Previous assessments of the complete RGI region (20–56° S) have shown that **both datasets (RGI6 and RGI7) show similar areas across different latitudes both datasets show similar latitudinal patterns in terms of area** (~3% of total area **according to national inventories relative to RGI6**; Zalazar et al., 2020). Nevertheless, the national inventories **included in RGI7** showed a higher number of glaciers ( $\Delta n = 8,493$ ) and area ( $\Delta = 651 \text{ km}^2$ ) for the smallest glaciers ( $< 0.5 \text{ km}^2$ ), and **a reduction of differences of less than 77% in the area covered by the largest glaciers in the icefields Patagonian Icefields** compared to RGI6.

Individual volumes for each glacier were derived from the thickness estimated from Farinotti et al. (2019) and Millan et al. (2022) (hereafter F19 and M22, respectively). F19 is a consensus estimate from five models that use principles of ice flow dynamics to infer ice thickness from surface properties. In contrast, M22 uses glacier flow mapping to reconcile the spatial distribution of ice masses with glacier dynamics, morphology, and ice divides. [In the southern Andes](#), Hock et al. (2023) reported that M22 had 13% more total ice volume than F19. ~~reported that the total ice volume of M22 showed a positive difference of 13% compared to F19 for the corresponding RGI region of the southern Andes.~~ Considering that [the two volume data both alternativesources](#) do not have a complete coverage of all glaciers in RGI6 (100% and 98.2% of the area for F19 and M22, respectively) and RGI7 (99.1% and 96.4% of the area for F19 and M22, respectively), we used a volume-area scaling (VAS, Hock et al., 2023) to complete the coverage ~~and compare the datasets at a regional and catchment scales.~~ In this approach, we calculated the VAS parameters for each hydrological zone (defined in Fig. 1) and [volume data sources dataset](#) separately.

### 3.2.2 Reference historical climate (1980–2015)

We used monthly precipitation and air temperature time series from ERA5 (0.25°; Hersbach et al., 2020) and three gauge-corrected alternatives that use ERA5 in the bias correction process (CR2MET v2.5, MSWEP v2.8/MSWX and PMET v1.0). CR2MET v2.5 (0.05°; Boisier, 2023) is the current national reference for hydrometeorological studies in Chile, and is based on a statistical downscaling technique that uses ERA5, meteorological records, satellite land surface temperature and topographic descriptors. MSWEP v2.8 (0.1°; Beck et al., 2019) is a global precipitation product that merges gauges, satellites and reanalysis data, and has outperformed other state-of-the-art precipitation products over Chile (Zambrano-Bigiarini, 2018). Precipitation from MSWEP v2.8 was complemented with air temperature from MSWX (0.1°; Beck et al., 2022), a bias-corrected meteorological product compatible with MSWEP. Finally, PMET v1.0 (Aguayo et al., 2024) was developed for Western Patagonia using statistical bias correction procedures, spatial regression models (random forest), and hydrological methods (Budyko framework) to correct the underestimation of precipitation reported in areas with pronounced elevation gradients and significant snowfall. ~~As part of the validation process,~~ PMET outperformed ERA5, CR2MET and MSWEP in terms of hydrological modelling performance (Aguayo et al., 2024).

### 3.2.3 Climate projections (2020–2099)

Climate projections of monthly precipitation and air temperature were obtained from 10 General Circulation Models (GCMs, Table [S4S2](#)) of the Coupled Model Intercomparison Project 6 (CMIP6; Eyring et al., 2016). Previous hydrological studies have suggested that 10 GCMs can ensure that the median of all possible combinations produces similar uncertainty components as the entire ensemble (Wang et al., 2020). ~~Using~~ [Considering the full CMIP6 ensemble only GCMs with at least one output in all emission scenarios, the selection of the 10 GCMs was based on the recommendations of Hausfather et al. \(2022\), who suggest focusing on a subset of GCMs that are most consistent with the assessed warming projections of the Sixth Assessment](#)

Report (AR6). In this case, the Following the recommendations of Hausfather et al. (2022), all selected GCMs show have a transient climate response (TCR; temperature change at the time of CO<sub>2</sub> doubling) that lies in the “likely” range of 1.4 - 2.2 °C (66% likelihood, Table S1S2), which is a good approximation of the assessed warming (Tokarska et al., 2020). –Given that the warming constraints assessed in the Sixth Assessment Report (AR6) are correlated with the TCR (Tokarska et al., 2020), this provides a good approximation of the assessed warming. Note that all GCMs have an equilibrium climate sensitivity (ECS) that falls in the “very likely” range, but only 80% of them fall in the ‘likely’ range of 2.5–4.0 °C (Table S1). Considering that future scenarios are the main source of uncertainty at the end of the century in the southern Andes (Marzeion et al., 2020), we used four different Shared Socioeconomic Pathways (SSPs; O’Neill et al., 2016): SSP1-2.6, SSP2-4.5, SSP3-7.0 and SSP5-8.5. Each GCM was initially resampled to 1.0° using a bilinear filter, and only the standard model realization-realisation was considered (r1i1p1f1 in all cases).

3.2.4 Bias correction method

Three statistical bias correction methods were evaluated to assess their impact on the glacier projections. The objective of bias correction is to minimize the systematic error of the climate projections obtained from general circulation models (Section 3.2.3) using the reference climate used in the calibration process (Section 3.2.2). The selected methods were: Mean and Variance Scaling (MVA; Chen et al., 2011), Quantile Delta Mapping (QDM; Cannon et al., 2015) and Multivariate Bias Correction with N-dimensional probability density function transformation (MBCn; Cannon, 2018). The MVA approach was commonly used in GlacierMIP2, as it guarantees that the bias-corrected time series has the same mean and standard deviation (i.e., variance) as the reference time series in the reference period. QDM is a hybrid method that combines quantile-based delta change and bias correction methods. Thus, it not only preserves the quantile changes predicted by climate projections, but also corrects the biases of the modelled series with respect to those of the reference time series. Finally, MBCn is a multivariate bias correction that has the advantage of transforming all aspects of the reference multivariate distribution to the multivariate distribution simulated by the climate models. The bias correction parameters of all methods were calculated on a monthly basis to account for the seasonality of GCM biases. Following the protocol of the Inter-Sectoral Impact Model Intercomparison Project (ISIMIP3b; Lange, 2021), the reference period was 1980–2015 for all correction methods. Climate outputs based on the QDM and MBCn approaches were obtained using the xclim package v0.4 (Logan et al., 2022).

3.3 Comparative Analysis of sources of uncertainty

Taking all glaciers into account, each source of data uncertainty was analysed to quantify the difference between the alternatives. In both cases, the area and volume were aggregated according to the location of the glacier terminus. For area and volume, we calculated the relative and absolute differences for each catchment and hydrological zone defined in Fig. 1. To calculate these differences, we aggregated glacier area and volume for a given catchment by selecting all glaciers with their terminus location within that catchment. It is assumed that, if the inventory outlines are correct, all the water flowing out of

Formatted: English (United States)

Formatted: English (United States)

Formatted: English (United States)

Formatted: English (United States)

Field Code Changed

Field Code Changed

~~the glacier will flow via its terminus.~~ In addition, we compared the acquisition dates of the glacier geometries for both inventories. ~~In both cases, the area and volume were aggregated according to the location of the glacier terminus.~~ To assess the influence of the reference climate on the glacier mass balance, we calculated the solid precipitation and positive degree-day sum in addition to precipitation and temperature. To isolate the effect of the spatial resolution, temperature from ERA5 and MSWEP/MSWX was downscaled to 0.05° using the same lapse rate used by OGGM (-6.5 °C km<sup>-1</sup>). ~~Precipitation was not downscaled.~~ ~~No downscaling was applied for precipitation.~~ Similarly, solid precipitation and positive degree-day sum were calculated using the ~~default parameter~~ thresholds indicated in Section 2.1 ~~as from OGGM~~ ( $T_{\text{melt}} = -1\text{ °C}$ ,  $T_{\text{solid}} = 0\text{ °C}$  and  $T_{\text{liquid}} = 2\text{ °C}$ ). Specifically, we calculated and compared annual means for each variable, catchment, and product for the reference period (1980–2015) using only the glacierized grid cells.

The climate projections were another source of uncertainty. To assess the impact of the raw climate projections, we calculated the relative change between the reference period (1980–2015) and the future period (2070–2099) for each GCM and SSP. In addition, we calculated the model agreement of precipitation following Iturbide et al. (2021), who defined a high model agreement when more than 80% of the GCMs agree on the sign of the change. Finally, to assess the individual impact of each climate uncertainty source, we calculated the standard deviation across different reference climates, GCMs, SSPs, and bias correction methods. Specifically, we calculated the standard deviation based on the long-term annual mean of each variable, catchment, and alternative. Analogous to the reference climate, we calculated the annual mean for the future period (2070–2099) using only the glacierized grid cells.

### 3.4 Glacio-hydrological runs

We used the OGGM model to estimate the evolution over the period 1980–2099 of all glaciers with an area > 1 km<sup>2</sup> in the Patagonian Andes (40–56° S). This corresponds to 2,034 and 1,837 glaciers that accumulate 99.0% and 98.5% of the total volume estimated by Millan et al. (2022) for RGI6 and RGI7, respectively. For each glacier, ~~we evaluated 16 scenarios generated by the historical sources of uncertainty: glacier outlines (n = 2), volume datasets (n = 2) and reference climates (n = 4). These scenarios were used to project the future evolution given by different we evaluated 1920 potential scenarios generated by all combinations of glacier outlines (n = 2), volume datasets (n = 2), reference climates (n = 4), GCMs (n = 10), future scenarios (n = 4), and bias correction methods (n = 3), resulting in 120 future scenarios for each historical simulation - (a total of 1920 potential scenarios; Fig. 2)-.~~ To estimate the glacier ~~mass-volume~~ that is unsustainable under current conditions, we additionally ~~run 16 scenarios based on historical conditions (2 × 2 × 4). For this, we ran a 16 simulations~~ for 80 years with a pseudo-random climate based on the historical climate (30 years) around the year 2000.

For all 1920 scenarios, we extracted the annual glacier area, volume, and specific mass balance of each modelled glacier. To assess the hydrological contribution, we additionally extracted glacier runoff which corresponds to all water originating from

Formatted: Subscript

Formatted: Subscript

Formatted: Subscript

the initially glacierized area (i.e., here year 1980; Huss and Hock, 2018). In this approach, OGGM calculates the glacier runoff from the sum of on- and off-glacier melt and on- and off-glacier liquid precipitation. To disaggregate the impact of projected precipitation changes ~~reductions in the climate projection~~, we also extracted the melt on ~~melt on the~~ glacier (hereafter glacier melt) ~~from the glacier runoff, which is the sum of ice and seasonal snow melt on the glacier~~ (Fig. 2c). As in the comparative analysis (Section 3.3), ~~The~~ the time series were initially aggregated at the catchment scale ~~at the catchment and hydrological zone scales~~ according to the location of the glacier terminus.

Glacier runoff and melt ~~on glacier~~ were characterised by 10 glacio-hydrological signatures (i.e., metrics) to describe the hydrological dynamic properties of each catchment (Table 1). The set of signatures was selected to cover the different categories proposed by Richter et al. (1996): magnitude, timing, frequency, duration, and rate of change. Poff et al. (1997) used these categories to characterize the hydrological regime and proposed that these components fully describe the streamflow characteristics that are important to the aquatic ecosystem. However, our analysis of glacier runoff should not be considered as downstream streamflow because our simulations considered only the initially glacierised area and did not include the interaction with other hydrological fluxes (e.g., evaporation and infiltration). ~~The set of selected signatures is presented in Table 2.~~

**Table 21.** Glacio-hydrological signatures used to characterize glacier runoff and melt ~~on glacier~~ time series of each catchment. The regime characteristics corresponds to the initial categories proposed by Richter et al. (1996). ~~The reference and future period correspond to 1980–2015 and 2070–2099, respectively.~~

Signature or metric	Regime characteristics	Description	Period	Units
Reference magnitude	Magnitude	Annual mean value (runoff and melt) <del>calculated from the reference period.</del> The value was normalized by the catchment area.	1980–2015	mm yr <sup>-1</sup>
Peak water year	Timing	Following Huss and Hock (2018), the peak water year was calculated using an 11-year moving average.	1980–2099	date (year)
Peak water magnitude	Magnitude Timing	Maximum annual value in the peak water year. The value was normalized by the catchment area.	1980–2099	mm yr <sup>-1</sup>
Peak water duration	Duration Timing	Number of years in which the annual value is greater than 90% of the peak water magnitude	1980–2099	years
Inter-annual variability	Frequency	Standard deviation of the detrended and normalized time series. For the detrending, we used the same 11-year moving average.	1980–2099	mm yr <sup>-1</sup>
Reference seasonal contribution	Duration Magnitude	Percentage of annual runoff that occurs during the summer season (DJF). <del>Value calculated from the reference period</del>	1980–2015	%
Reference seasonal variability	Frequency	Standard deviation of the percentage of the annual runoff that occurs during the summer season (DJF).	1980–2015	%

Formatted: Space After: 0 pt

Formatted Table

Formatted: English (United Kingdom)

Formatted: Space After: 0 pt

Formatted: Space After: 0 pt

Formatted: Font: 9 pt

Formatted: English (United Kingdom)

Formatted: Space After: 0 pt

Formatted: English (United Kingdom)

Formatted: Space After: 0 pt

Formatted: Space After: 0 pt

Formatted: Space After: 0 pt

Formatted: English (United Kingdom)

Formatted: Space After: 0 pt

Formatted: English (United Kingdom)

Formatted: Space After: 0 pt

Formatted: Space After: 0 pt

Formatted: English (United Kingdom)

Formatted: Space After: 0 pt

Formatted: English (United Kingdom)

Formatted: Space After: 0 pt

Formatted: Space After: 0 pt

Formatted: English (United Kingdom)

Formatted: Space After: 0 pt

Formatted: Space After: 0 pt

Formatted: English (United Kingdom)



Seasonal shift	Timing Rate of change	<u>Absolute change in summer contribution (DJF) between the reference period and the end of the 21st century</u> <del>Absolute change in summer contribution between the reference and future periods</del>	<u>1980–2015 vs. 2070–2099</u>	%
Long-term trend	<u>Timing</u> Rate of change <del>Timing</del>	Indicator of the long-term decline after reaching the peak water. The indicator is defined as the slope between the peak water year and 30 years later.	<u>1980–2099</u>	% dec <sup>-1</sup>
Long-term change	Rate of change Magnitude	<u>Relative change between reference magnitude and magnitude at the end of the 21st century</u> <del>Relative change between the reference magnitude and the mean annual value obtained from the future period</del>	<u>1980–2015 vs. 2070–2099</u>	%

### 3.5 Hydrological Uncertainty importance of sources of uncertainty analysis

We build random forest (RF) regression models based on the six sources of uncertainty to predict the glacio-hydrological signatures (~~n=10~~) of each catchment (Table 1). For this analysis, we selected 329 catchments with ~~with~~ at least one glacier (area > 1 km<sup>2</sup>) in both inventories (~~n=329~~). RF regression models generate predictions using an adaptation of Leo Breiman's random forest algorithm, a supervised machine learning method (Breiman, 2001; Svetnik et al., 2003). We used the permutation feature importance (PFI) to assess the influence of each source (Breiman, 2001) ~~(in this case, categorical predictors)~~. This technique ~~The PFI measures the change in model performance (in this case, the Root Mean Square Error; RMSE) after the values of a single model feature have been permuted (also known as shuffled), with more important features resulting in greater decreases in performance when permuted.~~ is defined as the decrease in a model score when a single feature or predictor value is randomly shuffled (Breiman, 2001). By breaking the association between the feature and the target (i.e., glacio-hydrological signatures), this procedure leads to a decrease in the model score, revealing the extent to which the model relies on the feature. This method has been successfully used as a sensitivity analysis tool in several studies (e.g., Bennett et al., 2022; Schmidt et al., 2020) (e.g., Ahn, 2020; Bennett et al., 2022; Schmidt et al., 2020). For each catchment and signature, the training set was selected to be 90% of the full dataset of scenarios, and the remaining 10% was used to measure the permutation importance. The importance of each feature ~~(in this case, categorical predictors)~~ was represented as the percentage of the average change in the ~~Root Mean Square Error~~ (RMSE) over 30 experiments of shuffling one feature. For all RF models, we used 500 regression trees as an ensemble, with each tree having a minimum leaf size of five. For each split, two variables were randomly selected as candidates. The complete procedure was performed using Scikit-learn v1.3.0 (Pedregosa et al., 2011).

Formatted: Space After: 0 pt

Formatted: Space After: 0 pt

Formatted: English (United Kingdom)

Formatted: Space After: 0 pt

Formatted: English (United Kingdom)

Formatted: Space After: 0 pt

Formatted: Space After: 0 pt

Formatted: Space After: 0 pt

Formatted: English (United Kingdom)

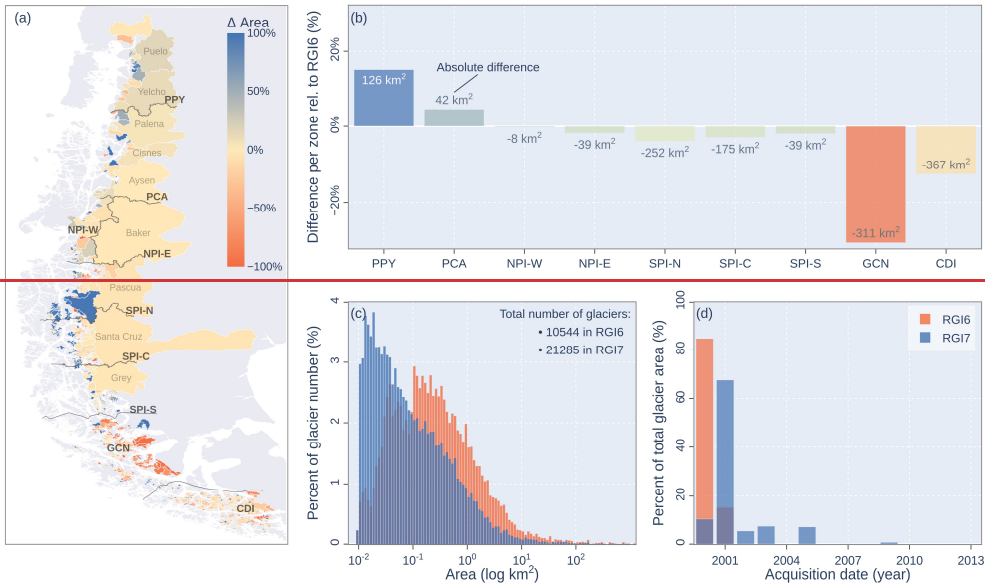
## 380 4 Results

### 4.1 Analysis of sources of uncertainty

#### 4.1.1 Historical conditions (1980–2015)

The historical conditions involved in the calibration process considered the geometry obtained from the glacier inventories (RGI6 and RGI7), the volume obtained from ice thickness datasets (F19 or M22), and the reference climate dataset (PMET, CR2MET, ERA5 and MSWEP). The incorporation of national inventories in RGI7 resulted in important differences compared to RGI6 (Fig. 3). The total number of glaciers increased from 10,544 in RGI6 to 21,285 in RGI7. Relative to this, RGI6 showed a higher number of glaciers with an area greater than 1.0 km<sup>2</sup>, but RGI7 has considerably more smaller glaciers (< 1.0 km<sup>2</sup>). The total glacier area decreased by 4.0% in RGI7 ( $\Delta = 1,024$  km<sup>2</sup>), with important regional differences (Fig. 3a,b). The northern area between the Puelo and Aysen catchments (PPY and PCA) showed ~~positive differences~~increases between ranging from 4% ~~and to~~ 15% relative to RGI6 (Fig. 3b). In contrast, the area located south of the SPI (GCN and CDI) showed ~~the maximum negative differences~~decreases with values as low as -31% (Fig. 3b). These regional differences may be due to several factors, including improved outlines and corrections from local inventories and differences in acquisition dates (Fig. 3d). ~~There were also differences in the date of acquisition of the two inventories, which made a direct comparison difficult (Fig. 3d).~~ While 84.7% of the glacier area in RGI6 ~~have~~has an acquisition date in ~~the year~~ 2000, only 10.5% of the glacier area in RGI7 ~~have~~has an acquisition date in the same year (91.7% between 2000–2003, including both years).

Formatted: Space After: 12 pt



Formatted: Normal (Web), Left

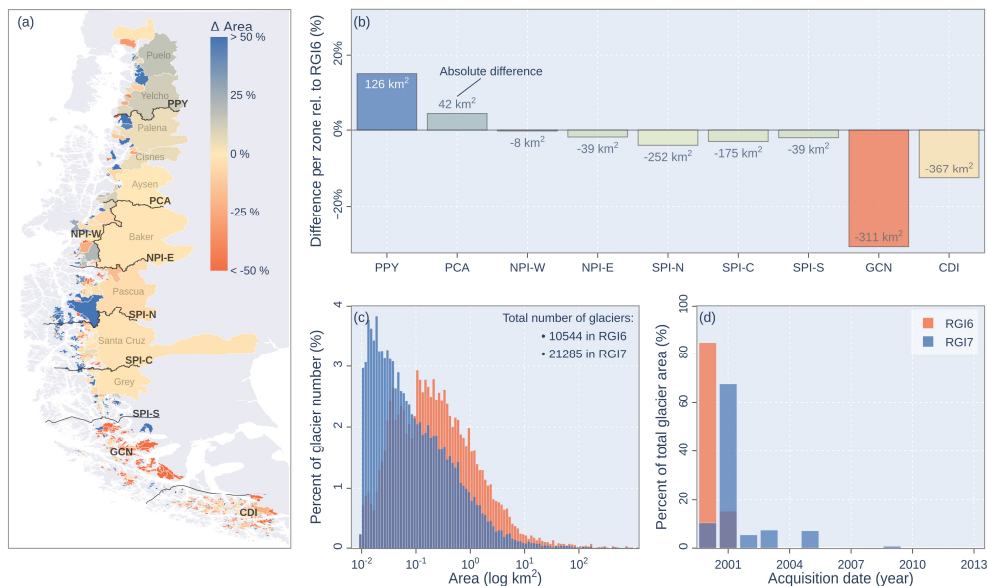
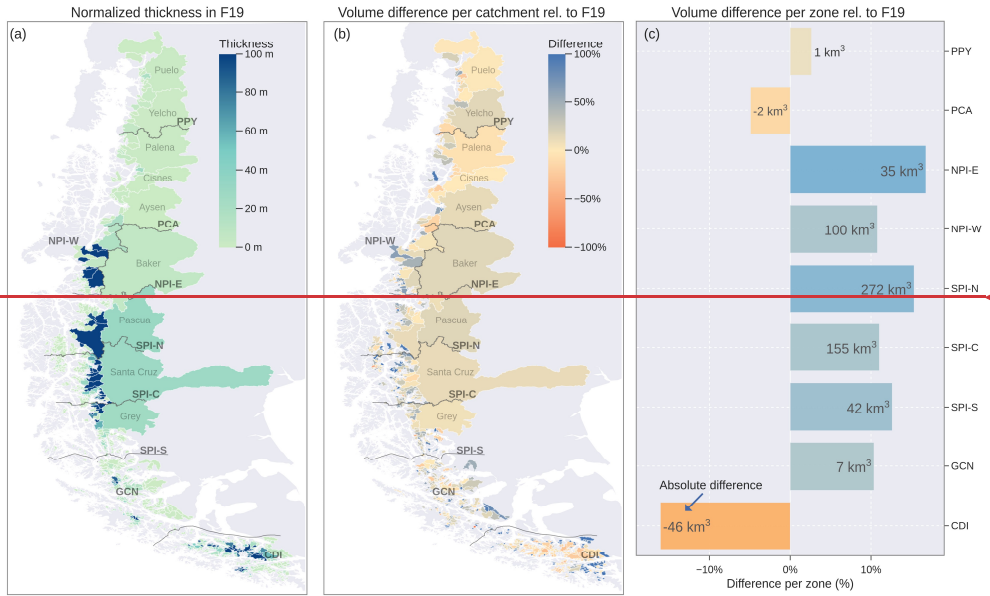
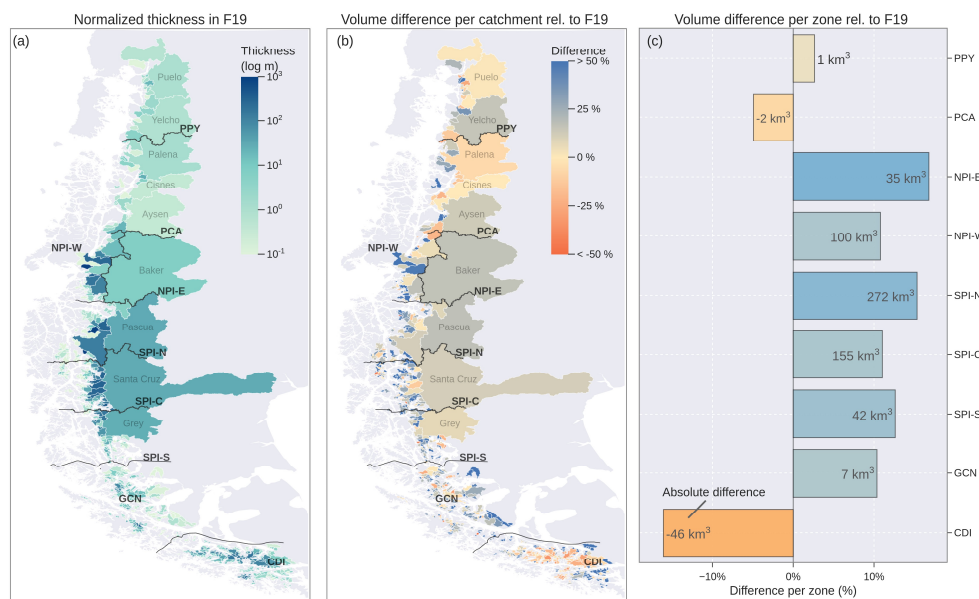


**Figure 3. Comparison between Randolph Glacier Inventory (RGI) versions 6 and 7. Difference in area a) per catchment and b) per hydrological zone considering RGI6 as reference. The area assigned to each catchment and zone was calculated according to the location of the glacier terminus. The names in grey in (a) correspond to the names of the main catchments, while the solid black line corresponds to the division between the hydrological zones defined in Fig. 1. The text in b) indicates the absolute difference in area (RGI7 – RGI6). c) Distribution of glacier area. d) Percent of glacier area per year of acquisition.**

Ice volume was another source of uncertainty analysed in this study (Fig. 4). According to the F19 dataset, the hydrological zones comprising the SPI have an ice volume of 3,526 km³, representing 68.89% of the study area. Conversely, the PPY, PCA, GCN and CDI zones accounted for only 8.98% of the total ice volume. The 26.67% of the total catchment area study domain had a normalized thickness (ice volume divided by catchment area) of less than 1.0 m (Fig. 4a). Based on RGI6, the M22 dataset showed more ice volume than the F19 dataset in 81.782% of the total catchment-glacier area (overall volume difference of 11.1%; Fig. 4b), mainly in the Patagonian Icefield (Fig. 4c). In this area, the NPI and SPI zones showed positive differences/increases of 135 km³ and 469 km³ (relative to F19), respectively. Only the PCA and CDI zones showed the opposite change, where the M22 dataset shows a lower total ice volume (Fig. 4c).



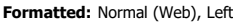
Formatted: Normal (Web)



**Figure 4. Volume comparison between Millan et al. (2022) (M22) and Farinotti et al. (2019) (F19) based on RGI6. a) Thickness normalized by the catchment area from F19 (in log scale). Percentage difference between M22 and F19 per b) catchment and c) hydrological zone considering F19 as reference. The grey names in (a) and (b) correspond to the names of the main catchments, while the solid black line corresponds to the division between the hydrological zones defined in Fig. 1. The text in c) indicates the absolute difference in volume (M22 - F19). The volume assigned to each catchment and zone was calculated according to the location of the glacier terminus.**

The historical climate of the glaciers of the southern Andes showed an important climatic diversity according to the PMET dataset, with an annual mean precipitation varying between 1,000 and 8,000 mm yr<sup>-1</sup> (Fig. 5a; 1980–2015). The spatial pattern of precipitation showed a clear difference between the western (> 4,000 mm yr<sup>-1</sup>) and the eastern (< 2,000 mm yr<sup>-1</sup>) side of the Andes (Fig. 5a). As a result of this orographic effect, mean precipitation was greater than 4,000 mm yr<sup>-1</sup> over 51.5% of the glacier area, and which represents only 22% of the catchment area. 95.0% of the total glacier area (99% of the catchment area) showed an annual mean temperature above 0 °C (Fig. 5b). The four climate products used to model the historical evolution of the glaciers (PMET, CR2MET, ERA5 and MSWEP/MSWX) showed important differences in precipitation and temperature (Fig. 5c-e). In relation to PMET, CR2MET-ERA5 and MSWEP showed contrast total differences in solid precipitation of close to 46.9% nearly 50% and -55.6% (glacier area weighted mean; Fig. 5c), respectively in solid precipitation a difference of nearly

435



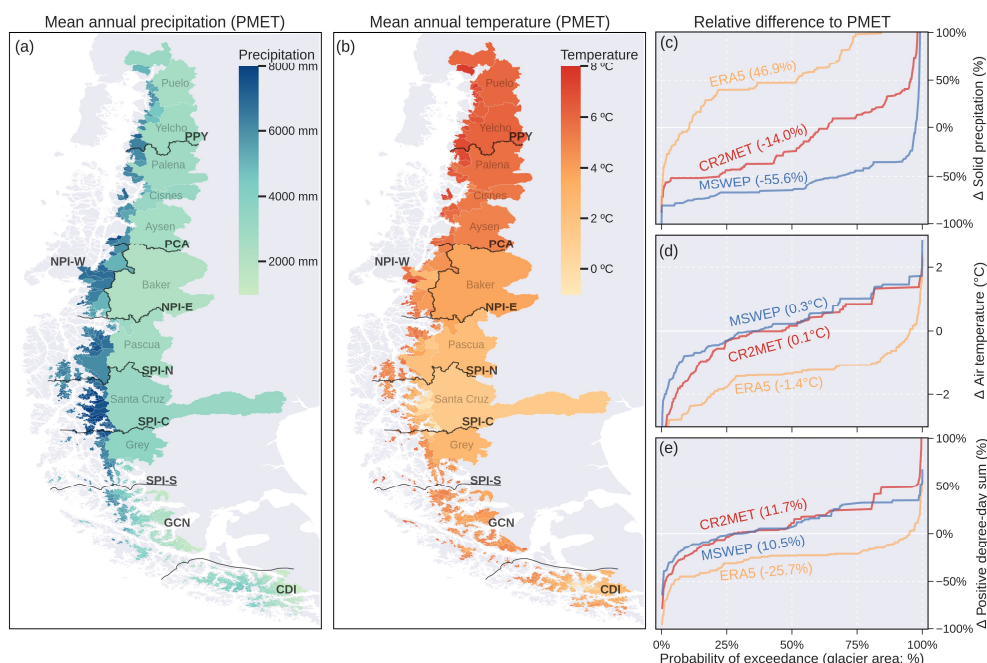


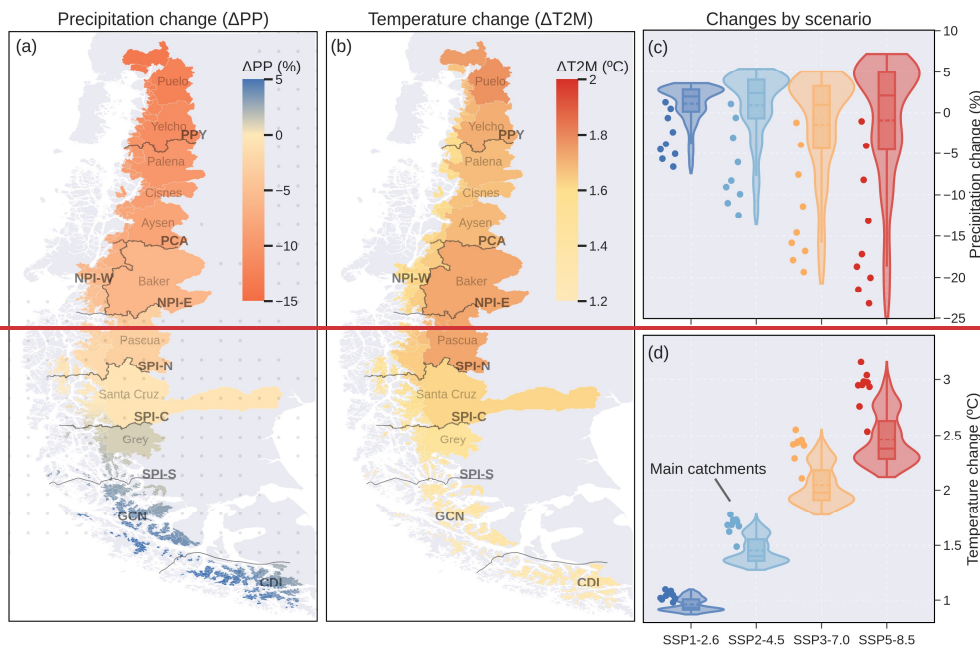
**Figure 5. Historical reference climate in terms of Mean-annual catchment-precipitation (a) and temperature (b) according to the PMET dataset (1980–2015). Long-term averages (1980–2015) Catchment-means** were calculated using only the glacierized grid cells of each catchment. The grey names in (a) and (b) correspond to the names of the main catchments, while the solid black line corresponds to the division between the hydrological zones defined in Fig. 1. **Relative differences in terms of glacier area between** Relative catchment-differences between-PMET and CR2MET, ERA5 and MSWEP/MSWX sorted per by glacier area for solid precipitation (c), temperature (d), and positive degree-day-sum (e). The values in parenthesis indicate the glacier area weighted means. The dots in (c-e) represent the values for the main catchments, which account for 68% of the total area. The dotted line corresponds to the mean value.

#### 4.1.2 Precipitation and temperature climate projections (2020–2099)

The climate projections for the end of the century (2070–2099) showed clear latitudinal patterns (Fig. 6a, b). Overall, the northern area was characterized by a warmer and drier future climate, while the southern area showed a slight increase in precipitation accompanied by a slight increase in temperature. The GCMs showed a high model agreement in all zones (> 80% of the models agree on the sign of the change), except in the SPI and GCN zones (Fig. 6a), areas characterized by a high ice volume (Fig. 4a). The climate projections for the catchments varied according to the SSP scenario.



Under the SSP1-2.6 scenario, the ~~67.55~~4% of the ~~catchment glacier~~ area (~~55% of the total glacier area~~) is projected to experience a decline in precipitation (Fig. 6c). This percentage increases to ~~91.83~~% under the SSP5-8.5 scenario. For temperature, the ~~mean glacier area weighted catchment~~-warming varies from ~~0.996 ± 0.05~~1.0 °C in SSP1-2.6 to ~~2.6746 ± 0.23~~°C in SSP5-8.5 (Fig. 6d). Overall, the main catchments showed a higher warming than the average of all catchments (Fig. 6d).



Formatted: Normal (Web), Left

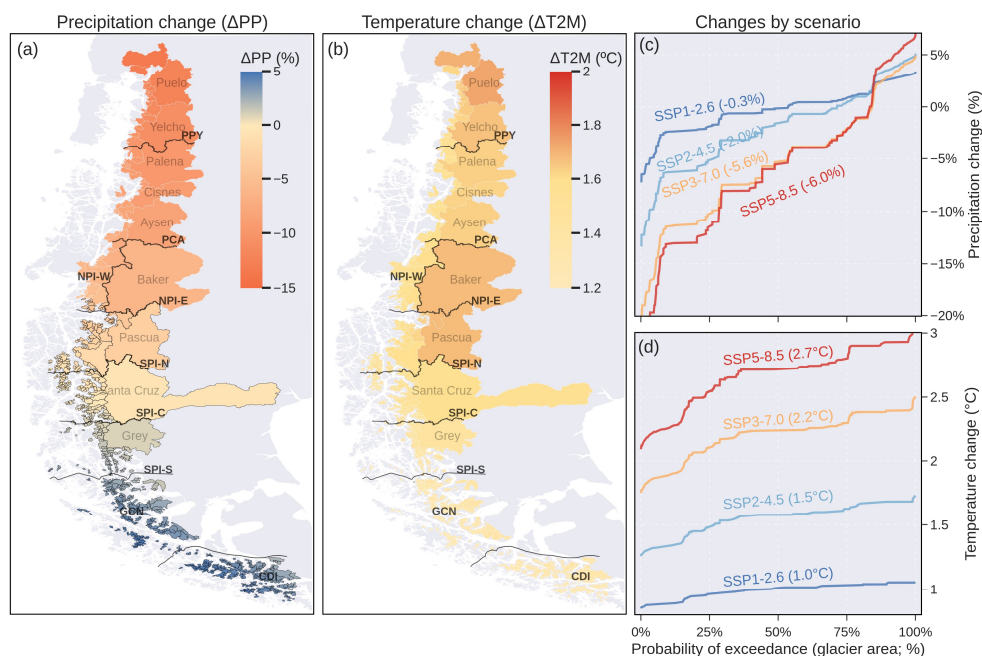
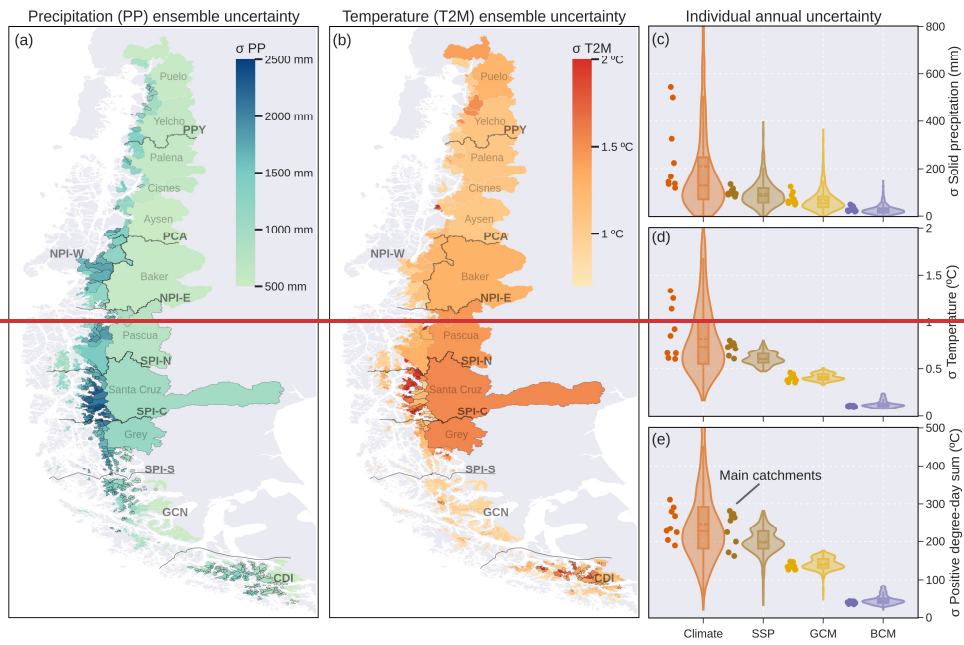


**Figure 6.** Multi-model catchment means ( $n = 10$ ) of future precipitation (a) and temperature change (b) considering the SSP 2-4.5 scenario (1980–2015 vs. 2070–2099). Catchment means were calculated using only the glacierized grid cells of each catchment. The catchments with black outlines indicate low model agreement, where less than 80% of the models agree on the sign of the change. The grey names in (a) and (b) correspond to the names of the main catchments, while the solid black line indicates the division between the hydrological zones defined in Fig. 1. Catchment differences by scenario for precipitation (c) and temperature (d). The values in parenthesis indicate the glacier area weighted means. The dots in (c) and (d) represent the values for the main catchments, which account the 68% of the total area. The dotted line corresponds to the mean value.

#### 4.1.3 Combined uncertainty of future climate

Future climate uncertainty considered four reference climate products, ten General Circulation Models (GCMs), four different Shared Socioeconomic Pathways (SSPs), and three bias correction methods (MVA, QDM, and MBCn), resulting in 480 possible combinations (Fig. 7). The standard deviation of the mean annual precipitation in the long term (2070–2099) was greater than 1,000 mm in 68.140% of the catchment-glacier area, which represents 68% of the glacier area (Fig. 7a). Similarly, the standard deviation of the temperature was greater than 1.0 °C in 88.990% of the catchment-glacier area (Fig. 7b); 88% of glacier area. The precipitation showed a greater variability (expressed as coefficient of variation) in the catchments-glaciers

located on the western side of the Southern Andes (Fig. 7a). On the other hand, the greater variability of temperature was concentrated in the SPI-C and CDI zones (Fig. 7b). For all variables, the reference climate was the most important source of uncertainty (Fig. 7c-e). The difference between SSPs and GCMs was more pronounced for temperature and positive degree-day sum (Fig. 7d,e) than for solid precipitation (Fig. 7c). The different bias correction methods (BCM) converged to similar values with no important differences between them.



Formatted: Normal (Web)

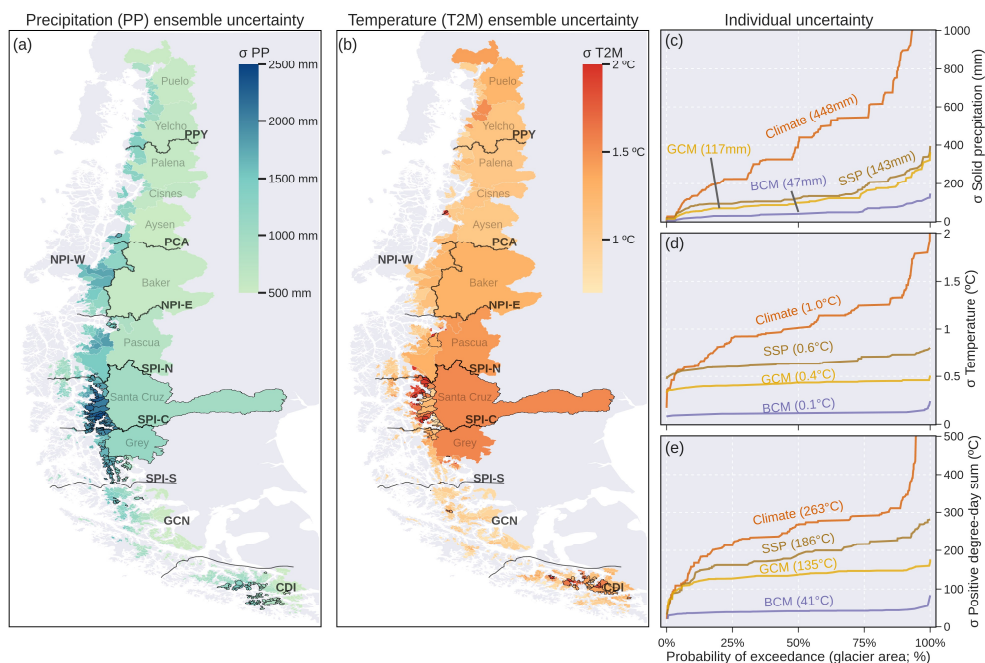
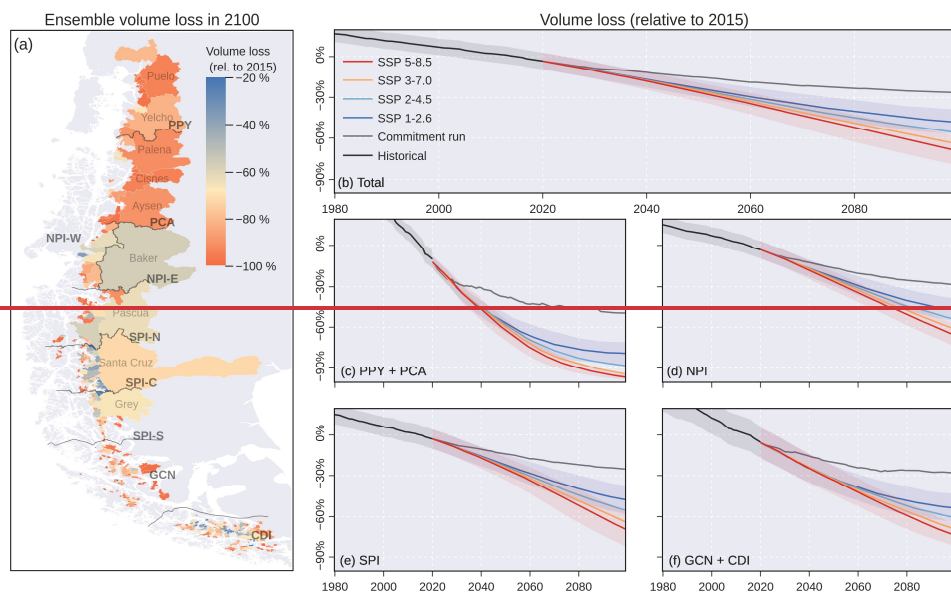


**Figure 7. Combined Future climate uncertainty (standard deviation;  $\sigma$ ) in mean annual precipitation (a) and temperature (b) obtained from the complete ensemble of future climate (2070–2099). Standard deviation ( $\sigma$ ) of mean annual precipitation (a) and temperature (b) obtained from the complete ensemble ( $n = 480$ ). The catchments with a coefficient of variation greater than 4035% have black outlines. Catchment Means were calculated using only the glacierized grid cells of each catchment. The grey names in (a) and (b) correspond to the names of the main catchments, while the solid black line indicates the division between the hydrological zones defined in Fig. 1. Individual uncertainty (in terms of glacier area) in standard deviation of solid precipitation (c), temperature (d) and positive degree-day sum (e) across different reference climates, emission scenarios (SSPs), general circulation models (GCMs) and bias correction methods (BCM). In all cases, the standard deviation was calculated from the annual mean of the 2070–2099 period. The values in parenthesis indicate the glacier area weighted means. The dots in (c), (d) and (e) represent the main catchments. The dotted line corresponds to the mean value.**

## 4.2 Glacio-hydrological projections

Glacier projections from OGGM indicate a prolongation of the glacier generalized mass volume loss of recent decades will continue (Fig. 8). Considering the mean derived from the full set of SSP scenarios ( $n = 1920$ ), 64318%  $\pm$  21% (mean  $\pm$  one standard deviation) of the total catchment glacier area w(18% of glacier area) will lose more than 850% of their current (year 2015/2020) volume by the end of the century (Fig. 8a). The results suggest that ice loss will vary according

500 to different sources of uncertainty. Considering ~~only historical sources~~ the prolongation of historical climate conditions ( $n =$   
~~46~~),  $246\% \pm 69\%$  of the total glacier ice is committed to melt in the long term (year 2099 in Fig. 8b). Aggregating the time  
series by emission scenario ( $n = 480$  per SSP), the volume loss varied from  $468 \pm 9\%$  in SSP1-2.6 to  $697 \pm 110\%$  in SSP5-8.5,  
with clear ~~regional-spatial~~ differences (Fig. 8c-f). In the northern region (PPY and PCA), the projected loss is exacerbated by  
the low ice volume (Fig. 4) and precipitation projections (Fig. 5), resulting in percentage losses exceeding 70% under all  
505 scenarios ~~regardless of the scenario~~ (Fig. 8c). Under the high emissions scenario (SSP 5-8.5)-In the northern region (PPY and  
~~PCA)~~, the percentage loss in NPI, SPI and the southern area (GCN and CDI) is projected to be ~~under the high emissions~~  
~~scenario (SSP 5-8.5)~~  $645\% \pm 8\%$ ,  $68\% \pm 12\%$  and  $712\% \pm 7\%$ , respectively (Fig. 8d-f). At the hydrological zone scale (Fig.  
S1), the confidence intervals for volume and area in the reference period are consistent with the differences found between the  
glacier inventories (Fig. 3) and ice thickness datasets (Fig. 4). Similar to the ice volume projections, the mean specific mass  
510 balance diverges strongly depending on the emission scenarios (Fig. S1).



Formatted: Normal (Web)



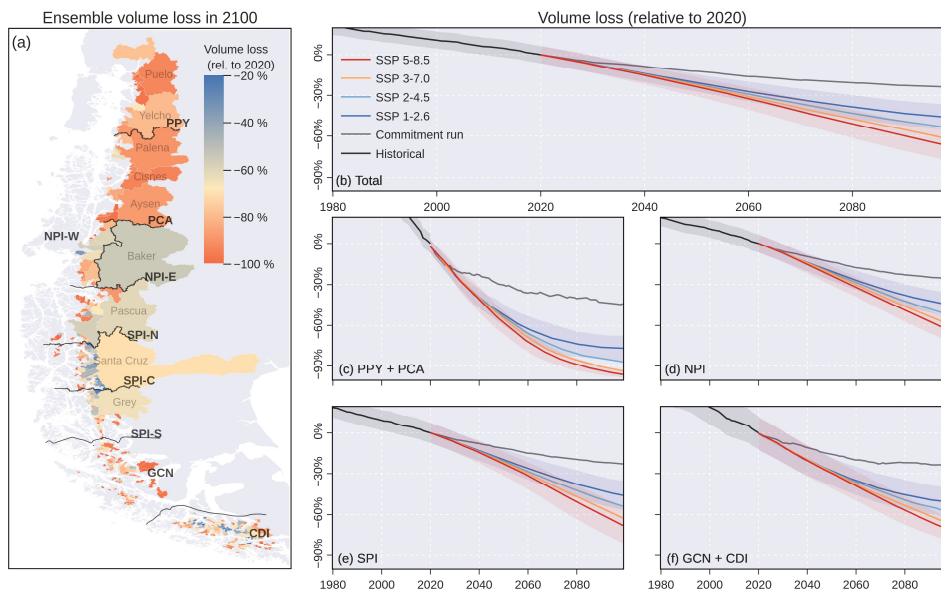
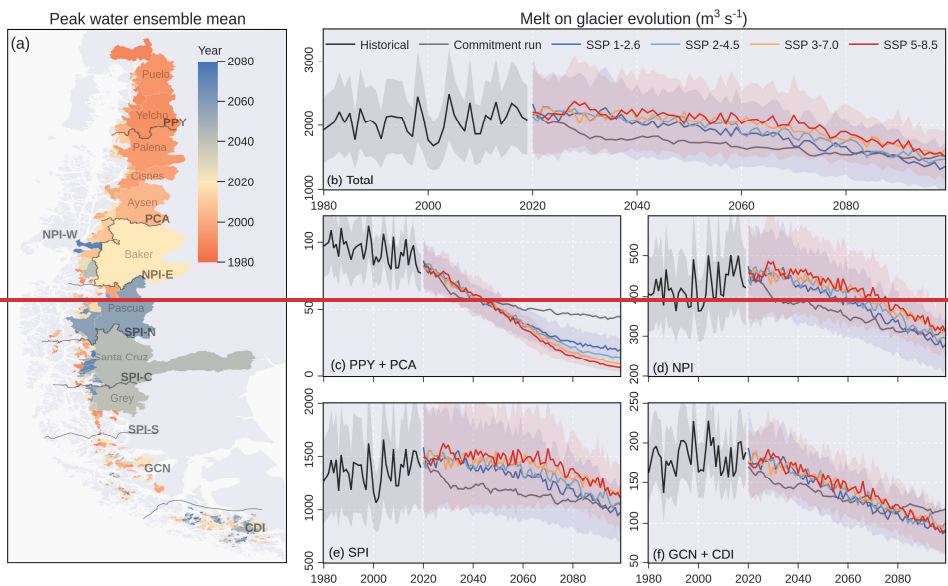


**Figure 8.** Glacier volume loss relative to 2015-2020. a) Mean volume loss in 2100 derived from the full ensemble ( $n = 1920$ ). Volume loss for the sum of all catchments (b), the northern area including PPY and PCA (c), the Northern Patagonian Icefield (d), the Southern Patagonian Icefield (e) and the southern area including GCN and CDI (f). The solid line represents the mean for each scenario, while the uncertainty bands are represent  $\pm$  calculated using one standard deviation (shown only for historical, SSP 1-2.6 and SSP 5-8.5 for visualization purposes). Volume, area and specific mass balance by hydrological zone are shown in Fig. S1. The commitment run considers a pseudo-random climate based on the period 1985–2015.

The mass-volume loss drives changes in the hydrological contribution of glaciers in the Patagonian Andes (Fig. 9). Considering the mean derived from the full set of SSP scenarios ( $n = 1920$ ),  $61.34\% \pm 13\%$  of the catchment-glacier area, which contains the 30% of the glacier area, has already peaked in terms of glacier melt (year 2020; Fig. 9a). The total glacier melt for the study domain on-glacier in the reference period (1980–2015) was  $2,0515 \pm 537499 \text{ m}^3 \text{ s}^{-1}$  (Fig. 9b). For this total, the northern area (PPY and PCA), NPI, SPI and the southern area (GCN and CDI) contributed with 4.67%, 20.5%, 66.0% and 8.8% (Fig. 9c-f), respectively. The evolution-projected trajectories of the glacier melt on-glacier varied slightly among emissions scenarios ( $n = 480$  per SSP), and the projections and their uncertainties tended to converge towards the end of the century (Fig. 9b). For example, the mean glacier melt on-glacier in 2070–2099 varies from  $1,555 \pm 424372 \text{ m}^3 \text{ s}^{-1}$  in SSP 1-2.6 to  $1,784 \pm 369465 \text{ m}^3 \text{ s}^{-1}$  in SSP 5-8.5 for the whole region. While most hydrological zones are projected to experience a steady decrease in glacier melt-on-glacier, the SPI zone shows slightly diverging trajectories in its mid-century meltwater contribution depending on the emission scenario (Fig. 9c-f). Relative to total glacier runoff (Fig. S2), the uncertainty (i.e., standard deviation) in the

glacier melt on glacier evolution was lower due to a lower influence of the reference climate (Fig. 5), the main contributor of climate uncertainty (Fig. 7). To the south of SPI, the slight increase in precipitation projections (Fig. 6) buffers the decrease in glacier melt on glacier, maintaining the contribution of total glacier runoff. In all hydrological zones, the ratio between glacier melt runoff and melt on glacier and the total glacier runoff is close to 60% in the reference period, percentage that decreases to 40% towards the end of the century (Fig. S2).



Formatted: Normal (Web)

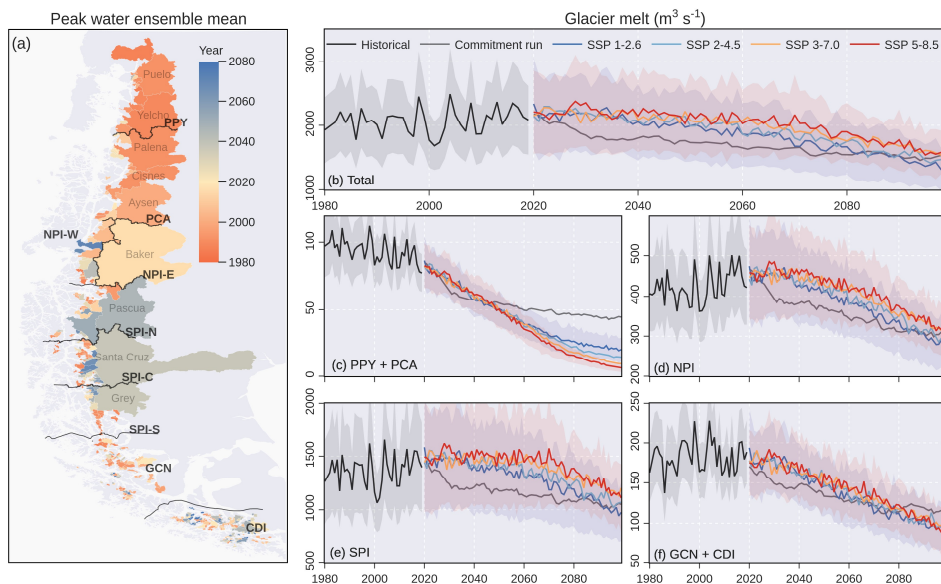


Figure 9. **Glacier melt on glacier** projections for the Patagonian Andes. a) Peak water year obtained from the complete ensemble ( $n = 1920$ ). **Glacier Melt melt on glacier** evolution for the sum of all catchments (b), the northern area including PPY and PCA (c), the Northern Patagonian Icefield (d), the Southern Patagonian Icefield (e) and the southern area including GCN and CDI (f). The solid line represents the mean for each scenario, while the uncertainty bands **represent  $\pm$  are calculated using one standard deviation** (shown only for historical, SSP 1-2.6 and SSP 5-8.5 for visualization purposes). **Total glacier runoff and, melt on glacier**, and the ratio between the two, disaggregated by hydrological zone, are shown in Fig. S2. The commitment run considers a pseudo-random climate based on the period 1985–2015. For visualization purposes, the commitment run was smoothed using a 10-year moving average.

#### 4.3 Influence on glacio-hydrological signature

The glacio-hydrological signature was represented by ten metrics that characterize the hydrological regime of each catchment (Table 21). Regardless of the variable (**glacier runoff melt or melt on glacier or total glacier runoff**), the permutation feature importance (**PFI**) of RF models showed that the differences between the historical reference climates contributed most to the total uncertainty (Fig. 10). This was especially clear for the reference magnitude, peak water magnitude, inter-annual variability and **reference** seasonal contribution **and variability**; metrics, where the reference climate accumulated more than **60XX50%** of the total RMSE loss after the permutations. **Considering glacier melt only**, **the** accumulated RMSE loss of the historical sources of uncertainty (**geometryglacier inventory, glacier** volume, and **reference** climate) was greater than that of the future

Formatted: Caption

Formatted: Not Highlight

555 sources (GCM, SSP, and BCM) in ~~six~~ **eight** signatures (**only five for glacier runoff**), including the peak water metrics. In the long-term (trend and change signatures), the historical sources accumulated a RMSE loss similar to that of the future sources. In these cases, the selection of ~~the~~ reference climate or ~~the~~ GCM was as important as the emission scenario (SSP). Overall ~~Despite the larger relative differences in glacier volume than in glacier inventories (Fig. 3 and 4),~~ **The selection of the glacier inventory was more important than the ice thickness dataset than the ice thickness dataset for most metrics (Fig. 10),** while ~~The~~ importance of the bias correction method (BCM) was significant (median > 10%) only for the **reference** seasonal variability and shift (Fig. 10). Consistently, the ~~RMSE loss~~ **relative importance** of future sources was 0% for all metrics calculated from the reference period (Table 21).

No clear spatial patterns were detected in the main source of uncertainty (i.e., the variable that accumulated most RMSE loss in each catchment; Fig. S3 and S4). Considering the ~~complete set of glacier melt~~ signatures ~~calculated from the glacier melt (Fig. S3) on glacier~~, the future sources of uncertainty were the main source in only ~~24XX~~ **17** %  $\pm$  ~~232~~ **1XX** % (mean  $\pm$  one standard deviation) of the total glacier area. In contrast, the reference climate was the main source of uncertainty in ~~74XX~~ **69** %  $\pm$  ~~23XX~~ **22** % of the glacier area. ~~The lower importance of the reference climate was limited to a few metrics and hydrological zones. For example, the GCMs and SSPs were the main source of uncertainty in the Patagonian Icefields for the long term trend, and in the northern area (PPY and PCA) for the long term change. In comparison to the glacier total runoff metries~~ **signatures**, the importance of the reference climate decreases to ~~57XX~~ **58** %  $\pm$  ~~XX~~ **31** % of the glacier area (Fig. S4 ~~not shown~~).

Formatted: Not Highlight

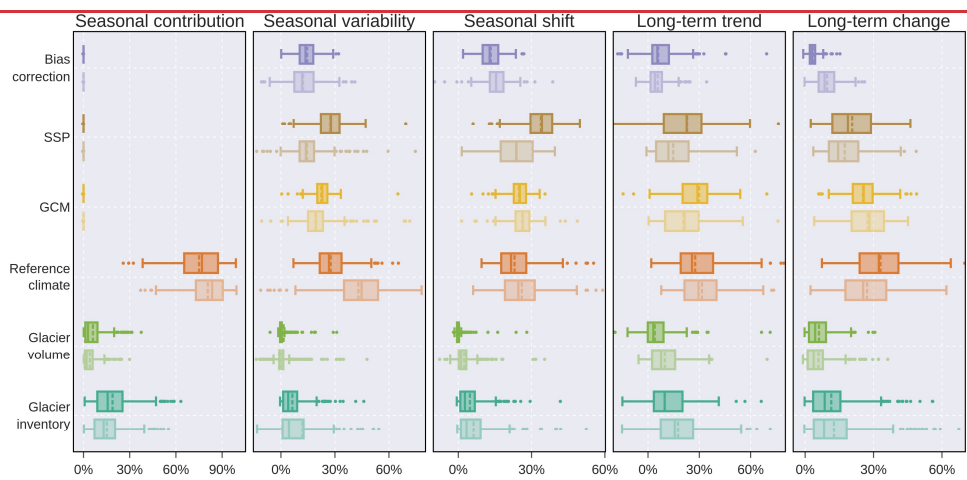
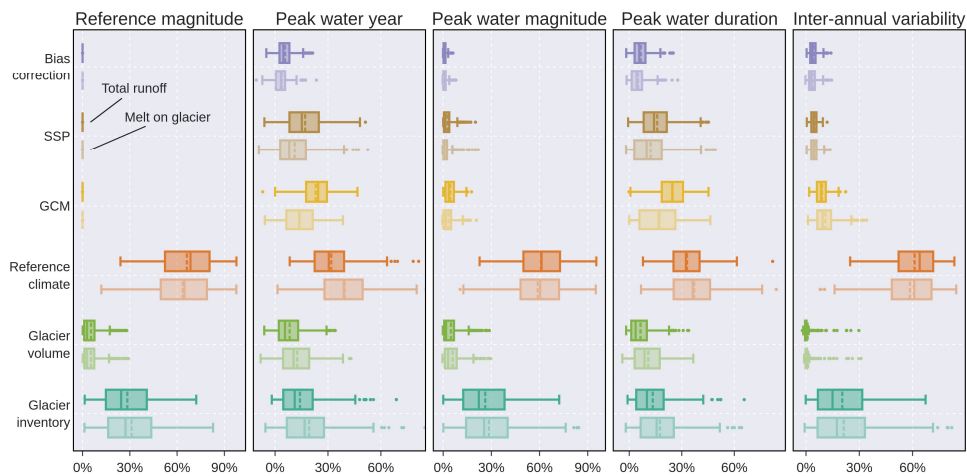
Formatted: Not Highlight

Formatted: Not Highlight

Formatted: Not Highlight

Formatted: Not Highlight

Formatted: Not Highlight



Feature importance (% of RMSE loss after permutations)

Formatted: Space Before: 0 pt, After: 0 pt

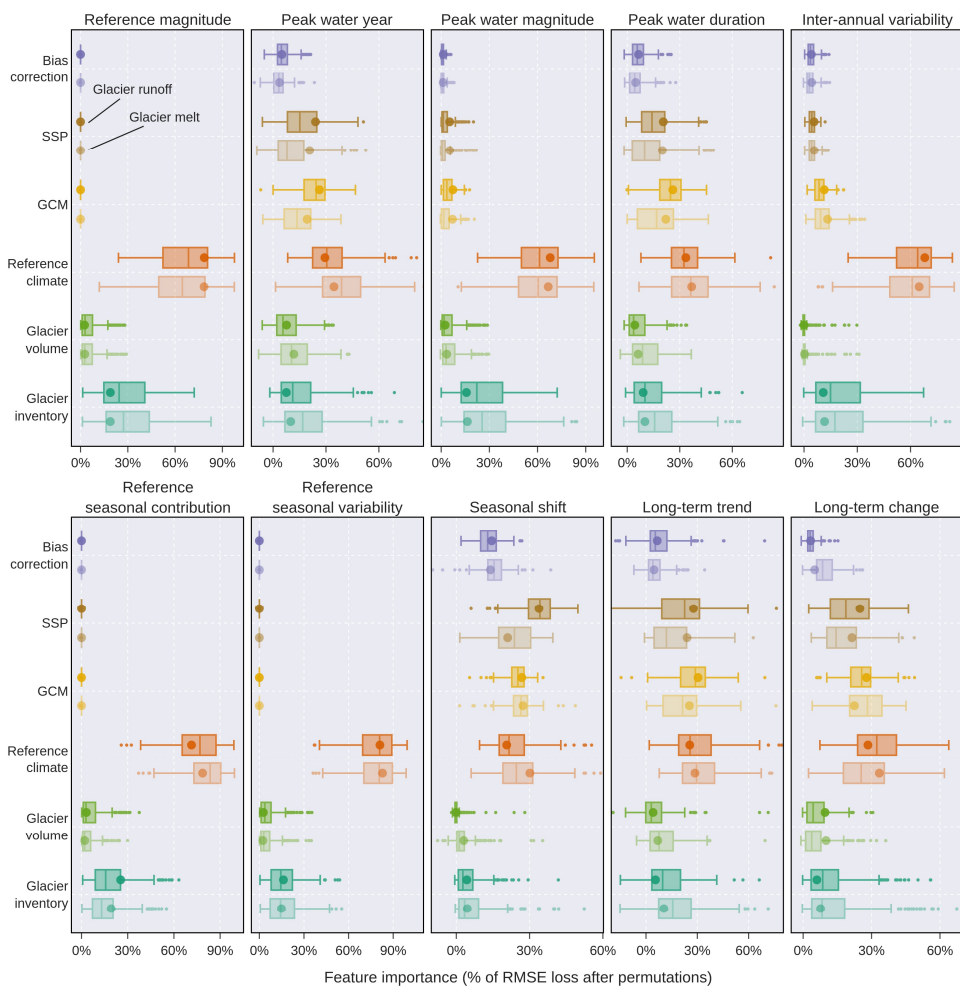


**Figure 10.** Importance of each source of uncertainty for the glacio-hydrological signatures obtained from the ~~total~~-glacier runoff (dark colours) and the melt on glacier (light colours). The importance of each source on the glacio-hydrological signatures (Table 2)

is represented as the percentage of the average change in the Root Mean Square Error (RMSE), with high values indicating a greater ~~relative importance for the signature~~. The ~~dotted circles line inside each boxplot correspond~~ s to the glacier area weighted mean ~~mean value~~. Note that each panel has a different range.



580 **5 Discussion**

**5.1 Changing and uncertain glacier hydrology**Hydrological response of Patagonian glaciers to climate change

The primary objective of glacio-hydrological modelling studies has been to assess the future impacts of climate change (Van Tiel et al., 2020), and therefore GCMs and SSP choices have commonly been part of the uncertainty analysis of previous modelling efforts. For the first time, this study incorporated sixfour additional different sources of data-uncertainty (both historical and future) to generate 1,920 possible future evolution scenarios in the Patagonian Andes.

As expected, The volume loss showed a strong dependence on the emission scenarios with total projected losses ranging from The persistent mass loss is expected to continue to drive changes in future glacier hydrology in the Patagonian Andes (Fig. 8 and 9). Considering the mean derived from the full set of SSP scenarios (n = 1920), 18% of the glacier area will lose more than 80% of its current ice volume (year 2015) this century (Fig. 8a). Aggregating the time-series by emission scenario (n = 480 per SSP), the 21<sup>st</sup>-century volume loss varied from  $48 \pm 9\%$  in SSP1-2.6 to  $69 \pm 10\%$  in SSP5-8.5 for the complete study domain (Fig. 8b). Compared to future mass loss, glacier melt showed a greater overall uncertainty, and the projections aggregated by SSP scenario tended to converge towards the end of the century (Fig. 9 and S2). Despite the dependence of the specific mass balance (units:  $\text{kg m}^{-2} \text{yr}^{-1}$ ) on the emission scenarios (Fig. S1), the glacierthe ice melt component of runoff (units:  $\text{m}^3 \text{s}^{-1}$ ) on the glacier doesdid not show a clear dependence on the emission scenario (Fig. 9), as it also depends on theis not normalized by glacier area, which decreases during the century (Fig. S1). This is shown, for example, by the regional glacier melt, which only varies from  $1,555 \pm 124 \text{ m}^3 \text{s}^{-1}$  in SSP1-2.6 to  $1,784 \pm 165 \text{ m}^3 \text{s}^{-1}$  in SSP5-8.5 in the long term (2070–2099; Fig. 9b). Only a few hydrological zones showed clear differences in their mid-century meltwater contribution between SSP scenarios, such as NPI-W and SPI-N. This is partly explained by the fact that  $61\% \pm 14\%$  of the catchment area, which contains  $30\% \pm 13\%$  of the glacier area, has already peaked in terms of glacier melt (year 2020; Fig. 9a). Compared to glacier total runoff (Fig. S2), the uncertainty (i.e., standard deviation) in the glacier melt component (i.e., standard deviation) was reducedis lower than that of total glacier runoff (Fig. S2), because the latter also entails the liquid precipitation and off-glacier snowmelt components, which are determined more by the reference climate more so than by model parameters, which is the primarymain source of climate uncertainty (Fig. 7), had less influence. This is because liquid precipitation, which is strongly dependent on the reference climate, is only included in the glacier runoff components, as the strongly past climate dependent liquid precipitation is only included in the total runoff components.

The slight increase in precipitation projections south of the SPI (Fig. 6) buffers the decrease in glacier melt, maintaining the contribution of glacier runoff throughout the 21<sup>st</sup> century (Fig. S2).

Formatted: Superscript

Formatted: Superscript

Formatted: Superscript

610 Although Glacio-hydrological studies are scarce in the Patagonian Andes, but the Baker River Basin (NPI-E in Fig. 1; 7.2%  
of glacier area) ~~has been~~ provides a point of comparison with previous studies due to its recent trends (Dussaillant et al., 2012)  
and historical glacial lake outburst floods (Vandekerkhove et al., 2020). Our study revealed a slight increase in glacier runoff  
(3% per decade) between 1980 and 2015. This finding is consistent with previous studies by (Dussaillant et al.,  
(2019) ~~Dussaillant et al. (2019)~~, who observed a similar trend from 2001 to 2017 using ASTER stereo images and stream  
gauges, and ~~Caro et al. (2023)~~, (Caro et al., (2024) who reported a 10% increase in glacier melt from 2000 to 2019 using the  
OGGM model (Table S1). In a longer time frame, Huss and Hock (2018) found that the peak water of the Baker River has  
615 already occurred or will occur in the coming years regardless of the emission scenario (2015  $\pm$  18 and 2020  $\pm$  16 for RCP 2.6  
and RCP 8.5, respectively), which is in agreement with our results indicating that the peak water year based on total glacier  
runoff may have been reached peaked (2021  $\pm$  15) considering all scenarios under all scenarios (2021  $\pm$  15). In a longer time  
frame, Huss and Hock (2018) found that the peak water of the Baker River has already occurred or will occur in the coming  
years regardless of the emission scenario (2015  $\pm$  18 and 2020  $\pm$  16 for RCP 2.6 and RCP 8.5, respectively), which is in  
620 agreement with our results indicating that the peak water year based on total glacier runoff may have been reached peaked  
(2021  $\pm$  15) considering all scenarios under all scenarios (2021  $\pm$  15).

**5.1.2 Uncertainty in the modelling chain** Hydrological importance of data uncertainty  
The variability of the All 10 glacio-hydrological metrics across the catchments is show a considerable uncertainty to modelling  
choices notably influenced by scenarios derived from the six sources of uncertainty (Fig. 10). Among these  
625 uncertainties Previous studies have shown that, accurate estimates of glacier inventory outlines areas (Li et al., 2022) and  
initial ice volumes (Gabbi et al., 2012)  
  
~~play have played~~ a pivotal role in ensuring reliable projections of volume and runoff.

accurate glacier inventory and ice volume estimates play pivotal roles in ensuring reliable projections of volume and runoff  
630 In this our study, despite the larger relative differences in glacier volume than in glacier inventories area (11.1% vs. 4.0%  
of overall difference; Fig. 3 and 4), the selection of glacier inventory was more important for most glacio-hydrological metrics  
(Fig. 10). The importance of these glacier attributes was ~~masked only superseded~~ by the choice of the climate in the historical  
period (Fig. 10). The Our uncertainty analysis showed that the reference climate was the most important source in 69%  $\pm$  22%  
of the glacier area for glacier melt (Fig. S3) and 58%  $\pm$  31% of the glacier area for glacier runoff (Fig. S4).  
635 The importance of the reference climate is that it establishes baseline conditions against which future changes can be assessed.  
In addition, its influence on temperature and precipitation directly shapes the seasonal response of glaciers, affecting both

Formatted: English (United States)

Field Code Changed

Field Code Changed

melting and accumulation processes. Finally, the reference climate will also influence the parameter calibration (see below) and therefore the model sensitivity to climate change. Mechanisms that underscore the importance of the reference climate as a major source of uncertainty are likely to include its role in defining the baseline conditions against which future changes are assessed. In addition, the influence of the reference climate on temperature and precipitation patterns directly affects seasonal glacier response (melt / accumulation), contributing to its importance in determining seasonal metrics.

Despite the large variability in climate, geography and glacier characteristics in the Patagonian Andes, ~~the only a few regions showed a low importance of sensitivity to the reference climate was limited to a few zones.~~ This is partly explained by the fact that some climate products showed overall relative differences of almost 50% in solid precipitation (Fig. 5), which dominates glacier runoff and melt evolution. For the long-term trend of glacier melt (Fig. S3), the GCMs and SSPs were the main source of uncertainty in the Patagonian Icefields (SPI, NPI and CDI), areas characterised by mostly neutral precipitation projections (Fig. 6) and the presence of high ice volumes (Fig. 4). The greater importance of the GCMs and SSPs was also observed in the northern area (PPY and PCA) for the long-term change in glacier melt. When considering glacier runoff (Fig. S4), which ~~considers includes~~ liquid precipitation as glaciers retreat, the importance of the SSP scenario increases in several metrics, such as seasonal shift and long-term change.

For the first time, this study incorporated six different sources of uncertainty (both historical and future) into the glacio-hydrological modelling chain, resulting in a total of 1920 future evolution scenarios. The historical scenarios (n = 16) considered the glacier inventory, the ice thickness dataset and the reference climate, while the future scenarios (n = 120) included different GCMs, SSPs, and bias correction methods (BCM). The exploratory analysis of both glacier inventories was consistent with Zalazar et al. (2020). While the northern area (PPY and PCA) showed an increase in glacier area in RGI7 relative to RGI6, the opposite was found in the southern zones (GCN and CDI) (Fig. 3). The decrease in glacier area in major ice masses may be due in part to differences in the acquisition dates (Fig. 3d), as only 10% of the glacier area in RGI7 has an acquisition date in the year 2000. The relative differences in glacier area were smaller than the reported differences in glacier volume (Fig. 3 and 4). ~~In terms of glacier area, XX% showed a relative difference of less than ± 10% between the two glacier inventories, while only XX% showed differences below this threshold when considering both ice volume estimates. While the 69XX% of the total catchment area glacier area showed a relative difference of less than ± 10% between the glacier inventories, only XX27% of the glacier area catchment area showed differences below this threshold when considering both ice volume~~

**Formatted:** Font: (Default) Times New Roman, 10 pt, Not Italic, English (United States)

**Formatted:** Normal

(i.e., ice thickness) estimates. The use of observational data can help to select a better dataset for the study area, potentially reducing the overall uncertainty. However, direct or indirect observations of ice thickness, such as those based on ground-penetrating radar or airborne surveys, are spatially and temporally scarce in the Patagonian Andes (e.g., Millan et al., 2019; Gacitúa et al., 2021). In addition, large-scale datasets of ice thickness require a large number of datasets which are derived from different acquisition dates (sometimes years or even decades), hindering an adequate regional validation (Hock et al., 2023).

The reference climate corresponds to one source of uncertainty that can be assessed using ground-based data. However, the current scarcity, poor quality control protocols, and lack of continuity and reliability of meteorological stations is a very important limitation to properly understand the atmospheric processes at high elevations that have driven glacio-hydrological changes in the Patagonian Andes (Masiokas et al., 2020; Condom et al., 2020). Recent studies have attempted to narrow the ranges of uncertainty using, for example, regional estimates of moisture flux. For example, Sauter (2020) reported that the icefield-wide precipitation averages (period 2010–2016) are likely to be within the range of 5,380 and 6,090 mm yr<sup>-1</sup> in the NPI and 5,060 and 5,990 mm yr<sup>-1</sup> in the SPI. Based on the catchment hydrological balance, Aguayo et al. (in review) derived gridded precipitation factors ( $P_f = 1.2 \pm 0.6$ ) to correct for the pronounced undercatch of mountainous areas. Using these factors, the PMET v1.0 showed long-term mean values of 6,050 mm yr<sup>-1</sup> and 5,900 mm yr<sup>-1</sup> for the NPI and SPI, respectively (Fig. 5a). Similar values of precipitation factors have been used to avoid underestimating mass accumulation (e.g., Temme et al., 2023) used  $P_f = 1.2$  in CDI).

The primary objective of glacio-hydrological modelling studies has been to assess the future impacts of climate change (Van Tiel et al., 2020), and therefore GCM and SSP have commonly been part of the uncertainty analysis. In the Patagonian Andes, the climate projections (Fig. 6) showed clear spatial patterns that follow the observed trends of the last decades (Aguayo et al., 2021; Pabón-Cañedo et al., 2020; Boisier et al., 2018; Weidemann et al., 2018). Compared to the global scale, the region is projected to experience a lower degree of warming in the long term ( $-3$  °C in SSP5-8.5), compared to the global continental warming of  $5.9 \pm 0.8$  °C under a high emissions scenario (1981–2010 vs. 2081–2100; Iturbide et al., 2021). The selected GCMs showed a high agreement in most hydrological zones, except in the SPI where less than 80% of the GCMs agreed on the sign of the change (Fig. 6). The GCM uncertainty was indirectly constrained by their selection. The ten selected GCMs showed a transient climate response (TCR) in the likely range of 1.4–2.2 °C (Table S1), which is a good approximation of the assessed warming (Hausfather et al., 2022). Future studies could potentially narrow the uncertainty based on the skill of GCMs to reproduce historical trends (Collazo et al., 2022), and key drivers of change in the Southern Hemisphere atmospheric circulation, such as ozone depletion (Revell et al., 2022; Ivanciu et al., 2021).

There are several sources of uncertainty that were not considered in this study, such as downscaling strategies (e.g., temperature lapse rates), the geodetic mass balance, the use of frontal ablation parameterization schemes, the surface mass balance model

(e.g., degree-day vs. energy balance), and the ice-flow model itself. These are acknowledged shortcomings of our study and should be further investigated in future studies. For example, Schuster et al. (2023) using the OGGM model showed that the use of spatially and seasonally variable lapse rates has the most systematic influence on glacier projections with smaller glacier volumes by the end of the century compared to the constant option. Similarly, Bravo et al. (2019a) reported spatial patterns in lapse rates for the SPI that can change the ablation rates by up to 60%, depending on the extrapolation method applied. The geodetic mass balance used in the dynamic calibration process was another source of uncertainty. In comparison to Hugonnet et al. (2021) who obtained a specific mass balance of  $-720 \pm 70 \text{ kg m}^{-2} \text{ yr}^{-1}$  for the complete RGI region (2000–2019), Braun et al. (2019) and Dussaillant et al. (2019) recently estimated values of  $-640 \pm 20 \text{ kg m}^{-2} \text{ yr}^{-1}$  (2000–2015) and  $-720 \pm 220 \text{ kg m}^{-2} \text{ yr}^{-1}$  (2000–2018), respectively. The complex dynamics of marine terminating and lake terminating glaciers is also a source of uncertainty in projections of regional glacier loss. In the Patagonian icefields, Minowa et al. (2021) estimated that frontal ablation was  $-24.1 \pm 1.7 \text{ Gt a}^{-1}$  (2000–2019), representing  $34 \pm 6\%$  of total ablation. The study of calving glaciers adds a layer of complexity, as additional processes require potential parameterizations and adjustments, which are also subject to uncertainty (Van Tiel et al., 2020). Using the OGGM model, Malles et al. (2023) found that the global mean sea level rise contribution at the end of this century is reduced by  $\sim 9\%$  when marine frontal processes were considered in Northern Hemisphere glaciers. Surface mass balance models can also play an important role in glacier evolution, but the lack of calibration and validation data hinders the assessment of the added value of more model complexity (e.g., Temme et al., 2023; Schuster et al., 2023; Huss and Hock, 2015). The ten metrics characterizing the hydrological regime of each catchment showed an important variability as a result of the 1920 scenarios generated from the six sources of uncertainty. The uncertainty analysis showed that the reference climate was the most important source in  $\text{XX}\% \pm \text{XX}\%$  of the glacier area (Fig. S3) and accumulated more than 60% of the total RMSE loss in the metrics relative to reference magnitude, peak water magnitude, inter-annual variability, and seasonal contribution (Fig. 10). Similar approaches have assessed the influence of the reference climate, but their focus has been limited to the mass loss evolution. For 18 glaciers in High Mountain Asia, Watanabe et al. (2019) showed that the differences between observed past climate datasets ( $n = 6$ ) introduced uncertainties of about 15% into projected changes in glacier mass. In Scandinavia and Iceland, Compagno et al. (2021) showed that the choice of the reference climate leads to differences of only 7% in the remaining ice volume by 2100. The small sensitivity was attributed to the model calibration scheme they used, which effectively reduces differences between climate forcing products by adapting precipitation and temperature corrections until they match glaciological observations. Our study, in turn, chooses not to correct the historical climate dataset, and therefore the historical climate uncertainty is incorporated into the model calibration and then into the projections.

In addition to other historical sources of uncertainty, the individual effects of different inventories and volumes on glacier mass projections have also been assessed. Using two different glacier inventories for China, Li et al. (2022) showed volume differences of  $30.4 \pm 2.5 \text{ km}^3$  by the end of the 21<sup>st</sup> century, differences that are higher than between adjacent emission

scenarios, highlighting the importance of regional inventories. Using a set of ice thickness measurements, Gabbi et al. (2012) analysed the sensitivity of glacier runoff projections to under- or overestimation of the total ice volume. The analysis revealed that reliable estimates of ice volume are essential, and that incorrect estimates could even lead to deviations in the sign of the projected runoff trend. In our study, the larger relative differences in area played a more important role than volume for most glacio-hydrological metrics (Fig. 10). However, the relative importance was masked by the choice of the climate in the historical period.

In the long term, the relative importance of the emission scenario was not as important as in previous studies that did not consider the reference climate in the uncertainty analysis (Fig. 10). In the Southern Andes, the Glacier Model Intercomparison Project Phase 2 (GlacierMIP2) showed that the uncertainty in the emission scenario is the largest source for the specific mass balance rate (Marzeion et al., 2020). Similarly, Mackay et al. (2019) found that the emission scenarios were also the dominant source for projections of mean monthly streamflow during the melt season, contributing up to 65% of the total projection uncertainty in glacio-hydrological modelling in Iceland. In our study, the accumulated RMSE loss of the historical sources (geometry, volume, and climate) was greater than that of the future sources (GCM, SSP, and BCM) in more than half of the signatures. Furthermore, the future sources of uncertainty were the main source in only  $18\% \pm 21\%$  of the total catchment area. The relatively greater influence of the future sources was limited to the long-term metrics (trend and change), where the selection of the emissions scenario or the GCM was as important as the reference climate (Fig. 10). This underscores that future glacio-hydrological projections are strongly shaped by modellers' choices, which should be guided by a systematic review of local datasets to adequately justify decisions in the modelling choices.

*Spatial differences: Importance of domain characteristics*

### 5.3 Influence of model calibration Parameters ()

The calibration of large-scale glacier model parameters is usually is glacier-specific and varies according to the glacier model and the available data (for an extensive overview, refer to Zekollari et al. 2022). For example, in the Global Glacier Evolution Model (GloGEM; (Huss and Hock, 2015)) In GloGEM, the calibration follows a sequential approach where glaciological observations are matched by adjusting the precipitation factor, factor is initially adjusted between 0.8-2.0 to match glaciological observations (i.e., the 20-year geodetic mass balance average) then a melt factor and finally a temperature bias parameter within predefined ranges. As a result This type of procedure will strongly adjusts the forcing climate data to match the expected values from the combination of a mass balance model and observations, which likely explaining explains why Compagno et al. (2021) found that the choice of the reference climate leads to differences of only 7% in the remaining ice volume by 2100 in Scandinavia and Iceland. However, of this reduction in differences between climate forcings, several

Formatted: Heading 2

studies using the sequential calibration approach have shown a low sensitivity to different climate forcings. In High Mountain Asia and using another methodology however, Watanabe et al. (2019) showed that the differences between the reference climate introduced uncertainties of about 15% into projected changes in glacier volume. In Scandinavia and Iceland, Compagno et al. (2021) showed that the choice of the reference climate leads to differences of only 7% in the remaining ice volume by 2100.

Considering the scaling effect of the precipitation factor on glacier runoff (Schuster et al., 2023), our study, in turn, chooses not to correct the historical climate dataset (i.e., maintaining  $P_0 = 1$ ), and therefore the historical climate uncertainty is incorporated into the model calibration and then into the projections. This approach recognises the inherent variability in precipitation estimates and aims to capture the range of potential 'true' precipitation values. In particular, certain regional climate datasets used in our analysis, such as PMET and CR2MET, are already subject to bias correction procedures to address potential underestimation of precipitation in high mountain areas. Thus, by incorporating historical climate uncertainty, our methodology aims to provide a robust framework for glacier runoff projections. Alternatively, future studies could use ensemble meteorological datasets (e.g., Tang et al. 2022) to incorporate uncertainty into their assessments.

In recent years, the calibration workflow of large-scale glacier models has evolved to incorporate model parameter uncertainty as a significant source of uncertainty. For example, Bayesian inference is used to calibrate the three parameters of the Python Glacier Evolution Model (PyGEM) uses Bayesian inference to calibrate the three parameters of for each glacier based on Markov Chain Monte Carlo (MCMC) methods (Rounce et al., 2020, 2023). Interestingly, despite the adoption of this alternative approach, our volume loss projections exhibit similarities to recent findings by Rounce et al. (2023).

The mass loss projections are similar to the recent projections from Rounce et al. (2023) (Fig. S45). When comparing the mean projected volume loss results disaggregated by hydrological zone and SSP scenario with (Rounce et al., 2023) projections, the difference RMSE between the two with our the two study studies calculated using the RMSE of the projected mass loss was only 4.4% (RMSE; Fig. S5) between the two studies. This suggests a remarkable consistency in projected glacier evolution despite potential differences in the sources of uncertainty considered between the studies.

Despite differences in the sources of uncertainty considered in the two studies, the uncertainty (i.e., standard deviation) associated with mass loss was similar, suggesting that GCMs and SSPs are the main source of variability in future mass loss.

## 5.2 Changing glacier hydrology

Glacier hydrology in the Patagonian Andes is expected to continue changing as a result of the sustained mass loss (Fig. 8 and 9). Considering the mean derived from the full set of SSP scenarios ( $n = 1920$ ), 43% of the catchment area, which contains 48% of the glacier area, will lose more than 80% of its current volume (year 2015) this century (Fig. 8a). Aggregating the time

Formatted: Subscript

Formatted: English (United States)

series by emission scenario ( $n = 480$  per SSP), the 21<sup>st</sup> century volume loss varied from  $48 \pm 9\%$  in SSP1-2.6 to  $69 \pm 10\%$  in SSP5-8.5 for the complete study domain (Fig. 8b). These mass loss projections are similar to the recent projections from Rounce et al. (2023) (Fig. S4). When comparing the mean results disaggregated by hydrological zone and SSP scenario, the RMSE of the projected mass loss was only 4.4% between the two studies. Despite differences in the sources of uncertainty considered in the two studies, the uncertainty (i.e., standard deviation) associated with mass loss was similar, suggesting that GCMs and SSPs are the main source of variability in future mass loss.

Compared to future mass loss, glacier melt showed a greater overall uncertainty, and the projections aggregated by SSP scenario tended to converge towards the end of the century (Fig. 9 and S2). Despite the dependence of the specific mass balance on the emission scenarios (Fig. S1), the melt on the glacier does not show a clear dependence, as it also depends on the glacier area, which decreases during the century (Fig. S1). This is shown, for example, by the regional melt on glacier, which only varies from  $1,555 \pm 124 \text{ m}^3 \text{ s}^{-1}$  in SSP1-2.6 to  $1,784 \pm 165 \text{ m}^3 \text{ s}^{-1}$  in SSP5-8.5 in the long term (2070–2099; Fig. 9b). Only a few hydrological zones showed clear differences in their mid-century meltwater contribution between SSP scenarios, such as NPI-W and SPI-N. This is partly explained by the fact that  $61\% \pm 14\%$  of the catchment area, which contains  $30\% \pm 13\%$  of the glacier area, has already peaked in terms of glacier melt (year 2020; Fig. 9a). Compared to total runoff (Fig. S2), the uncertainty (i.e., standard deviation) in melt on glacier was reduced because the reference climate, which is the primary source of climate uncertainty (Fig. 7), had less influence, as the strongly past climate-dependent liquid precipitation is only included in the total runoff components. The slight increase in precipitation projections south of the SPI (Fig. 6) buffers the decrease in melt on glacier, maintaining the contribution of glacier runoff throughout the 21<sup>st</sup> century (Fig. S2).

Glacio-hydrological studies are scarce in the Patagonian Andes, but the Baker River Basin (NPI-E in Fig. 1; 7.2% of glacier area) has been a point of comparison due to its recent trends (Dussailant et al., 2012) and historical GLOFs (Vandekerkhove et al., 2020). Using ASTER stereo images and stream gauges, Dussailant et al. (2019) found a slight increase in the decadal glacier contribution to streamflow from 2% to 3% over the period 2001–2017. In a similar period (2000–2019), Caro et al., (2023) modelled a volume change of  $-10.7\%$ , and a decadal increase in the mean annual glacier melt of  $10\%$  (66% of glacierized area modelled). In a longer time frame, Huss and Hoek (2018) found that regardless of the emissions scenario, the peak water of the Baker River has already occurred or will occur in the coming years ( $2015 \pm 18$  and  $2020 \pm 16$  for RCP 2.6 and RCP 8.5, respectively). In our study, we found that the peak water year based on total glacier runoff may have been reached under all scenarios ( $2021 \pm 15$ ), which coincides with a slight increase in glacier runoff of 3% per decade over the reference period 1980–2015.



5.3.4 Drivers of glacio-hydrological signature variability Limitations and potential implications

There are several sources of uncertainty that were not considered in this study, such as downscaling strategies (e.g., temperature lapse rates), the geodetic mass balance observation uncertainty, the use of frontal ablation parameterisation schemes, the surface mass balance model (e.g., degree-day vs. energy balance), and the ice-flow model itself. These are acknowledged shortcomings of our study and should be further investigated in future studies. For example, Schuster et al. (2023) using the OGGM model showed that the use of spatially and seasonally variable lapse rates has the most systematic influence on glacier projections with smaller glacier volumes by the end of the century compared to the constant option. The geodetic mass balance used in the dynamic calibration process was another source of uncertainty. In comparison to While Hugonnet et al. (2021) who obtained a specific mass balance of  $-720 \pm 70 \text{ kg m}^{-2} \text{ yr}^{-1}$  for the complete RGI region (2000–2019), Braun et al. (2019) and Dussaillant et al. (2019) estimated values of  $-640 \pm 20 \text{ kg m}^{-2} \text{ yr}^{-1}$  (2000–2015) and  $-720 \pm 220 \text{ kg m}^{-2} \text{ yr}^{-1}$  (2000–2018), respectively. The complex dynamics of marine terminating and lake terminating glaciers is also a source of uncertainty in projections of regional glacier loss. In the Patagonian icefields, Minowa et al. (2021) estimated that frontal ablation was  $-24.1 \pm 1.7 \text{ Gt a}^{-1}$  (2000–2019), representing  $34 \pm 6\%$  of total ablation. The study of calving glaciers adds a layer of complexity, as additional processes require potential parameterisations and adjustments, which are also subject to uncertainty (Van Tiel et al., 2020). Using the OGGM model, Malles et al. (2023) found that the global mean sea level rise contribution at the end of this century is reduced by  $\sim 9\%$  when marine frontal processes were considered in Northern Hemisphere glaciers. Surface mass balance models can also play an important role in glacier evolution, but the lack of data hinders the assessment of the added value of more model complexity (e.g., Temme et al., 2023; Schuster et al., 2023; Huss and Hock, 2015).

The use of ground-based observations can help to reduce the overall uncertainty. For example,

The use of direct or indirect observations of ice thickness, such as those based on ground-penetrating radar or airborne surveys, can help to select a better dataset for the study area, potentially reducing the data uncertainty. However, these observations are spatially and temporally scarce in the Patagonian Andes (e.g., Millan et al., 2019). Furthermore, the generation of large-scale ice thickness datasets requires the compilation of numerous datasets derived from different acquisition dates, often spanning years or even decades, which hinders regional validation (Hock et al., 2023). The reference climate can also be assessed using ground-based data. However, the current scarcity, poor quality control protocols, and lack of continuity and reliability of meteorological stations is a very important limitation to properly understand the atmospheric processes at high elevations (Condom et al., 2020; Masiokas et al., 2020). Recent studies have attempted to narrow the ranges of uncertainty using, for example, regional estimates of moisture flux (Sauter, 2020) and catchment hydrological balance (Aguayo et al., 2024). Future sources of uncertainty could potentially be reduced using a GCM screening approach. Using Chile as a case study, (Gateño et al., 2024) recently proposed an approach that goes beyond bias-related metrics to include metrics related to the ability of GCMs to reproduce teleconnection responses that can affect regional climate variability and trends. For example, Sauter

Field Code Changed

Formatted: French (France)

Formatted: French (France)

Formatted: French (France)

Field Code Changed

Formatted: Dutch (Belgium)

Field Code Changed

Formatted: Dutch (Belgium)

Formatted: Dutch (Belgium)

Field Code Changed

Field Code Changed

(2020) reported that the icefield-wide precipitation averages (period 2010–2016) are likely to be within in the range of 5,380 and 6,090 mm yr<sup>-1</sup> in the NPI and 5,060 and 5,990 mm yr<sup>-1</sup> in the SPI. Based on the catchment hydrological balance, Aguayo et al. (2024) derived gridded precipitation factors ( $P_i = 1.2 \pm 0.6$ ) to correct for the pronounced undercatch of mountainous areas. Using these factors, the PMET v1.1 showed long-term mean values of 6,050 mm yr<sup>-1</sup> and 5,900 mm yr<sup>-1</sup> for the NPI and SPI, respectively (Fig. 5a). Similar values of precipitation factors have been used to avoid underestimating mass accumulation (e.g., Temme et al. (2023) used  $P_i = 1.2$  in CDI). Future studies could potentially narrow the uncertainty based on the skill of GCMs to reproduce

capability of to replicate the main

features of monthly precipitation and temperature, as well as observed ENSO/SAM teleconnections (Gateño et al., in press; Salazar et al., 2024). Out of the 10 selected GCMs in our study, four are included in the screening recommendation of (Gateño et al., (2024) (more details in Table S2).

r climatological averages, interannual variability, seasonal cycles, monthly probabilistic distribution, spatial patterns of climatological means, and the capability of the GCMs to reproduce teleconnection responses to El Niño Southern Oscillation and the Southern Annular Mode

The implications of our study extend far beyond the Patagonian Andes and resonate with global concerns about the effects of climate change on the hydrological cycle in high mountain regions. These regions very often face challenges in constraining climate estimates due to a low density of meteorological stations (e.g., Beck et al., 2020). These limitations have led to substantial modelling uncertainties in the hydrological cycle (Tang et al., 2023), which can be projected into the future in climate change impact studies (Tarek et al., 2021). Our study is the first to integrate-assess the influence of the reference climate into uncertainty analyses of on evolution of glacier runoff evolution, resulting in differences from previous studies (Fig. 10). In the Southern Andes, the Glacier Model Intercomparison Project Phase 2 (GlacierMIP2) showed that the uncertainty in the emission scenario is the largest source for the specific mass balance rate (Marzeion et al., 2020). Similarly, Mackay et al. (2019) found that the emission scenarios were also the dominant source for projections of streamflow during the melt season in Iceland, contributing up to 65% of the total projected uncertainty. In our study, the relatively greater influence of the future sources was limited to the long-term metrics, where the selection of the emission scenario or the GCM was as important as the reference climate (Fig. 10). This underscores that future glacio-hydrological projections are strongly shaped by modellers' choices, which should be guided by a systematic review of local datasets to adequately justify modelling choices. In addition,

further research into the mechanisms driving the observed differences in precipitation and temperature, and their implications for glacier runoff dynamics, could provide valuable insights into the broader hydrological response of glaciated regions to changing climate conditions.

There are several sources of uncertainty that were not considered in this study, such as downscaling strategies (e.g., temperature lapse rates), the geodetic mass balance, the use of frontal ablation parameterization schemes, the surface mass balance model (e.g., degree-day vs. energy balance), and the ice flow model itself. These are acknowledged shortcomings of our study and should be further investigated in future studies. For example, Schuster et al. (2023) using the OGGM model showed that the use of spatially and seasonally variable lapse rates has the most systematic influence on glacier projections with smaller glacier volumes by the end of the century compared to the constant option. Similarly, Bravo et al. (2019a) reported spatial patterns in lapse rates for the SPI that can change the ablation rates by up to 60%, depending on the extrapolation method applied. The geodetic mass balance used in the dynamic calibration process was another source of uncertainty. In comparison to Hugonnet et al. (2021) who obtained a specific mass balance of  $-720 \pm 70 \text{ kg m}^{-2} \text{ yr}^{-1}$  for the complete RGI region (2000–2019), Braun et al. (2019) and Dussaillant et al. (2019) estimated values of  $-640 \pm 20 \text{ kg m}^{-2} \text{ yr}^{-1}$  (2000–2015) and  $-720 \pm 220 \text{ kg m}^{-2} \text{ yr}^{-1}$  (2000–2018), respectively. The complex dynamics of marine terminating and lake terminating glaciers is also a source of uncertainty in projections of regional glacier loss. In the Patagonian icefields, Minowa et al. (2021) estimated that frontal ablation was  $-24.1 \pm 1.7 \text{ Gt a}^{-1}$  (2000–2019), representing  $34 \pm 6\%$  of total ablation. The study of calving glaciers adds a layer of complexity, as additional processes require potential parameterizations and adjustments, which are also subject to uncertainty (Van Tiel et al., 2020). Using the OGGM model, Malles et al. (2023) found that the global mean sea level rise contribution at the end of this century is reduced by  $\sim 9\%$  when marine frontal processes were considered in Northern Hemisphere glaciers. Surface mass balance models can also play an important role in glacier evolution, but the lack of calibration and validation data hinders the assessment of the added value of more model complexity (e.g., Temme et al., 2023; Schuster et al., 2023; Huss and Hock, 2015).

Compared to the global scale, the region is projected to experience a lower degree of warming in the long term ( $\sim 3^\circ\text{C}$  in SSP5-8.5), compared to the global continental warming of  $5.9 \pm 0.8^\circ\text{C}$  under a high emissions scenario (1981–2010 vs. 2081–2100; Iturbide et al., 2021).

The ten metrics characterizing the hydrological regime of each catchment showed an important variability as a result of the 1920 scenarios generated from the six sources of uncertainty. The uncertainty analysis showed that the reference climate was the most important source in  $78\% \pm 21\%$  of the total catchment area ( $74\% \pm 23\%$  of the glacier area; Fig. S3), and accumulated more than 60% of the total RMSE loss in the metrics relative to reference magnitude, peak water magnitude, inter-annual

Field Code Changed

Formatted: Normal

variability, and seasonal contribution (Fig. 10). Similar approaches have assessed the influence of the reference climate, but their focus has been limited to the mass loss evolution. For 18 glaciers in High Mountain Asia, Watanabe et al. (2019) showed that the differences between observed past climate datasets ( $n = 6$ ) introduced uncertainties of about 15% into projected changes in glacier mass. In Scandinavia and Iceland, Compagno et al. (2021) showed that the choice of the reference climate leads to differences of only 7% in the remaining ice volume by 2100. The small sensitivity was attributed to the model calibration scheme they used, which effectively reduces differences between climate forcing products by adapting precipitation and temperature corrections until they match glaciological observations. Our study, in turn, chooses not to correct the historical climate dataset, and therefore the historical climate uncertainty is incorporated into the model calibration and then into the projections.

In addition to other historical sources of uncertainty, the individual effects of different inventories and volumes on glacier mass projections have also been assessed. Using two different glacier inventories for China, Li et al. (2022) showed volume differences of  $30.4 \pm 2.5 \text{ km}^3$  by the end of the 21<sup>st</sup> century, differences that are higher than between adjacent emission scenarios, highlighting the importance of regional inventories. Using a set of ice thickness measurements, Gabbi et al. (2012) analysed the sensitivity of glacier runoff projections to under- or overestimation of the total ice volume. The analysis revealed that reliable estimates of ice volume are essential, and that incorrect estimates could even lead to deviations in the sign of the projected runoff trend. In our study, the larger relative differences in area played a more important role than volume for most glacio-hydrological metrics (Fig. 10). However, the relative importance was masked by the choice of the climate in the historical period.

In the long term, the relative importance of the emission scenario was not as important as in previous studies that did not consider the reference climate in the modelling chain uncertainty (Fig. 10). In the Southern Andes, the Glacier Model Intercomparison Project Phase 2 (GlacierMIP2) showed that the uncertainty in the emission scenario is the largest source for the specific mass balance rate (Marzeion et al., 2020). Similarly, Mackay et al. (2019) found that the emission scenarios were also the dominant source for projections of mean monthly streamflows during the melt season, contributing up to 65% of the total projection uncertainty. In our study, the accumulated RMSE loss of the historical sources (geometry, volume, and climate) was greater than that of the future sources (GCM, SSP, and BCM) in more than half of the signatures. Furthermore, the future sources of uncertainty were the main source in only  $18\% \pm 21\%$  of the total catchment area. The relatively greater influence of the future sources was limited to the long-term metrics (trend and change), where the selection of the emissions scenario or the GCM was as important as the reference climate (Fig. 10). This underscores that future glacio-hydrological projections are strongly shaped by modellers' choices, which should be guided by a systematic review of local datasets to adequately justify decisions in the modelling chain.

## 6 Conclusions

In this study, we investigated the importance of six sources of data uncertainty ~~in in the modelling chain for~~ ten glacio-hydrological signatures covering the necessary categories to characterize the glacio-hydrological regime of each catchment (magnitude, timing, frequency, duration, and rate of change). For this purpose, we used the Open Global Glacier Model (OGGM) to project the potential change in the hydrological contribution of each glacier (area > 1km<sup>2</sup>; 2,034 glaciers in RGI6) in the Patagonian Andes (40–56° S) under 1920 potential scenarios. Based on these projections, we used the permutation importance of random forest regression models to calculate the relative importance of each source of data uncertainty. Our main findings are as follows:

- The six sources of data uncertainty showed relative differences of varying magnitude. The importance of the selection of glacier inventory and ice thickness source was masked by the reference climate. While the glacier inventory and ice thickness source showed overall differences close to 10%, the different climate alternatives showed differences of more than 50% for solid precipitation, for example. The relative differences between the different alternatives varied across the six sources of uncertainty. The relative differences in area due to different glacier inventories were lower than the reported differences in volume. While 69% of the total catchment area showed relative differences between glacier inventories of less than  $\pm 10\%$ , only 27% of the catchment area showed differences below this threshold when different volume estimates were considered. Among all contributors to future climate uncertainty (2070–2099), the reference climate was also the most important source for all variables, followed by the SSP, the GCM, and finally the bias correction method used.

- The volume loss of glaciers varies significantly with emission scenarios, ranging from  $46 \pm 9\%$  in SSP1-2.6 to  $67 \pm 11\%$  in SSP5-8.5. However, while the specific mass balance is influenced by emission scenarios, glacier melt doesn't show a clear dependence due to changes in glacier area over time. Uncertainty in glacier melt is reduced compared to glacier runoff due to the smaller influence of the reference climate, which mainly influences glacier runoff through past climate-dependent liquid precipitation. The hydrological patterns of glaciers in the Patagonian Andes are anticipated to undergo further changes due to the ongoing mass loss and the projected climate trends. By 2020,  $61\% \pm 14\%$  of the total catchment area ( $30\% \pm 13\%$  of the glacier area) has already peaked in terms of glacier melt. In addition,  $43\% \pm 8\%$  of the catchment area ( $18\% \pm 7\%$  of the glacier area) is projected to lose more than 80% of its glacier volume over the course of the century. Aggregating the time series by emission scenario, the projected volume loss varies from  $48 \pm 9\%$  in SSP1-2.6 to  $69 \pm 10\%$  in SSP5-8.5. Compared to future mass loss, glacier melt and runoff hydrological projections showed a greater overall uncertainty. In addition,, and glacier runoff and melt the projections aggregated by SSP scenario tended to converge towards an overall decrease throughout the 21st century, with particular exceptions (e.g., SPI).

965 --For ~~more than half of the eight~~ glacio-hydrological signatures obtained from the glacier melt evolution, the uncertainty from historical sources exceeded that from future sources, underscoring the critical role of modeler decisions during the calibration process. ~~Considering all glacier melt signatures, the reference climate was the main source of uncertainty in  $69\% \pm 22\%$  of the glacier area. In the Patagonian Andes ( $40-56^\circ\text{S}$ ), the primary source of uncertainty considering all metrics was the reference historical climate in  $78\% \pm 21\%$  of the catchment area ( $74\% \pm 23\%$  of the glacier area).~~ For long-term metrics (trend and change ~~over the period 2070–2099~~), factors not typically considered in regional studies, such as the selection of GCMs and reference climates, were as important as emission scenarios.

Our results shed light on the evolution of glacier runoff in the Patagonian Andes and provide new insights ~~into into the impacts of local calibration data choices~~ uncertainty. To our knowledge, the present study is the first large-scale assessment of the impact of multiple sources of data uncertainty (both historical and future) from a perspective beyond future glacier ~~mass-volume~~ loss. In order to advance with ~~climate change~~-adaptation plans for the long-term sustainability of local ecosystems, future studies should address sources of uncertainty not considered in this study (e.g., parameterization of frontal ablation, climate downscaling and surface mass balance and ice-flow models), and ~~extend the scope from glaciers to downstream hydrology~~ the relative contribution of non-glacial water sources (Drenkhan et al., 2022; He et al., 2021). ~~The Downstream hydrology latter will improve our understanding of the potential relative contribution of glaciers (e.g., Kaser et al., 2010), and the fluxes between the different water stores. The inclusion of surface and subsurface water stores, such as example snowpack, lakes and groundwater, can play a crucial critical role in the seasonal and interannual water release during dry seasons (Drenkhan et al., 2022) (e.g., Pokhrel et al., 2021), and thereby buffering attenuating the effects consequences of glacier shrinkage consequences (e.g., Somers et al., 2019) (Somers et al., 2019; Mackay et al., 2020).~~ Finally, we hope that ~~these new antecedents~~ our rigorous uncertainty quantification helps to prioritize future efforts (e.g., reference climate) to reduce glacio-hydrological modelling gaps in the Patagonian Andes.

#### Appendix A: dynamic calibration minimization algorithm

At the beginning, a first guess of the control variable ( $T_{\text{spinup}}$  or  $\mu^*$ ) is used and evaluated. If the mismatch between model and observation happens to be close enough, the algorithm stops. Otherwise, the second guess depends on the calculated first guess mismatch. For example, if the first resulting area is smaller (larger) than the searched one, the second temperature bias will be colder (warmer). This is because a colder (warmer) temperature leads to a larger (smaller) initial glacier state. The same idea is used for matching the geodetic mass balance. If the second guess is still unsuccessful, the previous value pairs (control variable, mismatch) are used for all subsequent guesses to determine the next guess. This is done by fitting a stepwise linear

function to these pairs and then setting the mismatch to 0 to obtain the next guess (this method is similar to the one described in Appendix A of Zekollari et al. (2019)).

**Code availability**

The complete code repository can be found at: [https://github.com/rodaguayo/glacier\\_uncertainties](https://github.com/rodaguayo/glacier_uncertainties)

**Data availability**

The glacier outlines from RGI6 and RGI7 were downloaded from <https://nsidc.org/data/nsidc-0770/versions/6> (last access: September–May 2816, 20232024) and <https://nsidc.org/data/nsidc-0770/versions/7> (last access: May 16September–28, 20232024), respectively. NASADEM was downloaded from: [https://lpdaac.usgs.gov/products/nasadem\\_hgtv001](https://lpdaac.usgs.gov/products/nasadem_hgtv001) (last access: May 16September–28, 20232024). Ice thicknesses datasets from Millan et al. (2022) and Farinotti et al. (2019) were downloaded from <https://doi.org/10.6096/1007> (last access: September 28, 20232024) and <https://doi.org/10.3929/ethz-b-000315707> (last access: May 16September–28, 20232024), respectively. PMET v1.0 was downloaded from <https://doi.org/10.5281/zenodo.7992761> (last access: May 16September–28, 2023). CR2MET v2.5 was downloaded from <https://doi.org/10.5281/zenodo.7529682> (last access: May 16September–28, 20232024). ERA5 was downloaded from <https://cds.climate.copernicus.eu#!/home> (last access: May 16September–28, 20232024). MSWEP v2.8 was downloaded from <https://www.gloh2o.org/mswep/> (last access: May 16September–28, 20232024). CMIP6 data was downloaded from the Google cloud storage provided by the Pangeo initiative (<https://storage.googleapis.com/cmip6/pangeo-cmip6.json>, last access: May 16September–28, 20232024). The complete set of results provided in this study is available at: <https://doi.org/10.5281/zenodo.11353065>(Aguayo et al., 2024a)(Aguayo et al., 2024a)

**Author contributions**

This study was conceived and designed by RA, FM and LS. RA collected the data and performed the modelling and core data analysis. PS implemented and developed the dynamic calibration algorithm. MS, AC, JL, MA, JM, and LU contributed to the analysis and discussion of the results and drafting of the manuscript. All authors revised the manuscript, provided feedback, and contributed to the preparation of the figures and tables. All authors approved the final version of the manuscript.

Acknowledgements

RA would like to acknowledge the support of the Open Global Glacier Model (OGGM) community for their valuable assistance, collaboration, and commitment to open science. JM publishes with the permission of the executive director, British Geological Survey (UKRI).

Financial support

RA was supported by the National Agency for Research and Development (ANID) PFCHA/DOCTORADO NACIONAL/2019 – 21190544 and by the European Research Council (ERC) under the European Union's Horizon Framework research and innovation programme (grant agreement N°101115565; ICE<sup>3</sup> project). LS's contribution was funded by her DOC Fellowship of the Austrian Academy of Sciences at the Department of Atmospheric and Cryospheric Sciences, University of Innsbruck (No. 25928). LS's, PS's and FM's contributions were funded from the European Union's Horizon 2020 research and innovation programme under grant agreement No. 101003687. This text reflects only the author's view, and that the Agency is not responsible for any use that may be made of the information it contains. JM's contribution was funded by the Natural Environment Research Council (NERC) MCNC Grant TerraFirma NE/W004895/1.

References

Aguayo, R., León-Muñoz, J., Aguayo, M., Baez-Villanueva, O. M., Zambrano-Bigiarini, M., Fernández, A., and Jacques-Coper, M.: PatagoniaMet: A multi-source hydrometeorological dataset for Western Patagonia, *Sci Data*, 11, 6, <https://doi.org/10.1038/s41597-023-02828-2>, 2024.

Ayala, Á., Farías-Barahona, D., Huss, M., Pellicciotti, F., McPhee, J., and Farinotti, D.: Glacier runoff variations since 1955 in the Maipo River basin, in the semiarid Andes of central Chile, *The Cryosphere*, 14, 2005–2027, <https://doi.org/10.5194/tc-14-2005-2020>, 2020.

Barcaza, G., Nussbaumer, S. U., Tapia, G., Valdés, J., García, J.-L., Videla, Y., Albornoz, A., and Arias, V.: Glacier inventory and recent glacier variations in the Andes of Chile, South America, *Annals of Glaciology*, 58, 166–180, <https://doi.org/10.1017/aog.2017.28>, 2017.

Beck, H. E., Wood, E. F., Pan, M., Fisher, C. K., Miralles, D. G., van Dijk, A. I. J. M., McVicar, T. R., and Adler, R. F.: MSWEP V2 Global 3-Hourly 0.1° Precipitation: Methodology and Quantitative Assessment, *Bulletin of the American Meteorological Society*, 100, 473–500, <https://doi.org/10.1175/BAMS-D-17-0138.1>, 2019.

Beck, H. E., Wood, E. F., McVicar, T. R., Zambrano-Bigiarini, M., Alvarez-Garretón, C., Baez-Villanueva, O. M., Sheffield, J., and Karger, D. N.: Bias correction of global high-resolution precipitation climatologies using streamflow observations from 9372 catchments, *Journal of Climate*, 33, 1299–1315, <https://doi.org/10.1175/JCLI-D-19-0332.1>, 2020.

Formatted: Bibliography, Widow/Orphan control, Adjust space between Latin and Asian text, Adjust space between Asian text and numbers



- Beck, H. E., Dijk, A. I. J. M. van, Larraondo, P. R., McVicar, T. R., Pan, M., Dutra, E., and Miralles, D. G.: MSWX: Global 3-Hourly 0.1° Bias-Corrected Meteorological Data Including Near-Real-Time Updates and Forecast Ensembles, *Bulletin of the American Meteorological Society*, 103, E710–E732, <https://doi.org/10.1175/BAMS-D-21-0145.1>, 2022.
- 1050 Bennett, K. E., Miller, G., Busey, R., Chen, M., Lathrop, E. R., Dann, J. B., Nutt, M., Crumley, R., Dillard, S. L., Dafflon, B., Kumar, J., Bolton, W. R., Wilson, C. J., Iversen, C. M., and Wulschleger, S. D.: Spatial patterns of snow distribution in the sub-Arctic, *The Cryosphere*, 16, 3269–3293, <https://doi.org/10.5194/tc-16-3269-2022>, 2022.
- Boisier, J. P.: CR2MET: A high-resolution precipitation and temperature dataset for the period 1960-2021 in continental Chile., <https://doi.org/10.5281/zenodo.7529682>, 2023.
- 1055 Braun, M. H., Malz, P., Sommer, C., Fariás-Barahona, D., Sauter, T., Casassa, G., Soruco, A., Skvarca, P., and Seehaus, T. C.: Constraining glacier elevation and mass changes in South America, *Nature Climate Change*, 9, 130–136, <https://doi.org/10.1038/s41558-018-0375-7>, 2019.
- Bravo, C., Quincey, D. J., Ross, A. N., Rivera, A., Brock, B., Miles, E., and Silva, A.: Air Temperature Characteristics, Distribution, and Impact on Modeled Ablation for the South Patagonia Icefield, *Journal of Geophysical Research: Atmospheres*, 124, 907–925, <https://doi.org/10.1029/2018JD028857>, 2019a.
- 1060 Bravo, C., Bozkurt, D., Gonzalez-Reyes, Á., Quincey, D. J., Ross, A. N., Fariás-Barahona, D., and Rojas, M.: Assessing Snow Accumulation Patterns and Changes on the Patagonian Icefields, *Frontiers in Environmental Science*, 7, 1–18, <https://doi.org/10.3389/fenvs.2019.00030>, 2019b.
- Breiman, L.: Random Forests, *Machine Learning*, 45, 5–32, <https://doi.org/10.1023/A:1010933404324>, 2001.
- 1065 Cannon, A. J.: Multivariate quantile mapping bias correction: an N-dimensional probability density function transform for climate model simulations of multiple variables, *Climate Dynamics*, 50, 31–49, <https://doi.org/10.1007/s00382-017-3580-6>, 2018.
- Cannon, A. J., Sobie, S. R., and Murdock, T. Q.: Bias correction of GCM precipitation by quantile mapping: How well do methods preserve changes in quantiles and extremes?, *Journal of Climate*, 28, 6938–6959, <https://doi.org/10.1175/JCLI-D-14-00754.1>, 2015.
- 1070 Caro, A., Condom, T., and Rabatel, A.: Climatic and Morphometric Explanatory Variables of Glacier Changes in the Andes (8–55°S): New Insights From Machine Learning Approaches, *Front. Earth Sci.*, 9, 713011, <https://doi.org/10.3389/feart.2021.713011>, 2021.
- Caro, A., Condom, T., Rabatel, A., Champollion, N., García, N., and Saavedra, F.: Hydrological response of Andean catchments to recent glacier mass loss, *The Cryosphere*, 18, 2487–2507, <https://doi.org/10.5194/tc-18-2487-2024>, 2024.
- 1075 Cauvy-Fraunié, S. and Dangles, O.: A global synthesis of biodiversity responses to glacier retreat, *Nat Ecol Evol*, 3, 1675–1685, <https://doi.org/10.1038/s41559-019-1042-8>, 2019.
- Chen, J., Brissette, F. P., and Leconte, R.: Uncertainty of downscaling method in quantifying the impact of climate change on hydrology, *Journal of Hydrology*, 401, 190–202, <https://doi.org/10.1016/j.jhydrol.2011.02.020>, 2011.
- 1080 Compagno, L., Zekollari, H., Huss, M., and Farinotti, D.: Limited impact of climate forcing products on future glacier evolution in Scandinavia and Iceland, *J. Glaciol.*, 67, 727–743, <https://doi.org/10.1017/jog.2021.24>, 2021.

- Condom, T., Martínez, R., Pabón, J. D., Costa, F., Pineda, L., Nieto, J. J., López, F., and Villacis, M.: Climatological and Hydrological Observations for the South American Andes: In situ Stations, Satellite, and Reanalysis Data Sets, *Frontiers in Earth Science*, 8, 1–20, <https://doi.org/10.3389/feart.2020.00092>, 2020.
- 1085 Davies, B. J. and Glasser, N. F.: Accelerating shrinkage of Patagonian glaciers from the Little Ice Age (~AD 1870) to 2011, *Journal of Glaciology*, 58, 1063–1084, <https://doi.org/10.3189/2012JG12J026>, 2012.
- Drenkhan, F., Buytaert, W., Mackay, J. D., Barrand, N. E., Hannah, D. M., and Huggel, C.: Looking beyond glaciers to understand mountain water security, *Nat Sustain*, 6, 130–138, <https://doi.org/10.1038/s41893-022-00996-4>, 2022.
- Dussailant, I., Berthier, E., Brun, F., Masiokas, M., Hugonnet, R., Favier, V., Rabatel, A., Pitte, P., and Ruiz, L.: Two decades of glacier mass loss along the Andes, *Nature Geoscience*, 1–7, <https://doi.org/10.1038/s41561-019-0432-5>, 2019.
- 1090 Eyring, V., Bony, S., Meehl, G. A., Senior, C. A., Stevens, B., Stouffer, R. J., and Taylor, K. E.: Overview of the Coupled Model Intercomparison Project Phase 6 (CMIP6) experimental design and organization, *Geoscientific Model Development*, 9, 1937–1958, <https://doi.org/10.5194/gmd-9-1937-2016>, 2016.
- Farinotti, D., Huss, M., Fürst, J. J., Landmann, J., Machguth, H., Maussion, F., and Pandit, A.: A consensus estimate for the ice thickness distribution of all glaciers on Earth, *Nat. Geosci.*, 12, 168–173, <https://doi.org/10.1038/s41561-019-0300-3>, 2019.
- 1095 Gabbi, J., Farinotti, D., Bauder, A., and Maurer, H.: Ice volume distribution and implications on runoff projections in a glacierized catchment, *Hydrology and Earth System Sciences*, 16, 4543–4556, <https://doi.org/10.5194/hess-16-4543-2012>, 2012.
- 1100 Garreaud, R. D., Alvarez-Garretón, C., Barichivich, J., Boisier, J. P., Christie, D., Galleguillos, M., LeQuesne, C., McPhee, J., Zambrano-Bigiarini, M., Pablo Boisier, J., Christie, D., Galleguillos, M., LeQuesne, C., McPhee, J., and Zambrano-Bigiarini, M.: The 2010–2015 megadrought in central Chile: impacts on regional hydroclimate and vegetation, *Hydrology and Earth System Sciences*, 21, 6307–6327, <https://doi.org/10.5194/hess-21-6307-2017>, 2017.
- Gateño, F., Mendoza, P. A., Vásquez, N., Lagos-Zúñiga, M., Jiménez, H., Jerez, C., Vargas, X., Rubio-Álvarez, E., and Montserrat, S.: Screening CMIP6 models for Chile based on past performance and code genealogy, *Climatic Change*, 177, 87, <https://doi.org/10.1007/s10584-024-03742-1>, 2024.
- 1105 Hanus, S., Schuster, L., Burek, P., Maussion, F., Wada, Y., and Viviroli, D.: Coupling a large-scale glacier and hydrological model (OGGM v1.5.3 and CWatM V1.08) – Towards an improved representation of mountain water resources in global assessments, <https://doi.org/10.5194/egusphere-2023-2562>, 22 January 2024.
- Hausfather, Z., Marvel, K., Schmidt, G. A., Nielsen-Gammon, J. W., and Zelinka, M.: Climate simulations: recognize the ‘hot model’ problem, *Nature*, 605, 26–29, <https://doi.org/10.1038/d41586-022-01192-2>, 2022.
- 1110 Hersbach, H., Bell, B., Berrisford, P., Hirahara, S., Horányi, A., Muñoz-Sabater, J., Nicolas, J., Peubey, C., Radu, R., Schepers, D., Simmons, A., Soci, C., Abdalla, S., Abellan, X., Balsamo, G., Bechtold, P., Biavati, G., Bidlot, J., Bonavita, M., De Chiara, G., Dahlgren, P., Dee, D., Diamantakis, M., Dragani, R., Flemming, J., Forbes, R., Fuentes, M., Geer, A., Haimberger, L., Healy, S., Hogan, R. J., Hólm, E., Janisková, M., Keeley, S., Laloyaux, P., Lopez, P., Lupu, C., Radnoti, G., de Rosnay, P., Rozum, I., Vamborg, F., Villaume, S., and Thépaut, J.-N.: The ERA5 global reanalysis, *Quarterly Journal of the Royal Meteorological Society*, 146, 1999–2049, <https://doi.org/10.1002/qj.3803>, 2020.
- 1115

Hock, R., Maussion, F., Marzeion, B., and Nowicki, S.: What is the global glacier ice volume outside the ice sheets?, *J. Glaciol.*, 69, 204–210, <https://doi.org/10.1017/jog.2023.1>, 2023.

Hugonnet, R., McNabb, R., Berthier, E., Menounos, B., Nuth, C., Girod, L., Farinotti, D., Huss, M., Dussailant, I., Brun, F., and Kääb, A.: Accelerated global glacier mass loss in the early twenty-first century, *Nature*, 592, 726–731, <https://doi.org/10.1038/s41586-021-03436-z>, 2021.

Huss, M. and Hock, R.: A new model for global glacier change and sea-level rise, *Frontiers in Earth Science*, 3, 1–22, <https://doi.org/10.3389/feart.2015.00054>, 2015.

Huss, M. and Hock, R.: Global-scale hydrological response to future glacier mass loss, *Nature Climate Change*, 8, 135–140, <https://doi.org/10.1038/s41558-017-0049-x>, 2018.

Huss, M., Zemp, M., Joerg, P. C., and Salzmann, N.: High uncertainty in 21st century runoff projections from glacierized basins, *Journal of Hydrology*, 510, 35–48, <https://doi.org/10.1016/j.jhydrol.2013.12.017>, 2014.

Huss, M., Bookhagen, B., Huggel, C., Jacobsen, D., Bradley, R. s., Clague, J. j., Vuille, M., Buytaert, W., Cayan, D. r., Greenwood, G., Mark, B. g., Milner, A. m., Weingartner, R., and Winder, M.: Toward mountains without permanent snow and ice, *Earth's Future*, 5, 418–435, <https://doi.org/10.1002/2016EF000514>, 2017.

Immerzeel, W. W., Lutz, A. F., Andrade, M., Bahl, A., Biemans, H., Bolch, T., Hyde, S., Brumby, S., Davies, B. J., Elmore, A. C., Emmer, A., Feng, M., Fernández, A., Haritashya, U., Kargel, J. S., Koppes, M., Kraaijenbrink, P. D. A., Kulkarni, A. V., Mayewski, P. A., Nepal, S., Pacheco, P., Painter, T. H., Pellicciotti, F., Rajaram, H., Rupper, S., Sinisalo, A., Shrestha, A. B., Viviroli, D., Wada, Y., Xiao, C., Yao, T., and Baillie, J. E. M.: Importance and vulnerability of the world's water towers, *Nature*, 577, 364–369, <https://doi.org/10.1038/s41586-019-1822-y>, 2020.

IPCC: High Mountain Areas, in: The Ocean and Cryosphere in a Changing Climate: Special Report of the Intergovernmental Panel on Climate Change, Cambridge, <https://doi.org/10.1017/9781009157964.004>, 2022.

Iriarte, J. L., Pantoja, S., and Daneri, G.: Oceanographic Processes in Chilean Fjords of Patagonia: From small to large-scale studies, *Progress in Oceanography*, 129, 1–7, <https://doi.org/10.1016/j.pocean.2014.10.004>, 2014.

Iturbide, M., Fernández, J., Gutiérrez, J. M., Bedia, J., Cimadevilla, E., Díez-Sierra, J., Manzanar, R., Casanueva, A., Baño-Medina, J., Milovac, J., Herrera, S., Cofiño, A. S., San Martín, D., García-Díez, M., Hauser, M., Huard, D., and Yelekci, Ö.: Repository supporting the implementation of FAIR principles in the IPCC-WGI Atlas, <https://doi.org/10.5281/ZENODO.3691645>, 2021.

Kaser, G., Großhauser, M., and Marzeion, B.: Contribution potential of glaciers to water availability in different climate regimes, *Proceedings of the National Academy of Sciences*, 107, 20223–20227, <https://doi.org/10.1073/pnas.1008162107>, 2010.

Lange, S.: ISIMIP3b bias adjustment fact sheet, 2021.

Li, F., Maussion, F., Wu, G., Chen, W., Yu, Z., Li, Y., and Liu, G.: Influence of glacier inventories on ice thickness estimates and future glacier change projections in the Tian Shan range, Central Asia, *J. Glaciol.*, 1–15, <https://doi.org/10.1017/jog.2022.60>, 2022.

- 150 [Logan, T., Aoun, A., Bourgault, P., Dupuis, É., Huard, D., Lavoie, J., Rondeau-Genesse, G., Smith, T. J., Alegre, R., Barnes, C., Biner, S., Caron, D., Ehbrecht, C., Fyke, J., Keel, T., Labonté, M.-P., Lierhammer, L., Low, J.-F., Quinn, J., Roy, P., Squire, D., Stephens, A., Tanguy, M., and Whelan, C.: Ouranosinc/xclim: v0.39.0, , <https://doi.org/10.5281/zenodo.7274811>, 2022.](#)
- 155 [Mackay, J. D., Barrand, N. E., Hannah, D. M., Krause, S., Jackson, C. R., Everest, J., Aðalgeirsdóttir, G., and Black, A. R.: Future evolution and uncertainty of river flow regime change in a deglaciating river basin, \*Hydrol. Earth Syst. Sci.\*, 23, 1833–1865, <https://doi.org/10.5194/hess-23-1833-2019>, 2019.](#)
- [Malles, J., Maussion, F., Ultee, L., Kochtitzky, W., Copland, L., and Marzeion, B.: Exploring the impact of a frontal ablation parameterization on projected 21st-century mass change for Northern Hemisphere glaciers, \*Journal of Glaciology\*, 2023.](#)
- [Marzeion, B., Jarosch, A. H., and Hofer, M.: Past and future sea-level change from the surface mass balance of glaciers, \*The Cryosphere\*, 6, 1295–1322, <https://doi.org/10.5194/tc-6-1295-2012>, 2012.](#)
- 160 [Marzeion, B., Hock, R., Anderson, B., Bliss, A., Champollion, N., Fujita, K., Huss, M., Immerzeel, W. W., Kraaijenbrink, P., Malles, J., Maussion, F., Radić, V., Rounce, D. R., Sakai, A., Shannon, S., van de Wal, R., and Zekollari, H.: Partitioning the Uncertainty of Ensemble Projections of Global Glacier Mass Change, \*Earth's Future\*, 8, <https://doi.org/10.1029/2019EF001470>, 2020.](#)
- 165 [Masiokas, M., Rabatel, A., Rivera, A., Ruiz, L., Pitte, P., Ceballos, J. L., Barcaza, G., Soruco, A., and Bown, F.: A review of the current state and recent changes of the Andean cryosphere, \*Frontiers in Earth Science\*, 8, 99, <https://doi.org/10.3389/FEART.2020.00099>, 2020.](#)
- [Masiokas, M. H., Cara, L., Villalba, R., Pitte, P., Luckman, B. H., Toum, E., Christie, D. A., Le Quesne, C., and Mauget, S.: Streamflow variations across the Andes \(18°–55°S\) during the instrumental era, \*Scientific Reports\*, 9, 17879, <https://doi.org/10.1038/s41598-019-53981-x>, 2019.](#)
- 170 [Maussion, F., Butenko, A., Champollion, N., Dusch, M., Eis, J., Fourteau, K., Gregor, P., Jarosch, A. H., Landmann, J., Oesterle, F., Recinos, B., Rothenpieler, T., Vlug, A., Wild, C. T., and Marzeion, B.: The Open Global Glacier Model \(OGGM\) v1.1, \*Geoscientific Model Development\*, 12, 909–931, <https://doi.org/10.5194/gmd-12-909-2019>, 2019.](#)
- 175 [McCarthy, M., Meier, F., Faticchi, S., Stocker, B. D., Shaw, T. E., Miles, E., Dussaillant, I., and Pellicciotti, F.: Glacier Contributions to River Discharge During the Current Chilean Megadrought, \*Earth's Future\*, 10, e2022EF002852, <https://doi.org/10.1029/2022EF002852>, 2022.](#)
- [McMillan, H. K.: A review of hydrologic signatures and their applications, \*WIREs Water\*, 8, e1499, <https://doi.org/10.1002/wat2.1499>, 2021.](#)
- 180 [Mernild, S. H., Liston, G. E., Hiemstra, C., and Wilson, R.: The Andes Cordillera. Part III: glacier surface mass balance and contribution to sea level rise \(1979–2014\), \*International Journal of Climatology\*, 37, 3154–3174, <https://doi.org/10.1002/joc.4907>, 2017.](#)
- [Millan, R., Rignot, E., Rivera, A., Martineau, V., Mouginot, J., Zamora, R., Uribe, J., Lenzano, G., De Fleurian, B., Li, X., Gim, Y., and Kirchner, D.: Ice Thickness and Bed Elevation of the Northern and Southern Patagonian Icefields, \*Geophysical Research Letters\*, <https://doi.org/10.1029/2019GL082485>, 2019.](#)
- 185 [Millan, R., Mouginot, J., Rabatel, A., and Morlighem, M.: Ice velocity and thickness of the world's glaciers, \*Nat. Geosci.\*, 15, 124–129, <https://doi.org/10.1038/s41561-021-00885-z>, 2022.](#)

- Milner, A. M., Khamis, K., Battin, T. J., Brittain, J. E., Barrand, N. E., Füreder, L., Cauvy-Fraunié, S., Gíslason, G. M., Jacobsen, D., Hannah, D. M., Hodson, A. J., Hood, E., Lencioni, V., Ólafsson, J. S., Robinson, C. T., Tranter, M., and Brown, L. E.: Glacier shrinkage driving global changes in downstream systems, *Proceedings of the National Academy of Sciences*, 114, 9770–9778, <https://doi.org/10.1073/pnas.1619807114>, 2017.
- 1190 Minowa, M., Schaefer, M., Sugiyama, S., Sakakibara, D., and Skvarca, P.: Frontal ablation and mass loss of the Patagonian icefields, *Earth and Planetary Science Letters*, 561, 116811, <https://doi.org/10.1016/j.epsl.2021.116811>, 2021.
- Morales, M. S., Cook, E. R., Barichivich, J., Christie, D. A., Villalba, R., LeQuesne, C., Srur, A. M., Ferrero, M. E., González-Reyes, A., Couvreur, F., Matskovsky, V., Aravena, J. C., Lara, A., Mundo, I. A., Rojas, F., Prieto, M. R., Smerdon, J. E., Bianchi, L. O., Masiokas, M. H., Urrutia-Jalabert, R., Rodríguez-Catón, M., Muñoz, A. A., Rojas-Badilla, M., Alvarez, C.,
- 1195 Lopez, L., Luckman, B. H., Lister, D., Harris, I., Jones, P. D., Williams, A. P., Velazquez, G., Aliste, D., Aguilera-Betti, I., Marcotti, E., Flores, F., Muñoz, T., Cuq, E., and Boninsegna, J. A.: Six hundred years of South American tree rings reveal an increase in severe hydroclimatic events since mid-20th century, *Proceedings of the National Academy of Sciences*, 117, 16816–16823, <https://doi.org/10.1073/pnas.2002411117>, 2020.
- NASA JPL: NASADEM Merged DEM Global 1 arc second V001 [Data set], 2020.
- 1200 O'Neill, B. C., Tebaldi, C., van Vuuren, D. P., Eyring, V., Friedlingstein, P., Hurtt, G., Knutti, R., Kriegler, E., Lamarque, J.-F., Lowe, J., Meehl, G. A., Moss, R., Riahi, K., and Sanderson, B. M.: The Scenario Model Intercomparison Project (ScenarioMIP) for CMIP6, *Geosci. Model Dev.*, 9, 3461–3482, <https://doi.org/10.5194/gmd-9-3461-2016>, 2016.
- Pasquini, A., Cosentino, N., and Depetris, P.: The Main Hydrological Features of Patagonia's Santa Cruz River: An Updated Assessment, 195–210, [https://doi.org/10.1007/978-3-030-89676-8\\_9](https://doi.org/10.1007/978-3-030-89676-8_9), 2021.
- 1205 Pedregosa, F., Varoquaux, G., Gramfort, A., Michel, V., Thirion, B., Grisel, O., Blondel, M., Prettenhofer, P., Weiss, R., Dubourg, V., Vanderplas, J., Passos, A., Cournapeau, D., Brucher, M., Perrot, M., and Duchesnay, É.: Scikit-learn: Machine Learning in Python, *Journal of Machine Learning Research*, 12, 2825–2830, 2011.
- Pesci, M. H., Schulte Overberg, P., Bosshard, T., and Förster, K.: From global glacier modeling to catchment hydrology: bridging the gap with the WaSiM-OGGM coupling scheme, *Frontiers in Water*, 5, 2023.
- 1210 Poff, N. L., Allan, J. D., Bain, M. B., Karr, J. R., Prestegard, K. L., Richter, B. D., Sparks, R. E., and Stromberg, J. C.: The Natural Flow Regime, *BioScience*, 47, 769–784, <https://doi.org/10.2307/1313099>, 1997.
- Pritchard, H. D.: Asia's shrinking glaciers protect large populations from drought stress, *Nature*, 569, 649–654, <https://doi.org/10.1038/s41586-019-1240-1>, 2019.
- 1215 Rasul, G. and Molden, D.: The Global Social and Economic Consequences of Mountain Cryospheric Change, *Frontiers in Environmental Science*, 7, 2019.
- RGI Consortium: Randolph Glacier Inventory - A Dataset of Global Glacier Outlines, Version 6, <https://doi.org/10.7265/4M1F-GD79>, 2017.
- RGI Consortium: Randolph Glacier Inventory - A Dataset of Global Glacier Outlines, Version 7, <https://doi.org/10.5067/F6JMOVY5NAVZ>, 2023.

- 1220 Richter, B. D., Baumgartner, J. V., Powell, J., and Braun, D. P.: A Method for Assessing Hydrologic Alteration within Ecosystems, *Conservation Biology*, 10, 1163–1174, <https://doi.org/10.1046/j.1523-1739.1996.10041163.x>, 1996.
- Rounce, D. R., Khurana, T., Short, M. B., Hock, R., Shean, D. E., and Brinkerhoff, D. J.: Quantifying parameter uncertainty in a large-scale glacier evolution model using Bayesian inference: application to High Mountain Asia, *J. Glaciol.*, 66, 175–187, <https://doi.org/10.1017/jog.2019.91>, 2020.
- 1225 Rounce, D. R., Hock, R., Maussion, F., Hugonnet, R., Kochtitzky, W., Huss, M., Berthier, E., Brinkerhoff, D., Compagno, L., Copland, L., Farinotti, D., Menounos, B., and McNabb, R. W.: Global glacier change in the 21st century: Every increase in temperature matters, *Science*, 379, 78–83, <https://doi.org/10.1126/science.abo1324>, 2023.
- Ruiz, L., Pitte, P., Rivera, A., Schaefer, M., and Masiokas, M. H.: Current State and Recent Changes of Glaciers in the Patagonian Andes (~37 °S to 55 °S), in: *Freshwaters and Wetlands of Patagonia: Ecosystems and Socioecological Aspects*, edited by: Mataloni, G. and Quintana, R. D., Springer International Publishing, Cham, 59–91, [https://doi.org/10.1007/978-3-031-10027-7\\_4](https://doi.org/10.1007/978-3-031-10027-7_4), 2022.
- 1230 Sauter, T.: Revisiting extreme precipitation amounts over southern South America and implications for the Patagonian Icefields, *Hydrology and Earth System Sciences*, 24, 2003–2016, <https://doi.org/10.5194/hess-24-2003-2020>, 2020.
- Schmidt, L., Heße, F., Attinger, S., and Kumar, R.: Challenges in Applying Machine Learning Models for Hydrological Inference: A Case Study for Flooding Events Across Germany, *Water Resources Research*, 56, e2019WR025924, <https://doi.org/10.1029/2019WR025924>, 2020.
- Schuster, L., Rounce, D. R., and Maussion, F.: Glacier projections sensitivity to temperature-index model choices and calibration strategies, *Ann. Glaciol.*, 1–16, <https://doi.org/10.1017/aog.2023.57>, 2023.
- 1240 Somers, L. D., McKenzie, J. M., Mark, B. G., Lagos, P., Ng, G. C., Wickert, A. D., Yarleque, C., Baraër, M., and Silva, Y.: Groundwater Buffers Decreasing Glacier Melt in an Andean Watershed—But Not Forever, *Geophysical Research Letters*, 46, 13016–13026, <https://doi.org/10.1029/2019GL084730>, 2019.
- Svetnik, V., Liaw, A., Tong, C., Culberson, J. C., Sheridan, R. P., and Feuston, B. P.: Random Forest: A Classification and Regression Tool for Compound Classification and QSAR Modeling, *Journal of Chemical Information and Computer Sciences*, 43, 1947–1958, <https://doi.org/10.1021/ci034160g>, 2003.
- 1245 Tang, G., Clark, M. P., and Papalexiou, S. M.: EM-Earth: The Ensemble Meteorological Dataset for Planet Earth, *Bulletin of the American Meteorological Society*, 103, E996–E1018, <https://doi.org/10.1175/BAMS-D-21-0106.1>, 2022.
- Tang, G., Clark, M. P., Knoben, W. J. M., Liu, H., Gharari, S., Arnal, L., Beck, H. E., Wood, A. W., Newman, A. J., and Papalexiou, S. M.: The Impact of Meteorological Forcing Uncertainty on Hydrological Modeling: A Global Analysis of Cryosphere Basins, *Water Resources Research*, 59, e2022WR033767, <https://doi.org/10.1029/2022WR033767>, 2023.
- 1250 Tarek, M., Brissette, F., and Arsenault, R.: Uncertainty of gridded precipitation and temperature reference datasets in climate change impact studies, *Hydrol. Earth Syst. Sci.*, 25, 3331–3350, <https://doi.org/10.5194/hess-25-3331-2021>, 2021.
- Temme, F., Fariás-Barahona, D., Seehaus, T., Jaña, R., Arigony-Neto, J., Gonzalez, I., Arndt, A., Sauter, T., Schneider, C., and Fürst, J. J.: Strategies for regional modeling of surface mass balance at the Monte Sarmiento Massif, Tierra del Fuego, *The Cryosphere*, 17, 2343–2365, <https://doi.org/10.5194/tc-17-2343-2023>, 2023.

- 255 [Tokarska, K. B., Stolpe, M. B., Sippel, S., Fischer, E. M., Smith, C. J., Lehner, F., and Knutti, R.: Past warming trend constrains future warming in CMIP6 models, \*Science Advances\*, 6, eaaz9549, <https://doi.org/10.1126/sciadv.aaz9549>, 2020.](#)
- [Ultee, L., Coats, S., and Mackay, J.: Glacial runoff buffers droughts through the 21st century, \*Earth System Dynamics\*, 13, 935–959, <https://doi.org/10.5194/esd-13-935-2022>, 2022.](#)
- 260 [Van Tiel, M., Stahl, K., Freudiger, D., and Seibert, J.: Glacio-hydrological model calibration and evaluation, \*WIREs Water\*, 7, e1483, <https://doi.org/10.1002/wat2.1483>, 2020.](#)
- [Van Tiel, M., Van Loon, A. F., Seibert, J., and Stahl, K.: Hydrological response to warm and dry weather: do glaciers compensate?, \*Hydrology and Earth System Sciences\*, 25, 3245–3265, <https://doi.org/10.5194/hess-25-3245-2021>, 2021.](#)
- 265 [Van Tiel, M., Weiler, M., Freudiger, D., Moretti, G., Kohn, I., Gerlinger, K., and Stahl, K.: Melting Alpine Water Towers Aggravate Downstream Low Flows: A Stress-Test Storyline Approach, \*Earth's Future\*, 11, e2022EF003408, <https://doi.org/10.1029/2022EF003408>, 2023.](#)
- [Viviroli, D., Kumm, M., Meybeck, M., Kallio, M., and Wada, Y.: Increasing dependence of lowland populations on mountain water resources, \*Nat Sustain\*, 3, 917–928, <https://doi.org/10.1038/s41893-020-0559-9>, 2020.](#)
- 270 [Vries, M. V. W. de, Romero, M., Penprase, S. B., Ng, G.-H. C., and Wickert, A. D.: Increasing rate of 21st century volume loss of the Patagonian Icefields measured from proglacial river discharge, \*Journal of Glaciology\*, 1–16, <https://doi.org/10.1017/jog.2023.9>, 2023.](#)
- [Wang, H., Chen, J., Xu, C., Zhang, J., and Chen, H.: A Framework to Quantify the Uncertainty Contribution of GCMs Over Multiple Sources in Hydrological Impacts of Climate Change, \*Earth's Future\*, 8, <https://doi.org/10.1029/2020EF001602>, 2020.](#)
- 275 [Watanabe, M., Yanagawa, A., Watanabe, S., Hirabayashi, Y., and Kanae, S.: Quantifying the range of future glacier mass change projections caused by differences among observed past-climate datasets, \*Clim Dyn\*, 53, 2425–2435, <https://doi.org/10.1007/s00382-019-04868-0>, 2019.](#)
- [Werder, M. A., Huss, M., Paul, F., Dehecq, A., and Farinotti, D.: A Bayesian ice thickness estimation model for large-scale applications, \*Journal of Glaciology\*, 66, 137–152, <https://doi.org/10.1017/jog.2019.93>, 2020.](#)
- 280 [Zalazar, L., Ferri, L., Castro, M., Gargantini, H., Gimenez, M., Pitte, P., Ruiz, L., Masiokas, M., Costa, G., and Villalba, R.: Spatial distribution and characteristics of Andean ice masses in Argentina: results from the first National Glacier Inventory, \*Journal of Glaciology\*, 66, 938–949, <https://doi.org/10.1017/jog.2020.55>, 2020.](#)
- [Zambrano-Bigiarini, M.: Temporal and spatial evaluation of long-term satellite-based precipitation products across the complex topographical and climatic gradients of Chile, in: Remote Sensing and Modeling of the Atmosphere, Oceans, and Interactions VII, Remote Sensing and Modeling of the Atmosphere, Oceans, and Interactions VII, <https://doi.org/10.1117/12.2513645>, 2018.](#)
- 285 [Zekollari, H., Huss, M., and Farinotti, D.: Modelling the future evolution of glaciers in the European Alps under the EURO-CORDEX RCM ensemble, \*The Cryosphere\*, 13, 1125–1146, <https://doi.org/10.5194/tc-13-1125-2019>, 2019.](#)
- [Zekollari, H., Huss, M., Farinotti, D., and Lhermitte, S.: Ice-Dynamical Glacier Evolution Modeling—A Review, \*Reviews of Geophysics\*, 60, e2021RG000754, <https://doi.org/10.1029/2021RG000754>, 2022.](#)

- 290 [Zekollari, H., Huss, M., Schuster, L., Maussion, F., Rounce, D. R., Aguayo, R., Champollion, N., Compagno, L., Hugonnet, R., Marzeion, B., Mojtavavi, S., and Farinotti, D.: 21<sup>st</sup> century global glacier evolution under CMIP6 scenarios and the role of glacier-specific observations, \*EGUsphere\*, 1–33, <https://doi.org/10.5194/egusphere-2024-1013>, 2024.](#)
- [Zhao, H., Su, B., Lei, H., Zhang, T., and Xiao, C.: A new projection for glacier mass and runoff changes over High Mountain Asia, \*Science Bulletin\*, 68, 43–47, <https://doi.org/10.1016/j.scib.2022.12.004>, 2023.](#)
- 295 [Aguayo, R., León-Muñoz, J., Aguayo, M., Baez-Villanueva, O. M., Zambrano-Bigiarini, M., Fernández, A., and Jacques-Coper, M.: PatagoniaMet: A multi-source hydrometeorological dataset for Western Patagonia, \*Sci Data\*, 11, 6, <https://doi.org/10.1038/s41597-023-02828-2>, 2024.](#)
- [Ayala, Á., Fariás-Barahona, D., Huss, M., Pellicciotti, F., McPhee, J., and Farinotti, D.: Glacier runoff variations since 1955 in the Maipo River basin, in the semiarid Andes of central Chile, \*The Cryosphere\*, 14, 2005–2027, <https://doi.org/10.5194/te-14-2005-2020>, 2020.](#)
- 300 [Bacaza, G., Nussbaumer, S. U., Tapia, G., Valdés, J., Garefá, J. L., Videla, Y., Albornoz, A., and Arias, V.: Glacier inventory and recent glacier variations in the Andes of Chile, South America, \*Annals of Glaciology\*, 58, 166–180, <https://doi.org/10.1017/aog.2017.28>, 2017.](#)
- [Beck, H. E., Wood, E. F., Pan, M., Fisher, C. K., Miralles, D. G., van Dijk, A. I. J. M., McVicar, T. R., and Adler, R. F.: MSWEP V2 Global 3-Hourly 0.1° Precipitation: Methodology and Quantitative Assessment, \*Bulletin of the American Meteorological Society\*, 100, 473–500, <https://doi.org/10.1175/BAMS-D-17-0138.1>, 2019.](#)
- 305 [Beck, H. E., Wood, E. F., McVicar, T. R., Zambrano-Bigiarini, M., Alvarez-Garretón, C., Baez-Villanueva, O. M., Sheffield, J., and Karger, D. N.: Bias correction of global high-resolution precipitation climatologies using streamflow observations from 9372 catchments, \*Journal of Climate\*, 33, 1299–1315, <https://doi.org/10.1175/JCLI-D-19-0332.1>, 2020.](#)
- [Beck, H. E., Dijk, A. I. J. M. van, Larraondo, P. R., McVicar, T. R., Pan, M., Dutra, E., and Miralles, D. G.: MSWX: Global 3-Hourly 0.1° Bias-Corrected Meteorological Data Including Near-Real-Time Updates and Forecast Ensembles, \*Bulletin of the American Meteorological Society\*, 103, E710–E732, <https://doi.org/10.1175/BAMS-D-21-0145.1>, 2022.](#)
- 310 [Bennett, K. E., Miller, G., Busey, R., Chen, M., Lathrop, E. R., Dann, J. B., Nutt, M., Crumley, R., Dillard, S. L., Dafflon, B., Kumar, J., Bolton, W. R., Wilson, C. J., Iversen, C. M., and Wullschleger, S. D.: Spatial patterns of snow distribution in the sub-Arctic, \*The Cryosphere\*, 16, 3269–3293, <https://doi.org/10.5194/te-16-3269-2022>, 2022.](#)
- 315 [Boisier, J. P.: CR2MET: A high-resolution precipitation and temperature dataset for the period 1960–2021 in continental Chile, <https://doi.org/10.5281/zenodo.7529682>, 2023.](#)
- [Braun, M. H., Malz, P., Sommer, C., Fariás-Barahona, D., Sauter, T., Casassa, G., Soruco, A., Skvarea, P., and Seehaus, T. C.: Constraining glacier elevation and mass changes in South America, \*Nature Climate Change\*, 9, 130–136, <https://doi.org/10.1038/s41558-018-0375-7>, 2019.](#)
- 320 [Bravo, C., Quincey, D. J., Ross, A. N., Rivera, A., Brock, B., Miles, E., and Silva, A.: Air Temperature Characteristics, Distribution, and Impact on Modeled Ablation for the South Patagonia Icefield, \*Journal of Geophysical Research: Atmospheres\*, 124, 907–925, <https://doi.org/10.1029/2018JD028857>, 2019a.](#)



Bravo, C., Bozkurt, D., Gonzalez-Reyes, Á., Quincey, D. J., Ross, A. N., Fariás-Barahona, D., and Rojas, M.: Assessing Snow Accumulation Patterns and Changes on the Patagonian Icefields, *Frontiers in Environmental Science*, 7, 1–18, <https://doi.org/10.3389/feenvs.2019.00030>, 2019b.

Breiman, L.: Random Forests, *Machine Learning*, 45, 5–32, <https://doi.org/10.1023/A:1010933404324>, 2001.

Cannon, A. J.: Multivariate quantile mapping bias correction: an N-dimensional probability density function transform for climate model simulations of multiple variables, *Climate Dynamics*, 50, 31–49, <https://doi.org/10.1007/s00382-017-3580-6>, 2018.

Cannon, A. J., Sobie, S. R., and Murdock, T. Q.: Bias correction of GCM precipitation by quantile mapping: How well do methods preserve changes in quantiles and extremes?, *Journal of Climate*, 28, 6938–6959, <https://doi.org/10.1175/JCLI-D-14-00754.1>, 2015.

Caro, A., Condom, T., and Rabatel, A.: Climatic and Morphometric Explanatory Variables of Glacier Changes in the Andes (8–55°S): New Insights From Machine Learning Approaches, *Front. Earth Sci.*, 9, 713011, <https://doi.org/10.3389/feart.2021.713011>, 2021.

Caro, A., Condom, T., Rabatel, A., Champollion, N., García, N., and Saavedra, F.: Hydrological response of Andean catchments to recent glacier mass loss, *The Cryosphere*, 18, 2487–2507, <https://doi.org/10.5194/te-18-2487-2024>, 2024.

Cauvy-Fraunié, S. and Dangles, O.: A global synthesis of biodiversity responses to glacier retreat, *Nat Ecol Evol*, 3, 1675–1685, <https://doi.org/10.1038/s41559-019-1042-8>, 2019.

Chen, J., Brissette, F. P., and Leconte, R.: Uncertainty of downscaling method in quantifying the impact of climate change on hydrology, *Journal of Hydrology*, 401, 190–202, <https://doi.org/10.1016/j.jhydrol.2011.02.020>, 2011.

Compagno, L., Zekollari, H., Huss, M., and Farinotti, D.: Limited impact of climate forcing products on future glacier evolution in Scandinavia and Iceland, *J. Glaciol.*, 67, 727–743, <https://doi.org/10.1017/jog.2021.24>, 2021.

Condom, T., Martínez, R., Pabón, J. D., Costa, F., Pineda, L., Nieto, J. J., López, F., and Villacis, M.: Climatological and Hydrological Observations for the South American Andes: In-situ Stations, Satellite, and Reanalysis Data Sets, *Frontiers in Earth Science*, 8, 1–20, <https://doi.org/10.3389/feart.2020.00092>, 2020.

Davies, B. J. and Glasser, N. F.: Accelerating shrinkage of Patagonian glaciers from the Little Ice Age (~AD 1870) to 2011, *Journal of Glaciology*, 58, 1063–1084, <https://doi.org/10.3189/2012JG12J026>, 2012.

Drenkhan, F., Buytaert, W., Mackay, J. D., Barrand, N. E., Hannah, D. M., and Huggel, C.: Looking beyond glaciers to understand mountain water security, *Nat Sustain*, 6, 130–138, <https://doi.org/10.1038/s41893-022-00996-4>, 2022.

Dussaillant, I., Berthier, E., Brun, F., Masiokas, M., Hugonnet, R., Favier, V., Rabatel, A., Pitte, P., and Ruiz, L.: Two decades of glacier mass loss along the Andes, *Nature Geoscience*, 1–7, <https://doi.org/10.1038/s41561-019-0432-5>, 2019.

Eyring, V., Bony, S., Meehl, G. A., Senior, C. A., Stevens, B., Stouffer, R. J., and Taylor, K. E.: Overview of the Coupled Model Intercomparison Project Phase 6 (CMIP6) experimental design and organization, *Geoscientific Model Development*, 9, 1937–1958, <https://doi.org/10.5194/gmd-9-1937-2016>, 2016.

Farinotti, D., Huss, M., Fürst, J. J., Landmann, J., Machguth, H., Maussion, F., and Pandit, A.: A consensus estimate for the ice thickness distribution of all glaciers on Earth, *Nat. Geosci.*, 12, 168–173, <https://doi.org/10.1038/s41561-019-0300-3>, 2019.

Gabbi, J., Farinotti, D., Bauder, A., and Maurer, H.: Ice volume distribution and implications on runoff projections in a glacierized catchment, *Hydrology and Earth System Sciences*, 16, 4543–4556, <https://doi.org/10.5194/hess-16-4543-2012>, 2012.

Garreaud, R. D., Alvarez-Garretón, C., Barichivich, J., Boisier, J. P., Christie, D., Galleguillos, M., LeQuesne, C., McPhee, J., Zambrano-Bigiarini, M., Pablo Boisier, J., Christie, D., Galleguillos, M., LeQuesne, C., McPhee, J., and Zambrano-Bigiarini, M.: The 2010–2015 megadrought in central Chile: impacts on regional hydroclimate and vegetation, *Hydrology and Earth System Sciences*, 21, 6307–6327, <https://doi.org/10.5194/hess-21-6307-2017>, 2017.

Gateño, F., Mendoza, P. A., Vázquez, N., Lagos-Zúñiga, M., Jiménez, H., Jerez, C., Vargas, X., Rubio-Álvarez, E., and Montserrat, S.: Screening CMIP6 models for Chile based on past performance and code genealogy, *Climatic Change*, 177, 87, <https://doi.org/10.1007/s10584-024-03742-1>, 2024.

Hanus, S., Schuster, L., Burek, P., Maussion, F., Wada, Y., and Viviroli, D.: Coupling a large-scale glacier and hydrological model (OGGM v1.5.3 and CWatM V1.08)—Towards an improved representation of mountain water resources in global assessments, <https://doi.org/10.5194/egusphere-2023-2562>, 22 January 2024.

Hausfather, Z., Marvel, K., Schmidt, G. A., Nielsen-Gammon, J. W., and Zelinka, M.: Climate simulations: recognize the ‘hot model’ problem, *Nature*, 605, 26–29, <https://doi.org/10.1038/d41586-022-01192-2>, 2022.

Hersbach, H., Bell, B., Berrisford, P., Hirahara, S., Horányi, A., Muñoz-Sabater, J., Nicolas, J., Peubey, C., Radu, R., Schepers, D., Simmons, A., Soci, C., Abdalla, S., Abellan, X., Balsamo, G., Beechold, P., Biavati, G., Bidlot, J., Bonavita, M., De Chiara, G., Dahlgren, P., Dee, D., Diamantakis, M., Dragani, R., Flemming, J., Forbes, R., Fuentes, M., Geer, A., Haimberger, L., Healy, S., Hogan, R. J., Hólm, E., Janisková, M., Keeley, S., Laloyaux, P., Lopez, P., Lupu, C., Radnoti, G., de Rosnay, P., Rozum, I., Vamborg, F., Villaume, S., and Thépaut, J.-N.: The ERA5 global reanalysis, *Quarterly Journal of the Royal Meteorological Society*, 146, 1999–2049, <https://doi.org/10.1002/qj.3803>, 2020.

Hoek, R., Maussion, F., Marzeion, B., and Nowicki, S.: What is the global glacier ice volume outside the ice sheets?, *J. Glaciol.*, 69, 204–210, <https://doi.org/10.1017/jog.2023.1>, 2023.

Hugonnet, R., McNabb, R., Berthier, E., Menounos, B., Nuth, C., Girod, L., Farinotti, D., Huss, M., Dussailant, I., Brun, F., and Käab, A.: Accelerated global glacier mass loss in the early twenty-first century, *Nature*, 592, 726–731, <https://doi.org/10.1038/s41586-021-03436-z>, 2021.

Huss, M. and Hoek, R.: A new model for global glacier change and sea-level rise, *Frontiers in Earth Science*, 3, 1–22, <https://doi.org/10.3389/feart.2015.00054>, 2015.

Huss, M. and Hoek, R.: Global-scale hydrological response to future glacier mass loss, *Nature Climate Change*, 8, 135–140, <https://doi.org/10.1038/s41558-017-0049-x>, 2018.

Huss, M., Zemp, M., Joerg, P. C., and Salzmann, N.: High uncertainty in 21st century runoff projections from glacierized basins, *Journal of Hydrology*, 510, 35–48, <https://doi.org/10.1016/j.jhydrol.2013.12.017>, 2014.

- 1390 Huss, M., Bookhagen, B., Huggel, C., Jacobsen, D., Bradley, R. s., Clague, J. j., Vuille, M., Buytaert, W., Cayan, D. r., Greenwood, G., Mark, B. g., Milner, A. m., Weingartner, R., and Winder, M.: Toward mountains without permanent snow and ice, *Earth's Future*, 5, 418–435, <https://doi.org/10.1002/2016EF000514>, 2017.
- 1395 Immerzeel, W. W., Lutz, A. F., Andrade, M., Bahl, A., Biemans, H., Bolch, T., Hyde, S., Brumby, S., Davies, B. J., Elmore, A. C., Emmer, A., Feng, M., Fernández, A., Haritashya, U., Kargel, J. S., Koppes, M., Kraaijenbrink, P. D. A., Kulkarni, A. V., Mayewski, P. A., Nepal, S., Pacheco, P., Painter, T. H., Pellicciotti, F., Rajaram, H., Rupper, S., Sinisalo, A., Shrestha, A. B., Viviroli, D., Wada, Y., Xiao, C., Yao, T., and Baillie, J. E. M.: Importance and vulnerability of the world's water towers, *Nature*, 577, 364–369, <https://doi.org/10.1038/s41586-019-1822-y>, 2020.
- IPCC: High Mountain Areas, in: *The Ocean and Cryosphere in a Changing Climate: Special Report of the Intergovernmental Panel on Climate Change*, Cambridge, <https://doi.org/10.1017/9781009157964.004>, 2022.
- 1400 Iriarte, J. L., Pantoja, S., and Daneri, G.: Oceanographic Processes in Chilean Fjords of Patagonia: From small to large-scale studies, *Progress in Oceanography*, 129, 1–7, <https://doi.org/10.1016/j.pocean.2014.10.004>, 2014.
- 1405 Iturbide, M., Fernández, J., Gutiérrez, J. M., Bedia, J., Cimadevilla, E., Díez-Sierra, J., Manzanar, R., Casanueva, A., Baño-Medina, J., Milovae, J., Herrera, S., Cofiño, A. S., San Martín, D., García-Díez, M., Hauser, M., Huard, D., and Yelekei, Ö.: Repository supporting the implementation of FAIR principles in the IPCC-WGI Atlas, <https://doi.org/10.5281/ZENODO.3691645>, 2021.
- Kaser, G., Großhauser, M., and Marzeion, B.: Contribution potential of glaciers to water availability in different climate regimes, *Proceedings of the National Academy of Sciences*, 107, 20223–20227, <https://doi.org/10.1073/pnas.1008162107>, 2010.
- Lange, S.: ISIMIP3b bias-adjustment fact sheet, 2021.
- 1410 Li, F., Maussion, F., Wu, G., Chen, W., Yu, Z., Li, Y., and Liu, G.: Influence of glacier inventories on ice thickness estimates and future glacier change projections in the Tian Shan range, Central Asia, *J. Glaciol.*, 1–15, <https://doi.org/10.1017/jog.2022.60>, 2022.
- 1415 Logan, T., Aoun, A., Bourgault, P., Dupuis, É., Huard, D., Lavoie, J., Rondeau-Genesee, G., Smith, T. J., Alegre, R., Barnes, C., Biner, S., Caron, D., Ehbrecht, C., Fyke, J., Keel, T., Labonté, M. P., Lierhammer, L., Low, J. F., Quinn, J., Roy, P., Squire, D., Stephens, A., Tanguy, M., and Whelan, C.: Ouranosine/xclim: v0.39.0, <https://doi.org/10.5281/zenodo.7274811>, 2022.
- Mackay, J. D., Barrand, N. E., Hannah, D. M., Krause, S., Jackson, C. R., Everest, J., Aðalgeirsdóttir, G., and Black, A. R.: Future evolution and uncertainty of river flow regime change in a deglaciating river basin, *Hydrol. Earth Syst. Sci.*, 23, 1833–1865, <https://doi.org/10.5194/hess-23-1833-2019>, 2019.
- 1420 Malles, J., Maussion, F., Ultee, L., Koeltitzky, W., Copland, L., and Marzeion, B.: Exploring the impact of a frontal ablation parameterization on projected 21st-century mass change for Northern Hemisphere glaciers, *Journal of Glaciology*, 2023.
- Marzeion, B., Jarosch, A. H., and Hofer, M.: Past and future sea-level change from the surface-mass balance of glaciers, *The Cryosphere*, 6, 1295–1322, <https://doi.org/10.5194/tc-6-1295-2012>, 2012.
- Marzeion, B., Hock, R., Anderson, B., Bliss, A., Champollion, N., Fujita, K., Huss, M., Immerzeel, W. W., Kraaijenbrink, P., Malles, J., Maussion, F., Radić, V., Rounce, D. R., Sakai, A., Shannon, S., van de Wal, R., and Zekollari, H.: Partitioning the

- 1425 Uncertainty of Ensemble Projections of Global Glacier Mass Change, *Earth's Future*, 8, <https://doi.org/10.1029/2019EF001470>, 2020.
- Masiokas, M., Rabatel, A., Rivera, A., Ruiz, L., Pitte, P., Ceballos, J. L., Barcaza, G., Soruco, A., and Bown, F.: A review of the current state and recent changes of the Andean cryosphere, *Frontiers in Earth Science*, 8, 99, <https://doi.org/10.3389/FEART.2020.00099>, 2020.
- 1430 Masiokas, M. H., Cara, L., Villalba, R., Pitte, P., Luckman, B. H., Toum, E., Christie, D. A., Le Quesne, C., and Mauget, S.: Streamflow variations across the Andes (18°–55°S) during the instrumental era, *Scientific Reports*, 9, 17879, <https://doi.org/10.1038/s41598-019-53981-x>, 2019.
- Maussion, F., Butenko, A., Champollion, N., Dusch, M., Eis, J., Fourteau, K., Gregor, P., Jarosch, A. H., Landmann, J., Oesterle, F., Recinos, B., Rothenpieler, T., Vlug, A., Wild, C. T., and Marzeion, B.: The Open Global Glacier Model (OGGM) v1.1, *Geoscientific Model Development*, 12, 909–931, <https://doi.org/10.5194/gmd-12-909-2019>, 2019.
- 1435 McCarthy, M., Meier, F., Fatichi, S., Stocker, B. D., Shaw, T. E., Miles, E., Dussailant, I., and Pellicciotti, F.: Glacier Contributions to River Discharge During the Current Chilean Megadrought, *Earth's Future*, 10, e2022EF002852, <https://doi.org/10.1029/2022EF002852>, 2022.
- McMillan, H. K.: A review of hydrologic signatures and their applications, *WIREs Water*, 8, e1499, <https://doi.org/10.1002/wat2.1499>, 2021.
- 1440 Mernild, S. H., Liston, G. E., Hiemstra, C., and Wilson, R.: The Andes Cordillera. Part III: glacier surface mass balance and contribution to sea level rise (1979–2014), *International Journal of Climatology*, 37, 3154–3174, <https://doi.org/10.1002/joc.4907>, 2017.
- Millan, R., Rignot, E., Rivera, A., Martineau, V., Mouginot, J., Zamora, R., Uribe, J., Lenzano, G., De Fleurian, B., Li, X., Gim, Y., and Kirchner, D.: Ice Thickness and Bed Elevation of the Northern and Southern Patagonian Icefields, *Geophysical Research Letters*, <https://doi.org/10.1029/2019GL082485>, 2019.
- 1445 Millan, R., Mouginot, J., Rabatel, A., and Morlighem, M.: Ice velocity and thickness of the world's glaciers, *Nat. Geosci.*, 15, 124–129, <https://doi.org/10.1038/s41561-021-00885-z>, 2022.
- Milner, A. M., Khamis, K., Battin, T. J., Brittain, J. E., Barrand, N. E., Füreder, L., Cauvy-Fraunié, S., Gíslason, G. M., Jacobsen, D., Hannah, D. M., Hodson, A. J., Hood, E., Lencioni, V., Ólafsson, J. S., Robinson, C. T., Tranter, M., and Brown, L. E.: Glacier shrinkage driving global changes in downstream systems, *Proceedings of the National Academy of Sciences*, 114, 9770–9778, <https://doi.org/10.1073/pnas.1619807114>, 2017.
- 1450 Minowa, M., Schaefer, M., Sugiyama, S., Sakakibara, D., and Skvarca, P.: Frontal ablation and mass loss of the Patagonian icefields, *Earth and Planetary Science Letters*, 561, 116811, <https://doi.org/10.1016/j.epsl.2021.116811>, 2021.
- 1455 Morales, M. S., Cook, E. R., Barichivich, J., Christie, D. A., Villalba, R., LeQuesne, C., Srur, A. M., Ferrero, M. E., González-Reyes, A., Couvreur, F., Matskovsky, V., Aravena, J. C., Lara, A., Mundo, I. A., Rojas, F., Prieto, M. R., Smerdon, J. E., Bianchi, L. O., Masiokas, M. H., Urrutia-Jalabert, R., Rodríguez-Catón, M., Muñoz, A. A., Rojas-Badilla, M., Alvarez, C., Lopez, L., Luckman, B. H., Lister, D., Harris, I., Jones, P. D., Williams, A. P., Velazquez, G., Aliste, D., Aguilera-Betti, I., Marcotti, E., Flores, F., Muñoz, T., Cug, E., and Boninsegna, J. A.: Six hundred years of South American tree rings reveal an increase in severe hydroclimatic events since mid-20th century, *Proceedings of the National Academy of Sciences*, 117, 16816–16823, <https://doi.org/10.1073/pnas.2002411117>, 2020.
- 1460

NASA JPL: NASADEM Merged DEM Global 1 arc-second V001 [Data set], 2020.

O'Neill, B. C., Tebaldi, C., van Vuuren, D. P., Eyring, V., Friedlingstein, P., Hurtt, G., Knutti, R., Kriegler, E., Lamarque, J.-F., Lowe, J., Meehl, G. A., Moss, R., Riahi, K., and Sanderson, B. M.: The Scenario Model Intercomparison Project (ScenarioMIP) for CMIP6, *Geosci. Model Dev.*, 9, 3461–3482, <https://doi.org/10.5194/gmd-9-3461-2016>, 2016.

Pasquini, A., Cosentino, N., and Depetris, P.: The Main Hydrological Features of Patagonia's Santa Cruz River: An Updated Assessment, 195–210, [https://doi.org/10.1007/978-3-030-89676-8\\_9](https://doi.org/10.1007/978-3-030-89676-8_9), 2021.

Pedregosa, F., Varoquaux, G., Gramfort, A., Michel, V., Thirion, B., Grisel, O., Blondel, M., Prettenhofer, P., Weiss, R., Dubourg, V., Vanderplas, J., Passos, A., Cournapeau, D., Brucher, M., Perrot, M., and Duchesnay, É.: Scikit-learn: Machine Learning in Python, *Journal of Machine Learning Research*, 12, 2825–2830, 2011.

Pesci, M. H., Schulte-Overberg, P., Bosshard, T., and Förster, K.: From global glacier modeling to catchment hydrology: bridging the gap with the WaSiM-OGGM coupling scheme, *Frontiers in Water*, 5, 2023.

Poff, N. L., Allan, J. D., Bain, M. B., Karr, J. R., Prestegard, K. L., Richter, B. D., Sparks, R. E., and Stromberg, J. C.: The Natural Flow Regime, *BioScience*, 47, 769–784, <https://doi.org/10.2307/1313099>, 1997.

Pritchard, H. D.: Asia's shrinking glaciers protect large populations from drought stress, *Nature*, 569, 649–654, <https://doi.org/10.1038/s41586-019-1240-1>, 2019.

Rasul, G. and Molden, D.: The Global Social and Economic Consequences of Mountain Cryospheric Change, *Frontiers in Environmental Science*, 7, 2019.

RGI Consortium: Randolph Glacier Inventory — A Dataset of Global Glacier Outlines, — Version — 6, <https://doi.org/10.7265/4M1F-GD79>, 2017.

RGI Consortium: Randolph Glacier Inventory — A Dataset of Global Glacier Outlines, — Version — 7, <https://doi.org/10.5067/F6JMOVY5NAVZ>, 2023.

Richter, B. D., Baumgartner, J. V., Powell, J., and Braun, D. P.: A Method for Assessing Hydrologic Alteration within Ecosystems, *Conservation Biology*, 10, 1163–1174, <https://doi.org/10.1046/j.1523-1739.1996.10041163.x>, 1996.

Rounce, D. R., Khurana, T., Short, M. B., Hock, R., Shean, D. E., and Brinkerhoff, D. J.: Quantifying parameter uncertainty in a large-scale glacier evolution model using Bayesian inference: application to High Mountain Asia, *J. Glaciol.*, 66, 175–187, <https://doi.org/10.1017/jog.2019.91>, 2020.

Rounce, D. R., Hock, R., Maussion, F., Hugonnet, R., Kochtitzky, W., Huss, M., Berthier, E., Brinkerhoff, D., Compagno, L., Copland, L., Farinotti, D., Menounos, B., and McNabb, R. W.: Global glacier change in the 21st century: Every increase in temperature matters, *Science*, 379, 78–83, <https://doi.org/10.1126/science.aba1324>, 2023.

Ruiz, L., Pitte, P., Rivera, A., Schaefer, M., and Masiokas, M. H.: Current State and Recent Changes of Glaciers in the Patagonian Andes (–37°S to 55°S), in: *Freshwaters and Wetlands of Patagonia: Ecosystems and Socioecological Aspects*, edited by: Mataloni, G. and Quintana, R. D., Springer International Publishing, Cham, 59–91, [https://doi.org/10.1007/978-3-031-10027-7\\_4](https://doi.org/10.1007/978-3-031-10027-7_4), 2022.

- 495 Sauter, T.: Revisiting extreme precipitation amounts over southern South America and implications for the Patagonian Icefields, *Hydrology and Earth System Sciences*, 24, 2003–2016, <https://doi.org/10.5194/hess-24-2003-2020>, 2020.
- Schmidt, L., Heße, F., Attinger, S., and Kumar, R.: Challenges in Applying Machine Learning Models for Hydrological Inference: A Case Study for Flooding Events Across Germany, *Water Resources Research*, 56, e2019WR025924, <https://doi.org/10.1029/2019WR025924>, 2020.
- 500 Sehuster, L., Rounce, D. R., and Maussion, F.: Glacier projections sensitivity to temperature index model choices and calibration strategies, *Ann. Glaciol.*, 1–16, <https://doi.org/10.1017/aog.2023.57>, 2023.
- Somers, L. D., McKenzie, J. M., Mark, B. G., Lagos, P., Ng, G. C., Wickert, A. D., Yarleque, C., Baraër, M., and Silva, Y.: Groundwater Buffers Decreasing Glacier Melt in an Andean Watershed—But Not Forever, *Geophysical Research Letters*, 46, 13016–13026, <https://doi.org/10.1029/2019GL084730>, 2019.
- 505 Svetnik, V., Liaw, A., Tong, C., Culberson, J. C., Sheridan, R. P., and Feuston, B. P.: Random Forest: A Classification and Regression Tool for Compound Classification and QSAR Modeling, *Journal of Chemical Information and Computer Sciences*, 43, 1947–1958, <https://doi.org/10.1021/ci034160g>, 2003.
- Tang, G., Clark, M. P., and Papalexiou, S. M.: EM-Earth: The Ensemble Meteorological Dataset for Planet Earth, *Bulletin of the American Meteorological Society*, 103, E996–E1018, <https://doi.org/10.1175/BAMS-D-21-0106.1>, 2022.
- 510 Tang, G., Clark, M. P., Knoben, W. J. M., Liu, H., Gharari, S., Arnal, L., Beck, H. E., Wood, A. W., Newman, A. J., and Papalexiou, S. M.: The Impact of Meteorological Forcing Uncertainty on Hydrological Modeling: A Global Analysis of Cryosphere Basins, *Water Resources Research*, 59, e2022WR033767, <https://doi.org/10.1029/2022WR033767>, 2023.
- Tarek, M., Brissette, F., and Arseneault, R.: Uncertainty of gridded precipitation and temperature reference datasets in climate change impact studies, *Hydrol. Earth Syst. Sci.*, 25, 3331–3350, <https://doi.org/10.5194/hess-25-3331-2021>, 2021.
- 515 Temme, F., Fariás-Barahona, D., Seehaus, T., Jaña, R., Arigony Neto, J., Gonzalez, I., Arndt, A., Sauter, T., Schneider, C., and Fürst, J. J.: Strategies for regional modeling of surface mass balance at the Monte Sarmiento Massif, Tierra del Fuego, *The Cryosphere*, 17, 2343–2365, <https://doi.org/10.5194/te-17-2343-2023>, 2023.
- Tokarska, K. B., Stolpe, M. B., Sippel, S., Fischer, E. M., Smith, C. J., Lehner, F., and Knutti, R.: Past warming trend constrains future warming in CMIP6 models, *Science Advances*, 6, eaaz9549, <https://doi.org/10.1126/sciadv.aaz9549>, 2020.
- 520 Ultee, L., Coats, S., and Mackay, J.: Glacial runoff buffers droughts through the 21st century, *Earth System Dynamics*, 13, 935–959, <https://doi.org/10.5194/esd-13-935-2022>, 2022.
- Van Tiel, M., Stahl, K., Freudiger, D., and Seibert, J.: Glacio-hydrological model calibration and evaluation, *WIREs Water*, 7, e1483, <https://doi.org/10.1002/wat2.1483>, 2020.
- Van Tiel, M., Van Loon, A. F., Seibert, J., and Stahl, K.: Hydrological response to warm and dry weather: do glaciers compensate?, *Hydrology and Earth System Sciences*, 25, 3245–3265, <https://doi.org/10.5194/hess-25-3245-2021>, 2021.
- 525 Van Tiel, M., Weiler, M., Freudiger, D., Moretti, G., Kohn, I., Gerlinger, K., and Stahl, K.: Melting Alpine Water Towers Aggravate Downstream Low Flows: A Stress-Test Storyline Approach, *Earth's Future*, 11, e2022EF003408, <https://doi.org/10.1029/2022EF003408>, 2023.

- 1530 Viviroli, D., Kummerow, M., Meybeck, M., Kallio, M., and Wada, Y.: Increasing dependence of lowland populations on mountain water resources, *Nat Sustain*, 3, 917–928, <https://doi.org/10.1038/s41893-020-0559-9>, 2020.
- Vries, M. V. W. de, Romero, M., Penprase, S. B., Ng, G. H. C., and Wickert, A. D.: Increasing rate of 21st-century volume loss of the Patagonian Icefields measured from proglacial river discharge, *Journal of Glaciology*, 1–16, <https://doi.org/10.1017/jog.2023.9>, 2023.
- 1535 Wang, H., Chen, J., Xu, C., Zhang, J., and Chen, H.: A Framework to Quantify the Uncertainty Contribution of GCMs Over Multiple Sources in Hydrological Impacts of Climate Change, *Earth's Future*, 8, <https://doi.org/10.1029/2020EF001602>, 2020.
- Watanabe, M., Yanagawa, A., Watanabe, S., Hirabayashi, Y., and Kanae, S.: Quantifying the range of future glacier mass change projections caused by differences among observed past climate datasets, *Clim Dyn*, 53, 2425–2435, <https://doi.org/10.1007/s00382-019-04868-0>, 2019.
- 1540 Werder, M. A., Huss, M., Paul, F., Dehecq, A., and Farinotti, D.: A Bayesian ice thickness estimation model for large-scale applications, *Journal of Glaciology*, 66, 137–152, <https://doi.org/10.1017/jog.2019.93>, 2020.
- Zalazar, L., Ferri, L., Castro, M., Gargantini, H., Gimenez, M., Pitte, P., Ruiz, L., Masiokas, M., Costa, G., and Villalba, R.: Spatial distribution and characteristics of Andean ice masses in Argentina: results from the first National Glacier Inventory, *Journal of Glaciology*, 66, 938–949, <https://doi.org/10.1017/jog.2020.55>, 2020.
- 1545 Zambrano-Bigiarini, M.: Temporal and spatial evaluation of long-term satellite-based precipitation products across the complex topographical and climatic gradients of Chile, in: *Remote Sensing and Modeling of the Atmosphere, Oceans, and Interactions VII, Remote Sensing and Modeling of the Atmosphere, Oceans, and Interactions VII*, <https://doi.org/10.1117/12.2513645>, 2018.
- Zekollari, H., Huss, M., and Farinotti, D.: Modelling the future evolution of glaciers in the European Alps under the EURO-CORDEX RCM ensemble, *The Cryosphere*, 13, 1125–1146, <https://doi.org/10.5194/tc-13-1125-2019>, 2019.
- 1550 Zekollari, H., Huss, M., Farinotti, D., and Lhermitte, S.: Ice Dynamical Glacier Evolution Modeling—A Review, *Reviews of Geophysics*, 60, e2021RG000754, <https://doi.org/10.1029/2021RG000754>, 2022.
- Zekollari, H., Huss, M., Schuster, L., Maussion, F., Rounce, D. R., Aguayo, R., Champollion, N., Compagno, L., Hugonnet, R., Marzeion, B., Mojtavavi, S., and Farinotti, D.: 21<sup>st</sup>-century global glacier evolution under CMIP6 scenarios and the role of glacier-specific observations, *EGU sphere*, 1–33, <https://doi.org/10.5194/egusphere-2024-1013>, 2024.
- 1555 Zhao, H., Su, B., Lei, H., Zhang, T., and Xiao, C.: A new projection for glacier mass and runoff changes over High Mountain Asia, *Science Bulletin*, 68, 43–47, <https://doi.org/10.1016/j.scib.2022.12.004>, 2023.